

HYDROGEN PRODUCTION FROM ETHANOL OVER MESOPOROUS  
ALUMINA BASED CATALYSTS AND MICROWAVE REACTOR  
APPLICATIONS

A THESIS SUBMITTED TO  
THE GRADUATE SCHOOL OF NATURAL AND APPLIED SCIENCES  
OF  
MIDDLE EAST TECHNICAL UNIVERSITY

BY

SEVAL GÜNDÜZ

IN PARTIAL FULFILLMENT OF THE REQUIREMENTS  
FOR  
THE DEGREE OF DOCTOR OF PHILOSOPHY  
IN  
CHEMICAL ENGINEERING

SEPTEMBER 2014



Approval of the thesis:

**HYDROGEN PRODUCTION FROM ETHANOL OVER MESOPOROUS  
ALUMINA BASED CATALYSTS AND MICROWAVE REACTOR  
APPLICATIONS**

submitted by **SEVAL GÜNDÜZ** in partial fulfillment of the requirements for the degree of **Doctor of Philosophy in Chemical Engineering Department, Middle East Technical University** by,

Prof. Dr. Canan Özgen  
Dean, Graduate School of **Natural and Applied Sciences**

Prof. Dr. Halil Kalıpçılar  
Head of Department, **Chemical Engineering**

Prof. Dr. Timur Doğu  
Supervisor, **Chemical Engineering Dept., METU**

**Examining Committee Members:**

Prof. Dr. İnci Eroğlu  
Chemical Engineering Dept., METU

Prof. Dr. Timur Doğu  
Chemical Engineering Dept., METU

Prof. Dr. Güzide Çalık  
Chemical Engineering Dept., Ankara University

Assoc. Prof. Dr. Naime Aslı Sezgi  
Chemical Engineering Dept., METU

Assoc. Prof. Dr. Sena Yaşyerli  
Chemical Engineering Dept., Gazi University

**Date:** 19.09.2014

**I hereby declare that all information in this document has been obtained and presented in accordance with academic rules and ethical conduct. I also declare that, as required by these rules and conduct, I have fully cited and referenced all material and results that are not original to this work.**

Name, Last name : Seval Gündüz

Signature :

## ABSTRACT

### HYDROGEN PRODUCTION FROM ETHANOL OVER MESOPOROUS ALUMINA BASED CATALYSTS AND MICROWAVE REACTOR APPLICATIONS

Gündüz, Seval  
Ph.D., Department of Chemical Engineering  
Supervisor: Prof. Dr. Timur Doğu

September 2014, 155 pages

Due to fast depletion of fossil fuel resources and related environmental impact of CO<sub>2</sub> emissions, the interest in hydrogen as a clean energy carrier has recently increased. Hydrogen production from bio-ethanol, which already contains large amount of water, by steam reforming process, has shown excellent potential with CO<sub>2</sub> neutrality and renewability. Steam reforming of ethanol (SRE) process has a highly complex reaction network including numerous side reactions which decrease hydrogen yield and have a negative effect on process economy. In addition, highly endothermic nature of the steam reforming of ethanol reaction raises the doubts on the economic feasibility of the process.

Therefore, the main objectives in the present study are; (i) designing and synthesizing novel mesoporous catalysts which are highly active for steam reforming of ethanol reaction and highly stable in the presence of steam at elevated temperature conditions and (ii) developing a new reaction system that uses an alternative heat source which is more efficient than conventional heating.

In the scope of the present study, Co-Mg and Ni-Mg incorporated mesoporous alumina type materials were synthesized following two different techniques; direct synthesis (one-pot) and impregnation routes with Co/Al or Ni/Al molar ratio of 0.10. Catalytic

activities of the synthesized materials were tested in both conventionally heated and focused-microwave reactor systems available in our laboratory. Afterwards, several characterization techniques were applied to both fresh and used catalysts in order to understand the reasons of catalytic performance differences obtained.

Co-Mg incorporated catalysts prepared by direct addition of Mg (Co-Mg-MA and Co@Mg-MA) and by impregnation/lack of Mg (Co-Mg@MA and Co@MA) showed very different behavior towards steam reforming of ethanol process. While catalysts synthesized by direct addition of Mg exhibited superior activity towards steam reforming of ethanol reaction with an average hydrogen yield of 5.2 out of the maximum hydrogen yield value of 6.0, the ones synthesized by impregnation/lack of Mg showed no activity for hydrogen production. The main product obtained with these catalysts was ethylene indicating that ethanol dehydration reaction dominated the reaction pathway over these catalysts. According to XRD and XPS analysis, Co-Mg-MA and Co@Mg-MA catalysts synthesized by direct addition of Mg involved  $\text{Co}^0$  and CoO phases which are the active structures for SRE reaction. However Co-Mg@MA and Co@MA catalysts were mainly composed of  $\text{CoAl}_2\text{O}_4$  structure and no  $\text{Co}^0$  and CoO phases were observed in their framework which resulted in low activity towards SRE reaction. Additionally, DRIFTS analysis of pyridine adsorbed samples showed that acidity of catalysts prepared by impregnation/lack of Mg (Co-Mg@MA and Co@MA) was very high which can be considered as the main reason of relatively high selectivity of ethanol dehydration reaction over these catalysts. The best catalyst towards SRE reaction, Co@Mg-MA, was also tested in focused-microwave reaction system and it was observed that microwave-assisted SRE reaction provided slightly higher and more stable hydrogen yield. The most surprising outcome of microwave-assisted SRE reaction was that coke elimination was achieved, most probably due to the uniform temperature distribution reached under microwave heating which eliminates Boudouard reaction that is the main route for coke deposition.

Unlike Co-Mg incorporated catalysts, a drastic difference was not observed between the hydrogen yields of Ni-Mg incorporated catalysts. Hydrogen yields obtained by Ni-

Mg-MA, Ni-Mg@MA and Ni@Mg-MA catalysts were 4.0, 4.5 and 5.0, respectively. This slight difference was attributed to different Ni particle sizes of materials synthesized by different routes. It is a known fact that large Ni particles show higher catalytic activity in the methanation of CO which result in higher CH<sub>4</sub> selectivity and lower H<sub>2</sub> yield. According to XRD analysis, particle sizes of Ni-Mg-MA and Ni@Mg-MA were 20 nm and 7 nm, respectively. Therefore it is obvious that lower hydrogen yield observed in Ni-Mg-MA catalyst was due to the higher Ni particles present in its structure. The activity tests carried out in focused-microwave reactor system provided more stable product distribution and coke elimination.

**Keywords:** Mesoporous Alumina, Hydrogen Production, Ethanol Steam Reforming, Microwave-Assisted Heterogeneous Reactions





## ÖZ

# MEZOGÖZENEKLİ ALUMİNA BAZLI KATALİZÖRLER İLE ETANOLDEN HİDROJEN ÜRETİMİ VE MİKRODALGA REAKTÖR UYGULAMALARI

Gündüz, Seval  
Yüksek Lisans, Kimya Mühendisliği Bölümü  
Tez Yöneticisi: Prof. Dr. Timur Doğu

Eylül 2014, 155 sayfa

Fosil yakıt rezervlerinin tükenmeye yüz tutması ve CO<sub>2</sub>'in çevreye verdiği zararlar nedeni ile son yıllarda temiz bir enerji taşıyıcısı olarak hidrojene ilgi artmaktadır. Yapısında hali hazırda yüksek miktarda su bulunan biyo-etanolden buharlı reformlama ile hidrojen üretimi, net CO<sub>2</sub> salımını sıfırlaması ve yenilenebilir oluşu ile büyük bir potansiyele sahiptir. Buharlı etanol reformlama prosesi hidrojen verimini azaltan ve proses ekonomisine negatif etkisi olan çok sayıda yan reaksiyon içeren kompleks bir reaksiyon ağına sahiptir. Ayrıca yüksek endotermik doğası nedeniyle prosesin ekonomik fizibilitesi tartışmalı bir konudur.

Bu çalışmamızın ana amaçları; (i) buharlı etanol reformlama reaksiyonuna karşı aktif ve yüksek sıcaklıklarda buharlı ortama dayanıklı yeni mezogözenekli katalizörler dizayn etme ve sentezleme, (ii) klasik ısıtma sisteminden daha verimli bir alternatif ısıtma sistemine sahip reaksiyon sisteminin tasarlanmasıdır.

Çalışmamız kapsamında, Co/Al ve Ni/Al mol oranı 0.10 olan Co-Mg ve Ni-Mg içeren mezogözenekli alumina tipi malzemeler doğrudan sentez ve impregnasyon olmak üzere iki farklı yöntemle sentezlenmiştir. Sentezlenen malzemelerin aktivite testleri laboratuvarımızda bulunan hem klasik ısıtmalı hem de mikrodalga reaktör

sistemlerinde gerçekleştirilmiştir. Daha sonra sentezlenen malzemeler ve reaksiyon sonrası malzemeler karakterize edilerek katalizörlerin performans farklarının sebepleri incelenmiştir.

Doğrudan sentez yöntemi ile hazırlanmış Co-Mg-MA ve Co@Mg-MA katalizörleri ile impregnasyon yöntemi ile hazırlanmış Co-Mg@MA ve Co@MA katalizörleri SRE reaksiyonuna karşı çok farklı aktivite göstermişlerdir. Doğrudan sentez yöntemi ile hazırlanan katalizörler maksimum hidrojen verimi olan 6.0 üzerinden 5.2'lik hidrojen verimi ile çok yüksek aktivite gösterirken, Mg'un impregne edilmesiyle sentezlenen katalizörler hidrojen verimine karşı aktivite göstermemişlerdir. Bu katalizörlerde ana ürün hidrojen yerine etilen olmuştur. Bu da göstermektedir ki etanol dehidrasyon reaksiyonu bu katalizörler üzerinde prosesi domine etmektedir. XRD ve XPS analizlerine göre Mg'un doğrudan eklendiği Co-Mg-MA ve Co@Mg-MA katalizörlerinde SRE reaksiyonunda aktif olan Co<sup>0</sup> ve CoO yapıları görülmüştür. Fakat Co-Mg@MA ve Co@MA katalizörleri büyük çoğunlukla CoAl<sub>2</sub>O<sub>4</sub> fazından oluşmuştur ve aktif Co<sup>0</sup> ve CoO fazlarının oluşmaması bu katalizörlerin SRE reaksiyonuna karşı düşük aktivite göstermesine neden olmuştur. Ek olarak, DRIFT analizleri, impregnasyon yöntemi ile hazırlanan katalizörlerin daha yüksek asiditeye sahip olduğunu göstermiştir. Aktivite açısından en iyi katalizör olan Co@Mg-MA ayrıca odaklı mikrodalga reaktörde denenmiş ve bu sistemde elde edilen hidrojen veriminin biraz daha yüksek ve çok daha kararlı olduğu görülmüştür. Mikrodalga sisteminde elde edilen en şaşırtıcı sonuç ise bu sistemde katalizör üzerindeki karbon birikiminin elimine edilmesidir. Mikrodalga sistemde sıcaklığın düzenli dağılmasından dolayı karbon birikiminin ana sebeplerinden biri olan Boudouard reaksiyonu en aza indirgenmiş ve karbon üretimi minimize edilmiştir.

Co-Mg içeren katalizörlerin aksine Ni-Mg içeren katalizörlerin hidrojen verimlerinde büyük bir fark gözlenmemiştir. Ni-Mg-MA, Ni-Mg@MA ve Ni@Mg-MA katalizörlerinin hidrojen verimleri sırasıyla 4.0, 4.5 ve 5.0'dır. Gözlenen küçük fark, farklı yollarla sentezlenen malzemelerdeki Ni parçacık boyutu farkına bağlanmıştır. Büyük Ni parçacıklarının yüksek CH<sub>4</sub> seçiciliğine ve düşük hidrojen verimine sebep

olan CO metanasyon reaksiyonuna karşı yüksek aktivite gösterdiği bilinen bir gerçektir. XRD analizine göre, Ni-Mg-MA ve Ni@Mg-MA katalizörlerindeki Ni parçacık boyutları sırasıyla 20 nm ve 7 nm'dir. Sonuç olarak Ni-Mg-MA katalizöründe gözlenen görece düşük hidrojen verimi bu katalizörde bulunan büyük Ni parçacıkları yüzündendir. Odaklı mikrodalga sisteminde gerçekleştirilen deneylerde daha kararlı ürün dağılımı ve karbon birikimi eliminasyonu gözlenmiştir.

**Anahtar Kelimeler:** Mezogözenekli Alumina, Hidrojen Üretimi, Buharlı Etanol Reformlama, Mikrodalga Enerjisi altında Heterojen Reaksiyonlar



To My Family



## ACKNOWLEDGEMENTS

I would like to express my deepest gratitude to my supervisor Prof. Dr. Timur Dođu who supported and guided me throughout my MSc and PhD studies. It is very comfortable to know that Professor Dođu is always here, by our side, with his infinite knowledge, endless patience and compassion like a father whenever we need. I cannot thank him enough for his inspiring guidance, encouragement, his kindly attitude in every aspect and for these enlightening six years during which I had the chance to work with him.

I would like to thank Assoc. Prof. Dr. Naime A. Sezgi for her valuable advices, support and encouragement throughout my undergraduate and graduate studies.

I would like to thank Prof. Dr. Sena Yaşyerli for her valuable and constructive comments and positive attitude during thesis supervision meetings.

I would like to offer my sincere thanks to Prof. Dr. Gülşen Dođu and her research group for their positive manner and support throughout my graduate study.

Special thanks are due to Arzu Arslan, Ayşegül Bayat, Burçin İkizer, Birce Pekmezci, Gökhan Çelik and Dr. Canan Şener for their friendship, support and motivation. Without them, this study could not be completed.

Special thanks are due to METU Central Laboratories for characterization analyses.

I would like to thank my friends Özgün Yalçın, Sevler Gökçe Avcıođlu and Cemre Aşar for all their support and friendship.

I would like to thank TUBITAK (Project No: 111M338) for the financial support.

Special thanks to my parents Müyesser Gündüz and Mustafa Gündüz and my brother Semih Gündüz for their endless support and love.



## TABLE OF CONTENTS

ABSTRACT.....	v
ÖZ.....	ix
ACKNOWLEDGEMENTS.....	xiii
TABLE OF CONTENTS.....	xvii
LIST OF FIGURES.....	xx
LIST OF TABLES.....	xxiv
CHAPTERS	
1. INTRODUCTION.....	1
1.1 Setting the Scene.....	1
1.2 Objectives of the Work.....	6
1.3 Thesis Context.....	7
2. DREAM FUEL OF THE FUTURE: HYDROGEN.....	9
2.1 Hydrogen.....	9
2.1.1 Historical Development of Hydrogen.....	9
2.2 Potential of Hydrogen as a Transportation Fuel & Challenges.....	10
2.3 Brief Review of Hydrogen Production Techniques.....	12
2.3.1 Thermochemical Technique for Hydrogen Production.....	13
2.3.2 Electrochemical Technique for Hydrogen Production.....	15
2.3.3 Photobiological Technique for Hydrogen Production.....	15
2.3.4 Photoelectrochemical Technique for Hydrogen Production.....	16
2.3.5 Economic aspects on Hydrogen Production Technology.....	16
3. STEAM REFORMING OF ETHANOL.....	19
3.1 Feedstock Selection in Steam Reforming Process for Hydrogen Production.....	19
3.2 General Aspects of Steam Reforming of Ethanol (SRE) Process.....	22
3.3 Thermodynamics of Steam Reforming of Ethanol Reaction.....	24
3.4 Review of Catalysts Used in Steam Reforming of Ethanol Process.....	27
4. CATALYST DESIGN.....	33

4.1	Properties and Characteristics of a Suitable Catalyst.....	35
4.2	Heterogeneous Catalysis.....	36
4.3	Porous Materials as Catalyst Support.....	36
4.3.1	Ordered Mesoporous Alumina-type Materials as Catalyst Support...37	
4.4	Active Metal Component of the Mesoporous Alumina (MA) Supported Catalysts.....	41
5.	MICROWAVE-ASSISTED STEAM REFORMING OF ETHANOL (SRE).....	45
5.1	History of Microwave.....	45
5.2	Characteristics of Microwave Radiation.....	45
5.3	Microwave Heating.....	47
5.3.1	Microwave Radiation-Material Interaction.....	49
5.3.2	Microwave Heating Mechanism.....	51
5.4	Microwave Applicators.....	52
5.5	Application of Microwave Heating in Heterogeneous Catalyzed Reactions.....	54
5.6	Application of Microwave Heating in Catalytic Hydrogen Production.....	57
6.	EXPERIMENTAL.....	61
6.1	Design and Synthesis of Catalysts.....	61
6.1.1	Mesoporous Alumina (MA) Synthesis.....	61
6.1.2	Mesoporous Alumina (MA) Supported Catalyst Synthesis.....	62
6.2	Characterization of the Catalysts.....	64
6.2.1	X-Ray Diffraction (XRD).....	64
6.2.2	Nitrogen Physisorption.....	64
6.2.3	X-Ray Photoelectron Spectroscopy (XPS).....	64
6.2.4	Diffuse Reflectance Infrared Fourier Transform Spectroscopy (DRIFTS).....	65
6.2.5	Scanning Electron Microscopy (SEM).....	65
6.2.6	Transmission Electron Microscopy (TEM).....	65
6.3	Catalytic Activity Tests in Conventionally Heated Reactor System.....	66
6.4	Installation of Focused-Microwave Reactor System & Activity Tests.....	67

6.5	Characterization of Used Catalysts.....	68
7.	RESULTS AND DISCUSSIONS.....	69
7.1	Results of Co-Mg Incorporated MA Type Catalysts.....	69
7.1.1	Characterization Results of Mesoporous Alumina (MA)-type Support Material.....	70
7.1.2	Characterization Results of Co-Mg Incorporated Catalysts.....	71
7.1.3	Activity Test Results of Co-Mg Incorporated Catalyst in Conventionally Heated reactor System.....	83
7.1.4	Activity Test Results of Co@Mg-MA Catalysts in Focused-Microwave Reactor System.....	90
7.2	Results of Ni-Mg Incorporated MA Type Catalysts.....	95
7.2.1	Characterization Results of Ni-Mg Incorporated Catalysts.....	96
7.2.2	Activity Test Results of Ni-Mg Incorporated Catalysts in Conventionally Heated Reactor System.....	102
7.2.3	Activity Test Results of Ni@Mg-MA Catalyst in Focused-Microwave Reactor System.....	107
7.2.4	Scanning Electron Microscopy (SEM) Analysis of Used Ni@Mg-MA Catalyst in both Conventionally Heated & Focused-Microwave Reactor Systems.....	112
8.	CONCLUSIONS.....	115
	REFERENCES.....	119
	APPENDICES.....	126
	A. Thermodynamic Analysis.....	133
	B. Focused-Microwave Reactor Components.....	137
	C. Sample Particle Size Calculation.....	143
	D. Calibration of Gas Chromatograph.....	145
	E. Sample Calculation for Catalyst Activity Towards SRE.....	147

## LIST OF FIGURES

Figure 1.1. World energy consumption, 1990-2040 (quadrillion Btu).....	2
Figure 1.2. World energy consumption by fuel type.....	2
Figure 1.3. World energy related CO <sub>2</sub> emissions (billion metric tons).....	4
Figure 2.1. Flowsheet of main hydrogen production technologies.....	13
Figure 3.1. Carbon cycle energy diagram for the hydrogen production from biomass derived ethanol.....	20
Figure 3.2. Global ethanol production data by country and year between 2007-2013.....	21
Figure 4.1. Catalytic processes in various sectors.....	33
Figure 4.2. EISA method for ordered mesoporous alumina synthesis.....	39
Figure 4.3. Typical small-angle XRD patterns of mesoporous alumina calcined at different temperatures.....	40
Figure 4.4. Schematic representation of the products obtained by impregnation and direct synthesis methods.....	42
Figure 5.1. The electromagnetic spectrum.....	46
Figure 5.2. Comparison of conventional heating and microwave heating wrt temperature gradients.....	48
Figure 5.3. Interaction of molecules with (A) conductive, (B) insulating, (C) absorbing materials.....	49
Figure 5.4. Types of dielectric polarization under microwave heating.....	51
Figure 5.5. Multimode microwave oven and its working principle.....	53
Figure 5.6. Single-mode microwave applicator and its working principle.....	54
Figure 6.1. Schematic representation of mesoporous alumina (MA) synthesis.....	62
Figure 6.2. Schematic representation of conventionally heated reactor system.....	66
Figure 6.3. Reaction system with focused-microwave.....	67
Figure 7.1. XRD pattern of MA type support material.....	70
Figure 7.2. N <sub>2</sub> physisorption curve of MA type support material.....	71
Figure 7.3. Nitrogen physisorption isotherms of Co-Mg incorporated catalysts.....	73
Figure 7.4. Pore size distribution of Co-Mg incorporated catalysts.....	74

Figure 7.5. XRD patterns of Co-Mg-MA and Co@Mg-MA .....	75
Figure 7.6. XRD patterns of Co-Mg@MA and Co@MA.....	76
Figure 7.7. Color of catalysts (a: Co-Mg-MA, b: Co-Mg@MA, c: Co@MA, d: Co@Mg-MA).....	77
Figure 7.8. X-ray photoelectron spectra of catalysts.....	78
Figure 7.9. DRIFT spectra of Co-Mg incorporated catalysts.....	79
Figure 7.10. TEM image of Co-Mg-MA catalyst.....	80
Figure 7.11. TEM images of Co-Mg@MA catalyst.....	81
Figure 7.12. TEM image of Co@Mg-MA catalyst.....	82
Figure 7.13. Mapping analysis of (a) Co-Mg@MA and (b) Co@Mg-MA.....	83
Figure 7.14. Hydrogen yield with respect to time data of Co-Mg incorporated catalysts.....	84
Figure 7.15. Product distribution of Co@Mg-MA catalyst.....	85
Figure 7.16. Product distribution of Co-Mg-MA catalyst.....	86
Figure 7.17. Product distribution of Co-Mg@MA catalyst.....	87
Figure 7.18. Product distribution of Co@MA catalyst.....	88
Figure 7.19. TGA curves of used Co-Mg incorporated catalysts.....	89
Figure 7.20. Picture of first moment of arc formation within the catalyst bed.....	90
Figure 7.21. Hydrogen yield of Co@Mg-MA in conventionally heated and microwave reactors.....	91
Figure 7.22. TGA curves of used Co@Mg-MA catalyst in conventionally heated and microwave reactors.....	92
Figure 7.23. Product distribution of Co@Mg-MA catalyst in microwave reactor system.....	93
Figure 7.24. Product distribution of Co@Mg-MA catalyst in conventionally heated reactor.....	93
Figure 7.25. Hydrogen yield of Co@Mg-MA in microwave reactor (long-term stability test).....	94
Figure 7.26. Product distribution of Co@Mg-MA in MW reactor (long-term stability test).....	95
Figure 7.27. Nitrogen physisorption isotherms of Ni-Mg incorporated catalysts.....	97

Figure 7.28. Pore size distribution of Ni-Mg incorporated catalyst.....	98
Figure 7.29. XRD patterns of Ni-Mg incorporated catalysts.....	99
Figure 7.30. DRIFT spectra of Ni-Mg incorporated catalyst.....	100
Figure 7.31. SEM images of Ni-Mg-MA catalyst.....	101
Figure 7.32. SEM image of Ni@Mg-MA catalyst.....	102
Figure 7.33. H <sub>2</sub> yield curves of Ni-Mg incorporated catalysts.....	103
Figure 7.34. Product distribution of Ni-Mg-MA.....	104
Figure 7.35. Product distribution of Ni-Mg@MA.....	105
Figure 7.36. Product distribution of Ni@Mg-MA.....	105
Figure 7.37. TGA curves of used Ni-Mg incorporated catalysts.....	106
Figure 7.38. Hydrogen yield of Ni@Mg-MA in both conventionally heated and microwave reactors.....	108
Figure 7.39. TGA curves of Ni@Mg-MA obtained in both conventionally heated and microwave reactors.....	108
Figure 7.40. Product distribution of Ni@Mg-MA obtained in conventionally heated system.....	109
Figure 7.41. Product distribution of Ni@Mg-MA obtained in focused-microwave reactor system.....	110
Figure 7.42. Hydrogen yield of Ni@Mg-MA in microwave reactor (long-term stability test).....	111
Figure 7.43. Product distribution of Ni@Mg-MA in MW reactor (long-term stability test).....	112
Figure 7.44. SEM image of used Ni@Mg-MA catalyst in conventionally heated reactor system.....	113
Figure 7.45. SEM image of used Ni@Mg-MA catalyst in microwave heating reactor system.....	114
Figure A.1. Equilibrium H <sub>2</sub> % in product stream between 400°C and 700°C with steam to ethanol ratio changing between 3 and 20.....	133
Figure A.2. Equilibrium H <sub>2</sub> % in product stream between 400°C and 700°C at pressure changing between 1 atm and 10 atm.....	134

Figure A.3. Equilibrium product distributions between 400°C and 700°C with steam to ethanol ratio of 3.....	134
Figure A.4. Equilibrium product distributions between 400°C and 700°C with steam to ethanol ratio of 3.2.....	135
Figure A.5. Equilibrium product distributions between 400°C and 700°C with steam to ethanol ratio of 5.....	135
Figure A.6. Equilibrium product distributions between 400°C and 700°C with steam to ethanol ratio of 10.....	136
Figure A.7. Equilibrium product distributions between 400°C and 700°C with steam to ethanol ratio of 15.....	136
Figure B.1. Power supply of focused-microwave reactor.....	137
Figure B.2. Front panel of the power supply.....	138
Figure B.3. Compact size-microwave head of focused-microwave reactor.....	138
Figure B.4. Adjustable iris of focused-microwave reactor.....	139
Figure B.5. H-bend waveguide element of microwave reactor.....	140
Figure B.6. Plasma downstream source of microwave reactor.....	141
Figure B.7. Sliding short circuit of microwave reactor.....	141

## LIST OF TABLES

Table 2.1. Properties of hydrogen as a fuel.....	9
Table 2.2. Historical development of hydrogen.....	10
Table 2.3. Comparison of key properties of hydrogen and other common fuels.....	11
Table 2.4. Comparison of reforming technologies.....	14
Table 3.1. Possible reaction pathways of steam reforming of ethanol process.....	23
Table 3.2. Non-noble metal-based catalysts used in SRE process for hydrogen production.....	28
Table 4.1. Some of noticeable properties of homogeneous and heterogeneous catalysts.....	34
Table 5.1. The dielectric constant, loss factor and loss tangent of common materials at room temperature.....	50
Table 7.1. Textural properties of synthesized materials.....	72
Table 7.2. Textural properties of synthesized materials.....	96
Table C.1. Raw XRD data of Co-Mg-MA.....	143
Table D.1. Calibration parameters of reaction gases.....	145
Table E.1. Raw data for 60 <sup>th</sup> minute of activity test of Co-Mg@MA catalyst at 550°C.....	147



## CHAPTER 1

### INTRODUCTION

#### 1.1 Setting the Scene

The most challenging issue of the 21<sup>st</sup> century characterized by growth is to achieve *sustainable development* in all parts of the world [1]. Although sustainable development has different meanings in different sources, in the report “Our Common Future”, it is defined as ‘sustainable development is development that meets the needs of the present without compromising the ability of future generations to meet their own needs’ [2]. Energy plays a vital role in achieving the vision of sustainable development.

According to the EIA (U.S. Energy Information Administration) International Energy Outlook 2013, world energy consumption increases from 524 quadrillion Btu in 2010 to 630 quadrillion Btu in 2020 and 820 quadrillion Btu in 2040 (Fig. 1.1), nearly 56% increase in the next 30 years [3].

At this point, it should be asked that, what are the resources available to meet such an enormous energy need in the next 30 years. According to IEO (International Energy Outlook) 2013 Reference case projection [3] , liquid fuels, natural gas and coal will continue to supply more than 75% of total world energy consumption (Fig. 1.2).

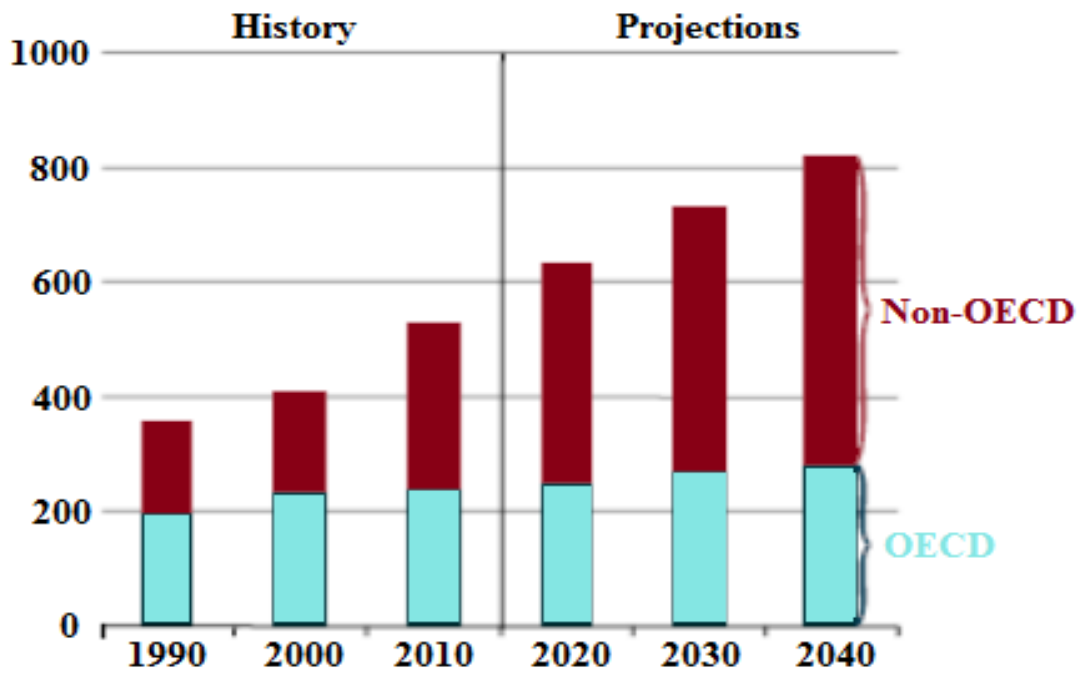


Figure 1.1. World energy consumption, 1990-2040 (quadrillion Btu) [3]

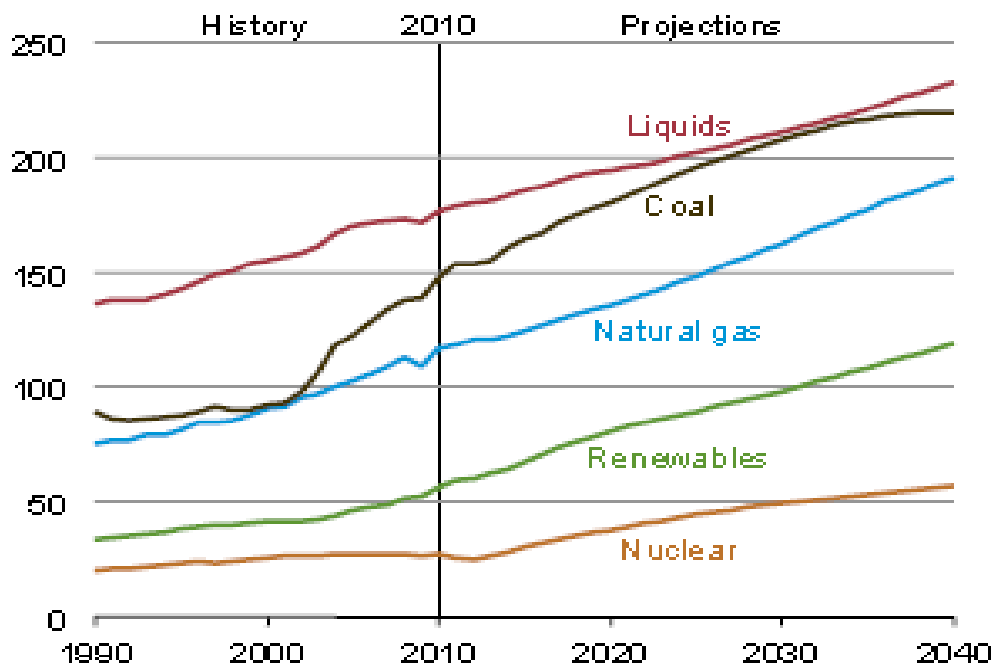
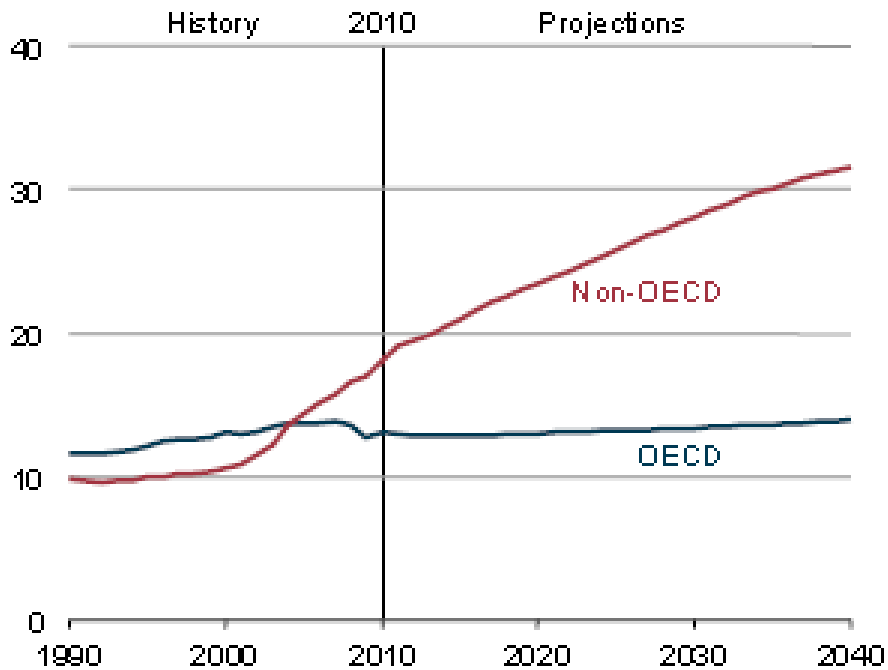


Figure 1.2. World energy consumption by fuel type [3]

A question therefore arises as to how much more fossil energy resources are there. Considering the annual consumption of petroleum which is 26.88 billion barrels in 1998, current worldwide reserves of petroleum (1033.2 billion barrels in 1999) would be consumed in about 40 years [4]. On the same basis, the known natural gas reserves in the world (5141.6 trillion cubic feet in 1999) would last for 63 years at the current annual consumption level of 82.19 trillion cubic feet in 1998 [4]. Although new exploration and production technologies will expand the oil and gas resources, two experts in oil industry, Campbell and Laherrere [5], have indicated that global production of conventional oil will begin to decrease sooner than most people think. Worldwide coal consumption in 1998 was 5013.5 million short tonnes [5]. The known world recoverable coal reserves in 1999 are 1087.19 billion short tonnes [4], which is over 215 times the world consumption level in 1998.

Unfortunately, these fossil-based resources are limited and geographically concentrated in some regions of the world. Additionally, un-controlled use of these fossil fuels to meet our energy demand cause environmental damage by emitting pollutants such as SO<sub>2</sub> and greenhouse gases such as CO<sub>2</sub> to the atmosphere. Researches show that there is a strong correlation between global energy consumption and global CO<sub>2</sub> emissions in developing non-OECD (Organization for Economic Co-operation and Development) nations that continue to rely on fossil fuels to meet their fast growth in energy demand (Fig. 1.3) [3].



**Figure 1.3.** World energy related CO<sub>2</sub> emissions (billion metric tons) [3]

In the IEO 2013 Reference case as shown in Fig. 1.3, which does not assume new policies to limit greenhouse gas emissions, total world energy-related carbon dioxide emissions increase from 31.2 billion metric tons in 2010 to 36.4 billion metric tons in 2020 and 45.5 billion metric tons in 2040 [3].

Therefore, a major change in the energy economy from fossil-based energy carriers to renewable sources, which are un-limited and environmentally friendly, is urgently required. Additionally, new energy conversion devices, instead of existing internal combustion and heat engines, which are not highly efficient are needed to achieve a sustainable energy development. Fuel cells are considered as promising candidates as energy efficient and truly clean conversion devices and it is believed that bio-hydrogen that is predominantly produced from biomass will become a major energy carrier of the future [6].

The potential benefits of using hydrogen as an energy carrier can be summarized as;

- H<sub>2</sub> can be produced from variety of primary resources such as biomass, wind, solar etc. which will reduce consumption of fossil based fuels.
- H<sub>2</sub> possesses the highest energy content per unit of weight (120.7 kJ/g) compared to any of the known fuels [7].
- Since H<sub>2</sub> burns cleanly, its use in internal combustion engines, gas turbines or fuel cells will reduce environmental pollutants such as SO<sub>2</sub> and greenhouse gases (GHGs) such as CO<sub>2</sub>.
- Use of H<sub>2</sub>-based fuel cells for electricity generation near the areas where the electricity is needed would enable distributed power generation.

Although H<sub>2</sub> is abundantly available in the universe, it is always present in bound form. Hydrogen can be produced from variety of feedstocks, such as natural gas, coal, liquified petroleum gas (LPG), jet fuel, biomass-derived liquid fuels (methanol, ethanol, biodiesel) and water. Many H<sub>2</sub> production technologies are known and these technologies can be examined under three main groups; *thermochemical technique*, *electrochemical technique* and *biological techniques*. The nature of feedstock defines the selection of an appropriate technology.

The present study focused on the production of hydrogen through steam reforming process. As discussed earlier, a vast number of feedstocks can be used for hydrogen production through reforming reaction. Among all the alternatives, bio-ethanol seems to be a good hydrogen source, because steam reforming of ethanol reaction allows to achieve closed carbon loop in such a way that CO<sub>2</sub> produced in steam reforming reaction is used in photosynthesis process and ethanol could be easily decomposed into hydrogen rich synthesis gas composed of H<sub>2</sub>, CO, CO<sub>2</sub> and

CH<sub>4</sub> in the presence of steam at a lower temperature than other hydrocarbons, like natural gas.

Unfortunately, due to the reversible nature of steam reforming of ethanol reaction, high amount of coke formation during process and undesired reactions, it is not easy to achieve ethanol steam reforming reaction alone. Catalyst which induces different reaction paths based on its physical and chemical properties plays vital role in ethanol steam reforming reaction.

Due to the highly endothermic nature of steam reforming of ethanol process, an efficient heating technology should be used in order to make the process economically feasible. Additionally, since steam reforming of ethanol process is very sensitive to temperature gradients, heating system should provide uniform temperature distribution within the catalyst bed.

## **1.2 Objectives of the Work**

The main objectives of the work presented in the present study are design and synthesis of highly stable and active catalysts for highly pure hydrogen production and testing the activity of these synthesized materials towards steam reforming of ethanol (SRE) reaction in both conventionally heated and focused-microwave reaction systems. To achieve these objectives, present study covers;

- Synthesis of novel Co-Mg and Ni-Mg incorporated mesoporous alumina (MA) type catalytic materials with very high hydrothermal stability and paramount physical and chemical properties.
- Performing activity tests of synthesized materials in conventionally heated reactor system in order to analyze the behavior of the catalyst under reaction conditions.

- Characterization of synthesized materials and used catalysts in order to explain both the differences in catalytic activities of the materials and the effect of reaction conditions on catalyst structure.
- Performing activity tests of synthesized materials in a focused-microwave reactor system, in order to get information about microwave-assisted heterogeneous reactions and the mechanism of microwave effect.

### **1.3 Thesis Context**

In the present study, Co-Mg and Ni-Mg incorporated novel mesoporous alumina type catalytic materials were synthesized, characterized and catalytic activity tests were performed both in conventionally heated and focused-microwave reactor systems.

In Chapter 2, properties of hydrogen as an energy carrier is researched. In subsections, general properties and historical development of hydrogen is presented and hydrogen product techniques and their economical aspects are discussed.

In Chapter 3, general aspects of steam reforming of ethanol reaction, thermodynamics of SRE process and the catalysts developed for hydrogen production through SRE reaction are given.

In Chapter 4, novel catalyst design and synthesis phenomenon is presented and particularly, mesoporous alumina based materials are discussed.

In Chapter 5, microwave energy application in chemistry field is investigated and microwave effect in microwave-assisted heterogeneous reactions is discussed.

In Chapter 6, experimental studies including catalyst synthesis and characterization and both conventionally heated and focused-microwave reactor systems are described.

In Chapter 7, activity test results obtained in both conventionally heated and focused-microwave reactor systems and characterization results of the synthesized materials are given.

In Chapter 8, conclusions and recommendations based on the results obtained in this study are displayed.



## CHAPTER 2

### DREAM FUEL OF THE FUTURE: HYDROGEN

#### 2.1 Hydrogen

Hydrogen comes from the Greek words ‘hydro’ and ‘genes’ which mean ‘water’ and ‘generator’, respectively [8]. It is the first element in the periodic table, most abundant element in the universe and appears in different forms in humans, animals, plants, fossil fuels and other chemical compounds.

Some properties of hydrogen are given in Table 2.1.

**Table 2.1.** Properties of hydrogen as a fuel [9-12]

Property	Unit	Value
Density	kg/m <sup>3</sup>	0.0838
HHV and LHV	MJ/kg (liquid)	141.9-119.9
HHV and LHV	MJ/m <sup>3</sup> (volumetric)	11.89-10.05
Boiling point	K	20.41
Freezing point	K	13.97
Ignition limits in air	% (volume)	4.75
Ignition temperature	K	585
Flame temperature in air	K	2318
Stoichiometric mixture in air	%	29.53
Stoichiometric air/fuel	kg/kg	34.3/1
Flame velocity	cm/s	2.75

##### 2.1.1 Historical Development of Hydrogen

In 16<sup>th</sup> century, Paracelsus and Van Helmot described hydrogen as a special gas and studied this ‘special gas’ in order to understand its properties including flammability.

In 17<sup>th</sup> century, Robert Boyle produced pure ‘special gas’ during an experiment that he conducted with iron and acids. 18<sup>th</sup> century was a very memorable century for our ‘special gas’; it was first accepted as a distinct element by Henry Cavendish and later it was called as ‘HYDROGEN’ by Lavoisier in this century. In 19<sup>th</sup> century, hydrogen was used in ammonia (key component of the fertilizer production process) production by Carl Bosh. Historical development of hydrogen is summarized in Table 2.2.

**Table 2.2.** Historical development of hydrogen [8]

<b>Time Period</b>	<b>Scientist</b>	<b>Contribution</b>
16 <sup>th</sup> Century	Paracelsus	Understanding of properties of hydrogen, including its flammability
16 <sup>th</sup> Century	Van Helmot	Described hydrogen as a special kind of gas
17 <sup>th</sup> Century	Robert Boyle	Produced hydrogen gas while experimenting with iron and acids
18 <sup>th</sup> Century	Henry Cavendish	First recognized hydrogen as a distinct element
18 <sup>th</sup> Century	Lavoisier	Hydrogen named
19 <sup>th</sup> Century	Anonymous	Development of idea that hydrogen could be an energy carrier that facilitates use of renewable energy sources
19 <sup>th</sup> Century	Carl Bosh	Hydrogen used in production of fertilizer
20 <sup>th</sup> Century	Kordesch	Hydrogen used in vehicles
20 <sup>th</sup> Century	T.N. Veziroğlu	Organization of symposia on hydrogen energy, leading to hydrogen energy study and utilization over the world

In 20<sup>th</sup> century, hydrogen was widely used in the manufacture of ammonia, methanol, gasoline, heating oil, fertilizers, glass, refined metals, pharmaceuticals, cosmetics, lubricants, margarine and rocket fuel. After 1974, many researches were conducted in order to investigate the uses of hydrogen as a transportation fuel [12, 13].

## **2.2 Potential of Hydrogen as a Transportation Fuel and Challenges**

It is projected that hydrogen will become an important actor of the energy supply field in the future. Hydrogen has several aspects as an energy carrier, considering energy demand, production techniques and application fields. Some of the advantages of hydrogen as an energy carrier are that it is clean, not harmful to the environment or life, renewable, broadly utilizable in various applications and

producible by different techniques and from various resources. A comparison of energy per unit mass/velocity and specific carbon emissions of hydrogen with other common fuels is presented in Table 2.3.

**Table 2.3.** Comparison of key properties of hydrogen and other common fuels [9, 11, 12, 14]

<b>Fuel Type</b>	<b>Energy per unit mass (J/kg)</b>	<b>Energy per unit volume (J/m<sup>3</sup>)</b>	<b>Specific carbon emission (kg C/kg fuel)</b>
Liquid H <sub>2</sub>	141.9	10.1	0.0
Gaseous H <sub>2</sub>	141.9	0.01	0.0
Fuel oil	45.5	38.7	0.8
Gasoline	47.4	34.9	0.9
Jet fuel	46.5	35.3	-
LPG	48.8	24.4	-
LNG	50.0	23.0	-
Methanol	22.3	18.1	0.5
Ethanol	29.9	23.6	0.5
Bio diesel	37.0	33.0	0.5
Natural gas	50.0	0.04	0.5
Charcoal	30.0	-	0.5

Several approaches are being proposed in order to extend the role of hydrogen in the near future. One approach is to use hydrogen as a fuel additive for internal combustion engines to improve engine performance and reduce pollution. Another approach involves producing hydrogen at certain locations and distributing it to refueling stations where it will be pumped into vehicles for use in fuel cell and other

power plants. According to Midilli et. al [8], a *hydrogen economy* will likely be introduced over a long time period and involve several phases which are;

- In the near term, hydrogen will be manufactured by steam reforming of hydrocarbons. Since the by-product of steam reforming process is a high purity CO<sub>2</sub> that can be collected and consumed or sequestered in many ways, steam reforming process gives an opportunity to decrease the amount of CO<sub>2</sub> released to the atmosphere [8].
- In the intermediate term, it is foreseen that hydrogen-powered fuel cells will provide on-site generation of electricity. Additionally, these fuel cells will also produce thermal energy for space heating and industrial applications. During this phase, the main hydrogen source will be biomass which resulting in no net CO<sub>2</sub> emissions. An increasing number of hydrogen-fueled-zero-emission vehicles will also be on the road due to the improvements in on-board production of hydrogen inside the vehicle or on-board storage of hydrogen [8].
- In the long term, advanced technologies that produce hydrogen from water and sun light will be emerged and grown [8].

### **2.3 Brief Review of Hydrogen Production Techniques**

Generally, hydrogen production technologies fall into four broad categories which are thermochemical, electrochemical, photobiological and photoelectrochemical.

An overview of the technologies for hydrogen production is illustrated in Figure 2.1. It is clear that all likely production techniques are related to the different resources.

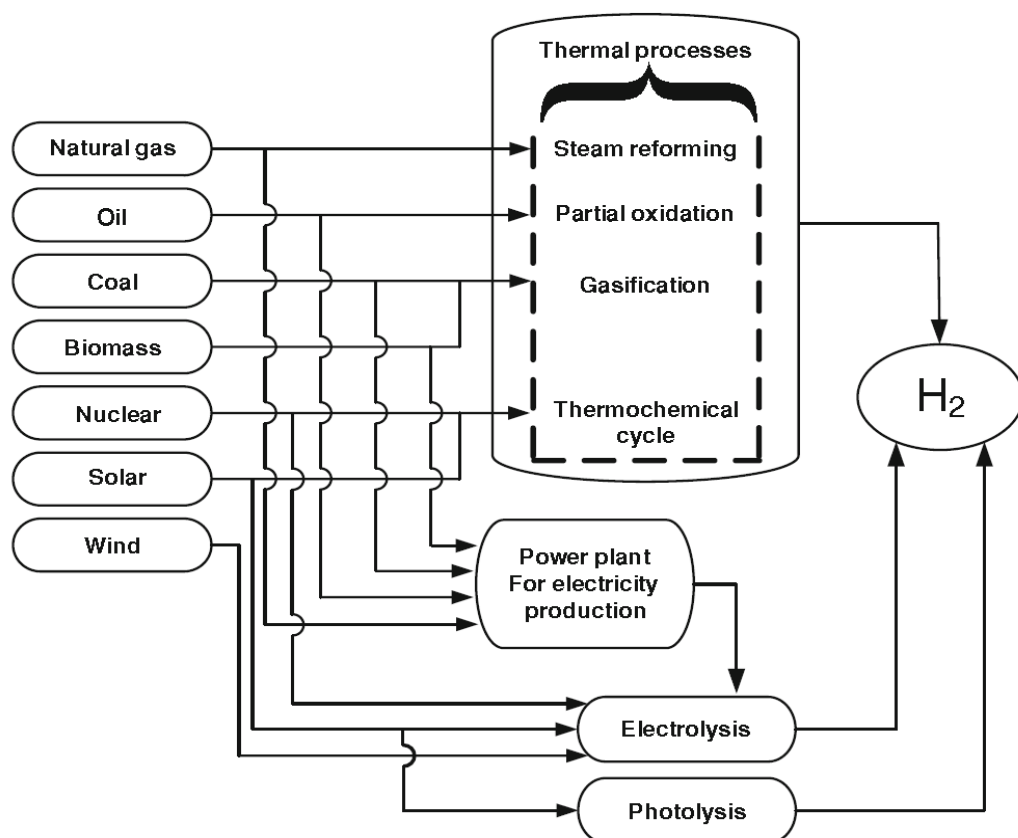


**Figure 2.1.** Flowsheet of main hydrogen production technologies [15]

### 2.3.1 Thermochemical Technology for Hydrogen Production

Thermochemical technology for hydrogen production involves reforming, gasification and pyrolysis processes briefly examined below. In this technology, usually catalysts are used.

#### **Reforming Process:**

Reforming technology has three primary techniques used to manufacture hydrogen from hydrocarbons; (i) steam reforming, (ii) partial oxidation (POX) reforming and (iii) autothermal reforming (ATR). The advantages and disadvantages of these three processes are listed in Table 2.4.

**Table 2.4.** Comparison of reforming technologies [16-18]

<b>Technology</b>	<b>Advantages</b>	<b>Disadvantages</b>
Steam Reforming	Widely used technique in industry O <sub>2</sub> is not needed Lowest reaction temperature High H <sub>2</sub> /CO	Highest air emission
Autothermal Reforming	Lower reaction temperature than POX	Limited commercialization O <sub>2</sub> is needed
Partial Oxidation	Desulfurization is not needed No catalyst required	Low H <sub>2</sub> /CO ratio High reaction temperature

In reforming process, a gas stream mainly composed of hydrogen, carbon monoxide and carbon dioxide is produced. Due to the highly endothermic nature of steam reforming process, an external heat source is needed. The advantages of steam reforming process over POX reforming and ATR are that steam reforming process does not require oxygen, it has a lower operating temperature and produces the reformat with a high H<sub>2</sub>/CO ratio which is beneficial for fuel cell applications [19]. In POX reforming, hydrocarbons are converted to hydrogen by partially oxidizing the hydrocarbon with oxygen. The heat needed for the reaction is provided by the partial combustion of this hydrocarbon. The advantages of POX reforming are that POX reforming process does not require a catalyst for operation, therefore it is the most sulfur tolerant reforming process. Autothermal reforming (ATR) uses the partial oxidation to provide the necessary heat for the reaction and steam reforming the enhance the hydrogen production.

Among the reforming technologies, steam reforming is typically the preferred process for hydrogen production in industry.

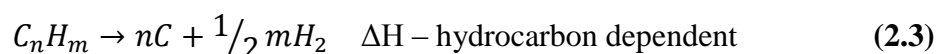
### **Gasification Process:**

Gasification is a very mature technology commonly used with solid biomass or coal. This process is based on the partial oxidation of the materials into a mixture of hydrogen, carbon monoxide, carbon dioxide, methane and nitrogen. Gasification

process suffers from low thermal efficiency due to the vaporization of moisture contained in the biomass. Gasification process can be achieved with or without a catalyst in a fixed bed or fluidized bed reactor.

### **Pyrolysis Process:**

Pyrolysis is a hydrogen production process where the hydrocarbon is decomposed into hydrogen and carbon without steam or oxygen present. Since no water or air is present in pyrolysis, no carbon oxides (CO and CO<sub>2</sub>) are formed. Advantages of this process are fuel flexibility, simplicity and reduction CO<sub>2</sub> and CO emissions. Pyrolysis reactions (Eqn 2.3) can be written as;



The major drawback of this process is the high possibility of fouling due to the carbon formation.

### **2.3.2. Electrochemical Technology for Hydrogen Production**

Electrolysis of water to produce hydrogen can be studied under electrochemical technology. Water splitting in its simplest form uses an electrical current passing through two electrodes to break water into hydrogen and oxygen [19]. The overall efficiency of the water electrolysis is significantly low, it is in the range of ~25% [20]. This technology will be competitive only if electricity costs are lower.

### **2.3.3. Photobiological Technology for Hydrogen Production**

In photobiological technology, hydrogen is produced by the natural photosynthetic activity of bacteria and green algae. The major disadvantage of this technology is that production rates in photobiological process is relatively slow [21]. Due to the lower mass transfer and slower kinetics, photobiological technology is not yet considered to be economical and it is still immature.

#### **2.3.4. Photoelectrochemical Technology for Hydrogen Production**

In photoelectrochemical technology, water splitting in the presence of a semiconductor, such as titania with sunlight is used for hydrogen production [22]. This technology is also still immature and can not be considered as economical.

#### **2.3.5. Economic Aspects on Hydrogen Production Technologies**

Presently, most of the hydrogen produced all over the world is by the process of steam reforming of methane. This method meets about half of the world hydrogen production, with a price about 7 USD/GJ [23]. Partial oxidation of hydrocarbons provide a comparable price for hydrogen production. However additional price of storage and capture of greenhouse gases generated during the thermochemical processes should be kept in mind [24].

Gasification and pyrolysis of biomass are also members of thermochemical process. The price of hydrogen obtained by these two methods is about three times greater than the price of hydrogen obtained by the steam reforming process. Therefore, these processes are generally not considered as economically feasible processes [23].

Electrolysis of water is a very simple hydrogen production technology without byproducts. Although this process is the cleanest hydrogen production technology, the input electricity cost is very high and plays a key role in the price of hydrogen produced.

The forecasts show that by the year 2030, the dominant hydrogen production method will be steam reforming of natural gas and catalyzed biomass gasification [25]. It is a small probability that both coal gasification and electrolysis will also be used. The use of solar energy in a given context is questionable but also possible. Probably, the role of solar energy will increase by 2050 [25].



There is now growing interest towards the development of H<sub>2</sub> production techniques. Currently, the most developed and used technology is the reforming of fossil-based resources. In order to decrease the dependence on fossil fuels, significant developments in other H<sub>2</sub> generation technologies from renewable resources such as biomass and water are considered. The advantages of these technologies are;

- H<sub>2</sub> production from renewable sources with minimal environmental impact may decrease the world's dependence on fuels that come primarily from unstable regions.
- The “in-house” H<sub>2</sub> production may increase both national energy and economic security.
- The ability of H<sub>2</sub> to be produced from a wide variety of feedstock and using a wide variety of processes may make every region of the world able to produce much of its own energy.



## CHAPTER 3

### STEAM REFORMING OF ETHANOL

As discussed in the previous chapter, among the alternatives, steam reforming is the most widely used and energy-efficient technology available. Although thermodynamic limitations limit the production of hydrogen through steam reforming process, the reaction is sufficiently fast. In addition, steam reforming process is a highly cost effective technology for hydrogen production.

#### **3.1. Feedstock Selection in Steam Reforming Process for Hydrogen Production**

Hydrogen can be produced from variety of feedstocks such as natural gas (methane), several hydrocarbons, liquid and dry biomass and biomass-derived liquids such as methanol, ethanol and biodiesel by steam reforming process. At present, the most widely used feedstock in steam reforming technology is methane. Although methane steam reforming is the most widely used and cheapest hydrogen production method available at the present time, it is not an environmentally friendly process due to the fossil-based nature of methane and high amount of CO<sub>2</sub> released during the process. Therefore, a source of hydrogen other than methane should be chosen in order to make the process environmentally friendly.

Among all the alternatives, bio-ethanol seems to be a good candidate for hydrogen production by steam reforming process, since;

- The use of hydrogen produced by reforming of bio-ethanol through fuel cells suggests that the overall process completes the carbon cycle adding little or no

net carbon to the atmosphere [26]. Carbon cycle energy diagram for the hydrogen production from biomass derived ethanol is illustrated in Figure 3.1.

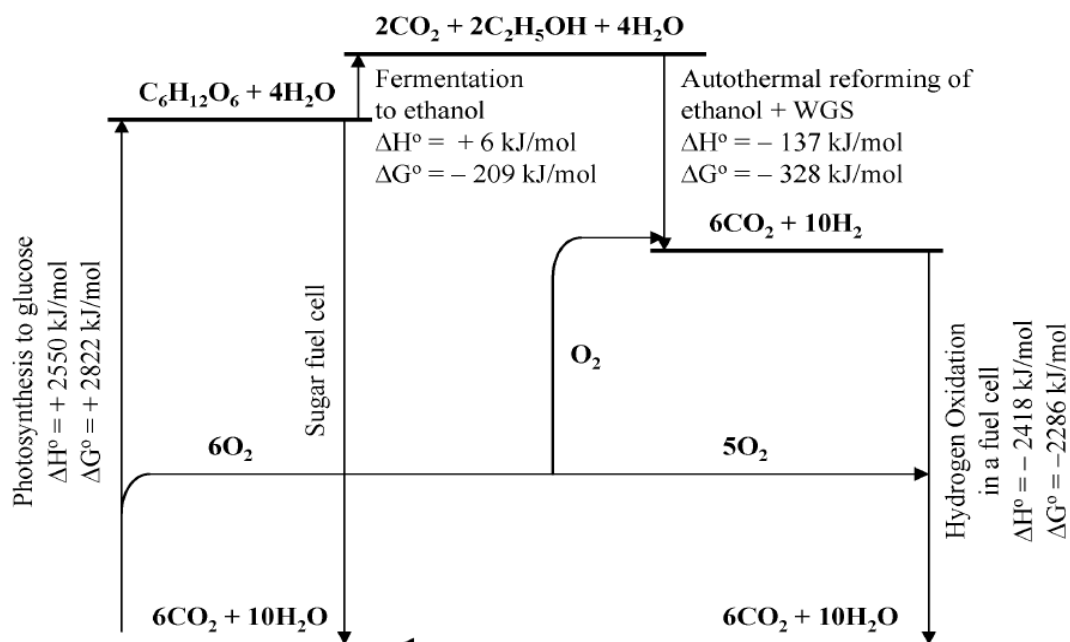


**Figure 3.1.** Carbon cycle energy diagram for the hydrogen production from biomass derived ethanol [26]

During photosynthesis,  $\text{CO}_2$  and  $\text{H}_2\text{O}$  are converted into sugars such as glucose ( $\text{C}_6\text{H}_{12}\text{O}_6$ ). Four moles of  $\text{H}_2\text{O}$  and six moles of  $\text{O}_2$  are also formed as byproducts during the photosynthesis. Glucose is converted into two moles of ethanol ( $\text{C}_2\text{H}_5\text{OH}$ ) and  $\text{CO}_2$  in fermentation process using a small amount of energy (approximately 6 kJ/mol of glucose converted) [1, 26]. Reforming of these two moles of ethanol with four moles of  $\text{H}_2\text{O}$  and one mole of  $\text{O}_2$  produced during photosynthesis followed by water-gas shift (WGS) reaction produces ten moles of  $\text{H}_2$  and four additional moles of  $\text{CO}_2$ . The  $\text{H}_2$  molecules produced in reforming process could be oxidized in a PEM fuel cell using the remaining 5 moles of  $\text{O}_2$  liberated in the photosynthesis process to generate electricity, while the byproduct  $\text{CO}_2$  will be used for the photosynthesis in the subsequent cycle to achieve closed carbon loop.

- Bio-ethanol is renewable and increasingly available. The worldwide ethanol production in 2013 reached to 25 billion gallons with USA being the largest producer in the world (Fig. 3.2).

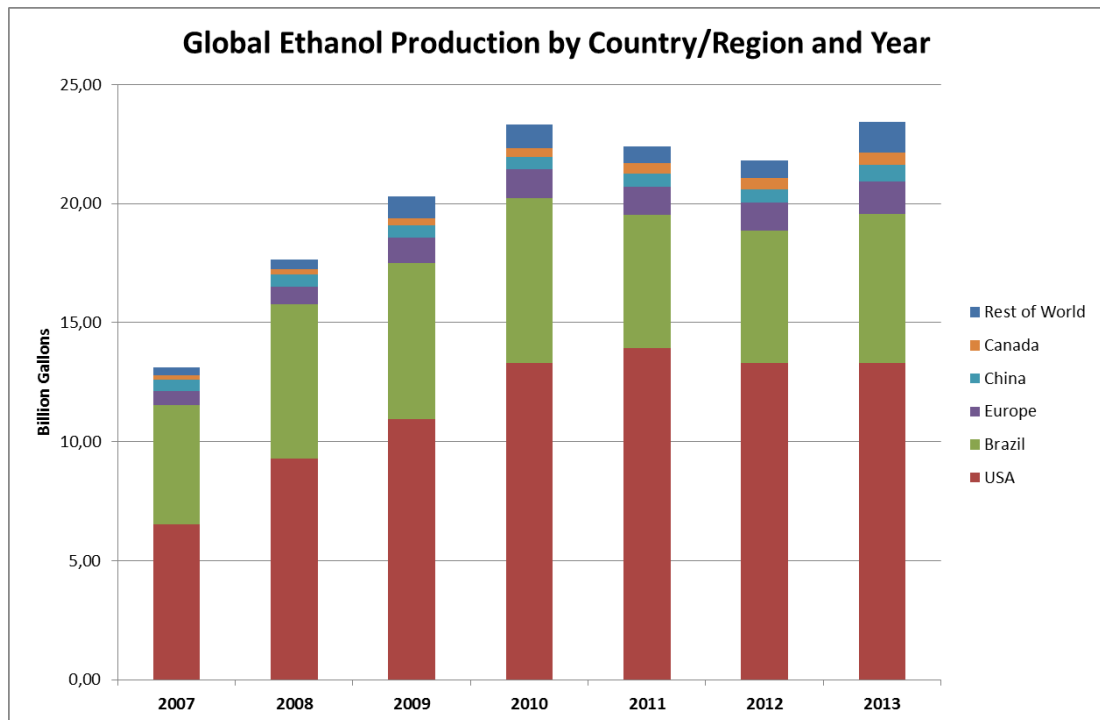
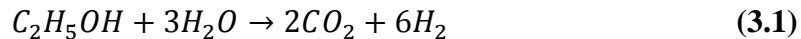


**Figure 3.2.** Global ethanol production data by country and year between 2007-2013 [27].

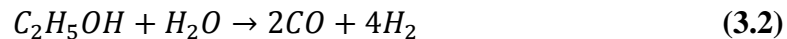
- Ease of transport, storage and distribution is another advantage of using bio-ethanol in steam reforming process for hydrogen production.
- Ethanol is not toxic for humans and nature and it is biodegradable.
- Ethanol could be easily broken down to a hydrogen rich mixture called syngas in the presence of steam.

### 3.2. General Aspects of Steam Reforming of Ethanol (SRE) Process

Steam reforming of ethanol (SRE) process involves reaction between ethanol and steam over a solid catalyst that has a capability of breaking the C-C bonds of ethanol in order to produce a mixture of H<sub>2</sub> and CO<sub>2</sub>. The overall steam reforming of ethanol reaction is represented as;



The overall SRE is a highly endothermic reaction with a standard enthalpy,  $\Delta H^{\circ}_{298} = +173.3$  kJ/mol of ethanol and occurs at relatively high temperatures between 400 and 800°C [1]. Overall SRE reaction is considered as a combination of steam reforming of ethanol and water-gas shift reaction (WGSR) illustrated in Eqn. 3.2 and Eqn. 3.3, respectively.



According to overall steam reforming of ethanol reaction (Eqn. 3.1), steam-to-ethanol molar ratio of 3.0 is stoichiometrically required. However, molar ratios, even up to 20 have been used, since bio-ethanol contains 12 vol% ethanol and 86 vol% water (corresponding steam-to-ethanol molar ratio is about 18). Excess water enhances WGSR (Eqn. 3.3) by increasing H<sub>2</sub> yield. Although high steam-to-ethanol molar ratios are preferable, considering hydrogen yield, the optimum H<sub>2</sub>O/EtOH molar ratio in the SRE reaction will be limited by the energy cost of the system. A higher steam-to-ethanol molar ratio represents a higher energy cost because of the extra steam to be generated.

Maximum hydrogen yield that can be achieved in overall steam reforming of ethanol reaction (Eqn. 3.1) is fixed by 6 moles of H<sub>2</sub> per mole of ethanol. However this

maximum hydrogen yield can not be achieved due to the complex nature of SRE process. Possible reactions that may occur during steam reforming of ethanol process have been studied in the literature [28, 29] and the major reactions are listed in Table 3.1.

**Table 3.1.** Possible reaction pathways of steam reforming of ethanol process [29]

Reaction	Equation	Remarks
Sufficient Steam Supply	$C_2H_5OH+3H_2O\rightarrow 2CO_2+6H_2$	Ideal pathway Highest H <sub>2</sub> yield
Insufficient Steam Supply	$C_2H_5OH+H_2O\rightarrow 2CO+4H_2$ $C_2H_5OH+2H_2\rightarrow 2CH_4+H_2O$	Undesired products Lower H <sub>2</sub> yield
Dehydrogenation Acetaldehyde decomposition Acetaldehyde steam reforming	$C_2H_5OH\rightarrow C_2H_4O+H_2$ $C_2H_4O\rightarrow CH_4+CO$ $C_2H_4O+H_2O\rightarrow 3H_2+2CO$	H <sub>2</sub> production paths in practice
Dehydration Coke formation	$C_2H_5OH\rightarrow C_2H_4+H_2O$ $C_2H_4\rightarrow$ polymeric deposits (coke)	Undesired pathway Acidic catalysts Main source of coke formation
Decomposition	$C_2H_5OH\rightarrow CO+CH_4+H_2$ $2C_2H_5OH\rightarrow C_3H_6O+CO+3H_2$ $C_2H_5OH\rightarrow 0.5CO_2+1.5CH_4$	Coke formation Low H <sub>2</sub> yield
Methanation Methane decomposition Boudouard reaction	$CO+3H_2\rightarrow CH_4+H_2O$ $CO_2+4H_2\rightarrow CH_4+2H_2O$ $CH_4\rightarrow 2H_2+C$ $2CO\rightarrow CO_2+C$	Possible reactions of decomposition products
Water gas shift reaction (WGSR)	$CO+H_2O\rightarrow CO_2+H_2$	Minimize coke Enhance H <sub>2</sub> yield

As illustrated in Table 3.1, hydrogen rich gaseous mixture may be obtained through different reaction pathways. The key points in enhancing hydrogen yield are supply

of sufficient steam to the system and designing a catalyst that minimize ethanol dehydration, decomposition and dehydrogenation reactions.

### **3.3. Thermodynamics of Steam Reforming of Ethanol Reaction**

The thermodynamic studies of steam reforming of ethanol process have received great attention [28, 30-38].

Steam reforming of ethanol (SRE) has a complex reaction network composed of numerous desired and undesired reactions. The selectivity of these desired and undesired reactions strongly depends on the reaction parameters and the physical and chemical properties of the catalyst used. In order to understand how the reaction parameters affect product distribution, a detailed thermodynamic analysis should be performed. There are many studies in literature which focus on the thermodynamic analysis of the steam reforming of ethanol process and some of them are listed and summarized in this part of the present study.

In the study conducted by Garcia et. al. [34], thermodynamic equilibrium of steam reforming of ethanol process has been studied over a temperature range of 400-800°C, pressure range of 1-9 atm and water to ethanol feed ratio range of 0:1-10:1. In this study, non-stoichiometric formulation has been used to investigate the effect of reaction parameters on the product distribution and the best conditions for achieving maximum hydrogen yield. They concluded that the best conditions for maximum H<sub>2</sub> production occurs at temperatures higher than 650 K, in the presence of excess water in the feed and at atmospheric pressure.

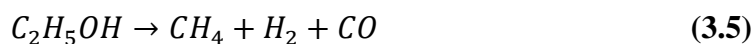
The study conducted by Vasudeva et. al. [35] showed that the selectivity of steam reforming of CH<sub>4</sub> which is one of the most important reactions for relatively high H<sub>2</sub> production would increase at higher water to ethanol ratios and at higher temperatures.



According to the study conducted by Fishtik et. al [36], due to the instability of the product gaseous mixture composed of H<sub>2</sub>, CO, CO<sub>2</sub>, CH<sub>4</sub> and H<sub>2</sub>O, product composition can not be calculated from chemical thermodynamics but rather from kinetics. In that case, their suggestion was to use the experimental data to analyze product composition and to interpret the product composition in terms of the major reactions called response reactions. At the end of this study performed using Response Reactions (RERs) approach, it was concluded that at low steam to ethanol ratios and at lower temperatures, ethanol decomposes according to the reaction (Eqn. 3.4);



In the case of low steam to ethanol ratios and higher temperatures, the reaction given below is dominant.



Therefore, in order to maximize hydrogen production, relatively high temperatures (700-800 K and above), low pressure and high steam to ethanol ratio in the feed are needed.

In addition to the effect of pressure, steam to ethanol ratio and temperature, Wang et. al. [37] studied the effect of addition of an inert gas such as argon (Ar) to the reaction system. They concluded that changing argon to ethanol ratio in the feed from 0 to 100 affect H<sub>2</sub> yield at a given temperature and steam to ethanol ratio. Higher Ar to ethanol ratio enhances hydrogen production.

Different from the previous studies, Ionnides [38] suggested that steam to ethanol ratio in the feed should not be much higher than stoichiometric value which is 3.0 in

order to make the process economically feasible since high amounts of water in feed stream needs high energy to be evaporated.

As a summary, thermodynamic studies of steam reforming of ethanol process conducted up to now suggested that; high temperature above 600°C, high steam-to-ethanol ratio (in the range of 4-10) and low pressure (atmospheric pressure) enhance ethanol conversion and hydrogen yield and reduce the by-product concentration [39-41].

In order to investigate the effects of reaction parameters on the hydrogen yield and product distribution, a detailed thermodynamic analysis of steam reforming of ethanol process was performed by using GASEQ chemical equilibrium program and the results are illustrated in Appendix A. GASEQ chemical equilibrium program was developed by Chris Morley and distributed free of charge. GASEQ program is based on the minimization of gibbs free energy method. This program can be used to calculate chemical equilibrium for the following cases;

- Equilibrium at given temperature and pressure,
- Adiabatic composition and temperature at a given pressure,
- Equilibrium at a given temperature and at constant volume,
- Adiabatic composition and temperature at a given constant volume,
- Adiabatic compression/expansion.

In the present study, “*equilibrium at given temperature and pressure*” case of the GASEQ program was used. Calculations were made assuming that product stream contains H<sub>2</sub>, CO, CO<sub>2</sub>, CH<sub>4</sub>, C<sub>2</sub>H<sub>4</sub> and CH<sub>2</sub>O. Obtained results were in good agreement with the literature, such that increasing temperature and steam to ethanol ratio enhance hydrogen yield and pressure increase has a negative effect on hydrogen production.

### **3.4. Review of Catalysts Used in Steam Reforming of Ethanol Process**

Steam reforming of ethanol is a very complex process, due to the presence of numerous side reactions that negatively affect both ethanol conversion and hydrogen yield. Therefore, catalyst selection plays a critical role in this process due to the fact that each catalyst induces different reaction paths.

A wide variety of catalysts containing noble metals such as Pt, Pd, Ru and Rh or non-noble metals such as Co, Ni and Cu have been investigated in the steam reforming of ethanol process [1]. Although noble metals show good performance towards SRE reaction, due to the higher cost of them, it is not economically feasible to use these noble metals as catalyst. In Table 3.2, the type of catalysts containing non-noble metals used in SRE process, reaction operating conditions and paramount results achieved in literature are summarized.

With the discovery of novel mesoporous materials, metal incorporated novel mesoporous materials have gained great attention. Detailed literature survey of novel mesoporous materials and catalyst design is given in Chapter 4.

**Table 3.2.** Non-noble metal-based catalysts used in SRE process for hydrogen production (adapted from (Subramani and Song)) [1]

<b>Catalyst</b>	<b>Reaction Conditions</b>	<b>Paramount Results</b>	<b>Reference No:</b>
35 wt% Ni/Al <sub>2</sub> O <sub>3</sub> derived from layered double hydroxide precursors	500°C, 0.84 g catalyst, H <sub>2</sub> O/EtOH=1-6	Ethanol and methane steam reforming reactions were studied. The competition for the same active site for ethanol and methane reforming maximizes the H <sub>2</sub> and CO <sub>2</sub> production and minimizes the CO formation	42
10–20 wt% Ni on ZnO, La <sub>2</sub> O <sub>3</sub> , MgO and Al <sub>2</sub> O <sub>3</sub>	300–650°C, 3 ml catalyst, H <sub>2</sub> O/EtOH=3-12	Catalysts were prepared by incipient wet impregnation. 20 wt% Ni supported on ZnO exhibited better performance compared to others.	43
1–25 wt% Ni on ZnO–Al <sub>2</sub> O <sub>3</sub>	500–600°C, 300 mg catalyst, H <sub>2</sub> O/EtOH = 3.6–3.8	Catalysts containing 1–25 wt% Ni were synthesized by citrate sol gel method. Catalyst with Ni loading between 18–25% exhibited better performance.	44

10–25 wt% Ni on Al <sub>2</sub> O <sub>3</sub>	320–520°C, 1 g catalyst, H <sub>2</sub> O/EtOH=2-18	Catalysts prepared by precipitation, co-precipitation and impregnation methods were compared. Catalyst containing 15 wt% Ni synthesized by precipitation method produced smaller Ni crystallite sizes and better reducibility and hence a better catalytic performance.	45
Ni/Y <sub>2</sub> O <sub>3</sub>	250–350°C, 4 g catalyst, H <sub>2</sub> O/EtOH=3	Catalysts were prepared in three different methods, impregnation, impregnation followed by treatment with NaBH <sub>4</sub> . A high ethanol conversion of about 98% and H <sub>2</sub> selectivity of 55% were obtained at 380°C. H <sub>2</sub> selectivity did not increase above 500° C.	46
35 wt% Ni on Al <sub>2</sub> O <sub>3</sub>	300–500°C, 0.1–0.9 g catalyst, H <sub>2</sub> O/EtOH=1–6	High activity and H <sub>2</sub> yield are obtained at higher temperatures, above 500°C, but at this temperature large amount of CO also produced.	47

17 wt% Ni on La <sub>2</sub> O <sub>3</sub> , Al <sub>2</sub> O <sub>3</sub> , YSZ and MgO	550–850° C, 0.1 g catalyst, H <sub>2</sub> O/EtOH = 2–3	Among the catalysts, Ni/La <sub>2</sub> O <sub>3</sub> exhibited high activity and selectivity for H <sub>2</sub> production in the SRE reaction. The enhanced activity has been attributed to cleaning of coke deposited on the Ni surface by lanthanum oxycarbonate species.	48
8–18 wt% Co on Al <sub>2</sub> O <sub>3</sub> 8–18 wt% Co on SiO <sub>2</sub>	400°C, 0.15 g catalyst, H <sub>2</sub> O/EtOH = 3	Catalysts were prepared by incipient wetness impregnation of commercial Al <sub>2</sub> O <sub>3</sub> and SiO <sub>2</sub> . Catalytic activity increased with increasing Co content.	49
8.6% Co on Al <sub>2</sub> O <sub>3</sub> 7.8% Co on SiO <sub>2</sub> 18% Co on MgO	400°C, 0.15 g catalyst, H <sub>2</sub> O/EtOH = 3	Catalysts were prepared by incipient wetness impregnation of commercial supports using cobalt nitrate as a precursor. Ethylene, methane and CO are formed over Co supported on Al <sub>2</sub> O <sub>3</sub> , SiO <sub>2</sub> and MgO, respectively.	50

10 wt% Co on ZnO	300–400°C, 0.1 g catalyst, H <sub>2</sub> O/EtOH = 13	Nitrate and carbonyl precursors of Co were used for the impregnation of ZnO support. Catalyst synthesized using carbonyl precursor was stable and selective for the production of CO-free H <sub>2</sub> .	51
1 wt% Co on MgO, Al <sub>2</sub> O <sub>3</sub> , SiO <sub>2</sub> TiO <sub>2</sub> , ZnO, La <sub>2</sub> O <sub>3</sub> , CeO <sub>2</sub>	300–450°C H <sub>2</sub> O/EtOH = 13	Catalysts were prepared by impregnation of supports using Co <sub>2</sub> (CO) <sub>8</sub> as a Co precursor. In situ magnetic characterization indicated that a mixed Co <sup>0</sup> and Co <sup>2+</sup> contributes to catalytic activity in the SRE reaction.	52
7.4% Co on Al <sub>2</sub> O <sub>3</sub> , SiO <sub>2</sub> , MgO, ZrO <sub>2</sub> and carbon	400°, 0.3 g catalyst	Catalysts were prepared by impregnation using cobalt (II) nitrate. Co/Al <sub>2</sub> O <sub>3</sub> was the most active and selective catalyst by suppressing the ethanol decomposition and CO methanation reactions.	53





## CHAPTER 4

### CATALYST DESIGN

The universal definition of '*catalyst*' is given as 'a substance that increases the rate of approach to equilibrium of a chemical reaction without itself being substantially consumed in the reaction process' [54].

Catalysis has played a crucial role in modern society. Catalysts improve quality of life by contributing in environmentally benign processes for the production of various valuable chemical products. Over 85% of industrial processes are based on catalysis [54]. Sectors that involve catalytic processes are illustrated in Figure 4.1.

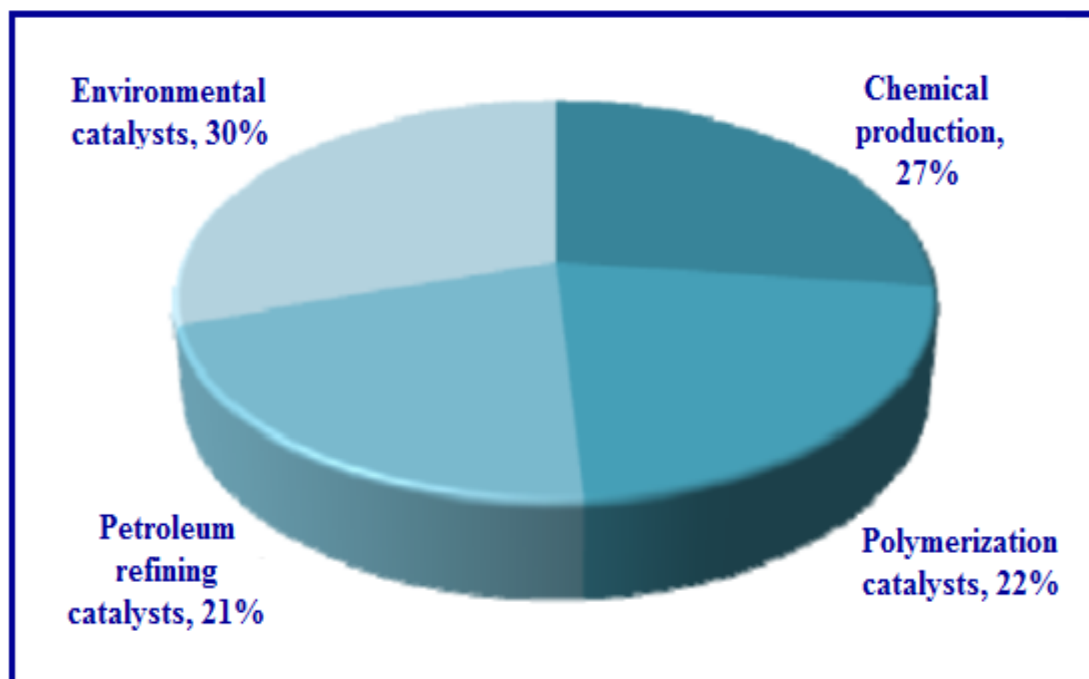


**Figure 4.1.** Catalytic processes in various sectors [54]

Catalysts can be divided into two groups depending upon the phase of the catalytic material;

- *Homogeneous catalyst*; in which catalyst, reactants and products are in the same phase.
- *Heterogeneous catalyst*; in which catalyst is in different phase than reactants and products.

Some of noticeable properties of homogeneous and heterogeneous catalysts are summarized in Table 4.1.

**Table 4.1.** Some of noticeable properties of homogeneous and heterogeneous catalysts [54]

	Advantages	Disadvantages
Homogeneous Catalyst	<ul style="list-style-type: none"> <li>• Mild reaction conditions</li> <li>• High activity &amp; selectivity</li> <li>• Efficient heat transfer</li> <li>• No mass transfer limitation</li> </ul>	<ul style="list-style-type: none"> <li>• Toxic waste water after catalyst recycling</li> <li>• Contamination of product with catalyst</li> <li>• High cost due to catalyst lost</li> <li>• Difficulties in separation &amp; recycling</li> <li>• Corrosion problems</li> </ul>
Heterogeneous Catalyst	<ul style="list-style-type: none"> <li>• Facile separation of catalyst</li> <li>• Continuous processing</li> <li>• Elimination of corrosion</li> </ul>	<ul style="list-style-type: none"> <li>• Heat transfer problems</li> <li>• Lower selectivity</li> <li>• Mass transfer limitation</li> </ul>

Heterogeneous catalysts have distinct advantages over homogeneous catalysts, such as easy recovery and recycle. Accordingly, the present study deals with the heterogeneous catalyst design for steam reforming of ethanol reaction.

#### **4.1. Properties and Characteristics of a Suitable Catalyst**

A suitable catalyst for a given process should have fundamental properties that come from the definition of the catalyst which are activity, selectivity and stability. Additionally, it is required that a catalyst be regenerable, reproducible, mechanically and thermally stable and economical.

##### ***Activity of a Catalyst***

High activity of a catalyst will be reflected either in high productivity from relatively small reactors and catalyst volumes or in mild operating conditions that enhance selectivity and stability if the thermodynamics is more favorable.

##### ***Selectivity of a Catalyst***

High selectivity enhances yield of a desired product while suppressing undesired reactions. The textural properties of a catalyst such as pore volume and pore distribution should be improved to reduce limitations by internal diffusion, which in the case undesired reaction reduce selectivity.

##### ***Stability of a Catalyst***

A catalyst with good stability shows small changes under reaction conditions and during regeneration. Some factors that cause activity or selectivity loss are;

- Coke formation during reaction,
- Poisoning of active sites of the catalyst by the reactants or products during reaction,
- Loss of volatile agents of the catalyst during reaction,
- Change in the crystalline structure of the catalyst (loss of mechanical strength)
- Progressive adsorption of trace poisons in the feed or products.

##### ***Regenerability of a Catalyst***

All catalysts age in time and they should be regenerated through a process that will return part or all of their catalytic properties when their activities or selectivities have been partly or totally lost. The most common regeneration treatments are burning off

carbon that accumulates during the reaction and scrubbing of used catalyst with certain gases to desorb poisons.

## **4.2. Heterogeneous Catalysis**

Heterogeneous catalysts can be examined roughly under two groups which are *unsupported* and *supported* heterogeneous catalysts [55]. Due to the difficulty in preparation and estimation of active metal component, characterization problems and possibility of sintering, homogeneous catalysts are generally not preferred.

Supported catalysts mainly composed of a support material (discussed in Section 4.3) that provide better dispersion of active metal for efficient use of catalyst and an active metal component (discussed in Section 4.4). Support materials are generally porous materials having relatively high surface area.

## **4.3. Porous Materials as Catalyst Support**

Porous materials can be classified into three groups according to IUPAC definition which are microporous materials, mesoporous materials and macroporous materials [56]. Pore diameters of microporous materials, mesoporous materials and macroporous materials are less than 2 nm, between 2 nm and 50 nm and larger than 50 nm, respectively.

Microporous materials such as zeolites has gained great attention within industrial areas like oil refining, petrochemistry and chemical synthesis and they are also very important as adsorbents. Their success in catalytic applications is based on [57]:

- High surface area
- High adsorption capacity and controlled adsorption properties (vary from hydrophobic to hydrophilic type materials)
- Active sites in the materials' framework,

- Their channel structure, which allows zeolites to present different types of shape selectivity such as product, reactant and transition state, which can be used to direct a given catalytic reaction towards the desired product, avoiding the side reactions.

“Despite the advantages listed above, zeolites have a vital limitation that they are not able to process molecules that are larger than their pore diameters (1-1.2 nm). Because of that, attention of researchers is focused on increasing the pore diameter to bring them into mesoporous region without damaging the porous structure of the material. Besides the transport (diffusion) limitations, microporous materials were reported to be more susceptible to catalyst deactivation due to coke formation, than the mesoporous catalytic materials. Researchers at Union Carbide discovered  $\text{AlPO}_4$  structures having a pore size range of 1.3-1.5 nm. Soon after, related materials such as SAPO’s (silicoaluminophosphates) and MeAPOs (metal aluminophosphates) were synthesized” [56]. The common problems of these materials are their lack of thermal and hydrothermal stability.

In 1992, Mobil scientists discovered a new family of nanostructured porous materials, named as M41S family [58]. This discovery was the solution of zeolite pore diameter limitation and opened a new avenue in the porous material research and catalysis.

Although the textural properties of members of M41S family (MCM-41, MCM-48 and MCM-50) are very promising due to their weakness in hydrothermal stability, researchers’ attention has switched to novel more stable metal oxide materials having mesoporous structure.

#### **4.3.1. Ordered Mesoporous Alumina-type Materials as Catalyst Support**

Compared to silica-based M41S family materials, mesoporous alumina (MA) is more popular in catalysis area for its broad applications as catalyst support in petroleum refinement, automobile emission control and others [59]. Due to its highly uniform

channels, large surface area, narrow pore size distribution, tunable pore sizes and most importantly its relatively high hydrothermal stability, mesoporous alumina possesses much more excellent properties.

#### **4.3.1.1. Synthesis of Mesoporous Alumina-type Materials (MA)**

Aluminum oxides with porous structure have been synthesized by several methods such as;

- High-temperature dehydration of bulk powders [60]
- Aerosol generation of particles with use of block copolymers [61]
- Modified sol-gel method in the presence of organic structural agents [62, 63], cationic and anionic surfactants [64], block copolymers [65-67], using ordered mesoporous carbon templates [68].
- Evaporation-induced self-assembly (EISA) method with block copolymers [69, 70]

Among various synthesis routes, those employing poly(ethylene oxide)-poly(propylene oxide)-poly(ethylene oxide) block copolymers [(EO)<sub>x</sub>(PO)<sub>y</sub>(EO)<sub>x</sub>] as soft templates attracted a lot of attention, because they are inexpensive, commercially available, biodegradable, and afford materials. The first successful synthesis of ordered mesoporous alumina (MA) in the presence of block copolymers was reported by Niesz et al. [66]. However, this procedure required a strict control of experimental conditions.

In 2008, Yuan *et al.* were among the first to present a facile synthesis procedure for the preparation of nanostructured mesoporous Al<sub>2</sub>O<sub>3</sub> powders [69]. By employing amphiphilic block copolymers such as Pluronic® P123 and P127, which are composed of ethylene oxide (EO) and propyleneoxide (PO) groups (EO<sub>20</sub>PO<sub>70</sub>EO<sub>20</sub>) and EO<sub>100</sub>PO<sub>65</sub>EO<sub>100</sub>, respectively), in an evaporation-induced self-assembly process (EISA). Highly ordered mesoporous organic-inorganic nanocomposites were obtained under controlled evaporation at 60 °C.

Several groups have tried to use P123 as structuring agent for the nanostructuring of alumina. However without the use of EISA process no ordered alumina phases have been obtained. [72]. Among the different proposed EISA processes, the one proposed by Yuan et al. [69] seems to be the simplest and the fastest to get mesoporous alumina powder. Schematic representation of mesoporous alumina synthesis procedure proposed by Yuan et al. (EISA method) is illustrated in Figure 4.2. “In this acidic EISA process, it is assumed that the multivalent hydrolysed and partly condensed Al (Aluminum) species are preferentially assembled in the ethylene oxide blocks of the structure-directing co-polymer via weak coordination bonds. As concentrated acids are employed as catalysts, this association is even enhanced by hydrogen bonding, allowing a systematic growth of the Al oligomers in the hydrophilic domains, which finally results in the formation of a mesoscopically ordered inorganic organic nanocomposite” [69].

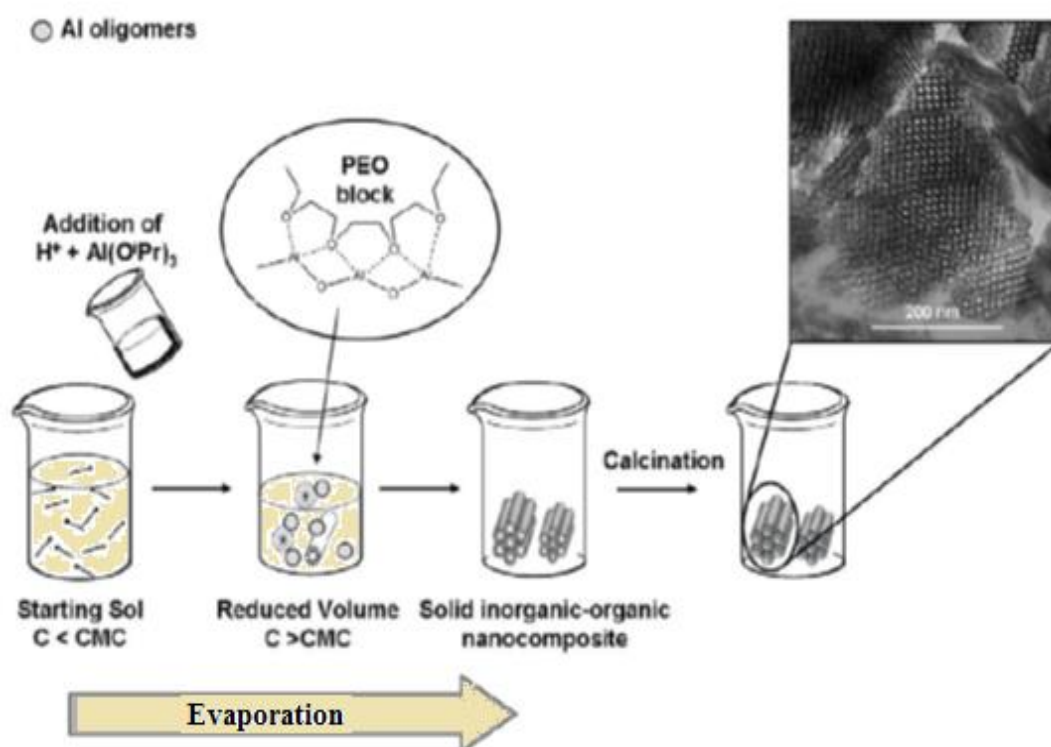


**Figure 4.2.** EISA method for ordered mesoporous alumina synthesis [72]

In the original publication of Yuan et al. [69], the recipe for the synthesis of nanostructured alumina is not clearly formulated, as a wide range of concentrations for each reactant and of acids is given. It is important to avoid washing or liquid extraction before drying is completed, as the organic template prevents the mesoporous structure to collapse during the drying step. Only after a substantial drying at 60°C leading to the solidification of the amorphous alumina phase, the calcination can be proceed and a free accessible 2D-hexagonally arranged mesopore system is achieved [72].

#### 4.3.1.2. Characterization of Mesoporous Alumina-type Materials (MA)

Mesostructure formation in the mesoporous alumina framework can be proved by low-angle X-ray diffraction (XRD) analysis. Mesoporous materials exhibit a very strong diffraction peak at a 2theta range of 0° and 5° and smaller reflection peaks at higher 2theta values. A typical small-angle XRD pattern obtained by Yuan et al. is illustrated in Figure 4.3.

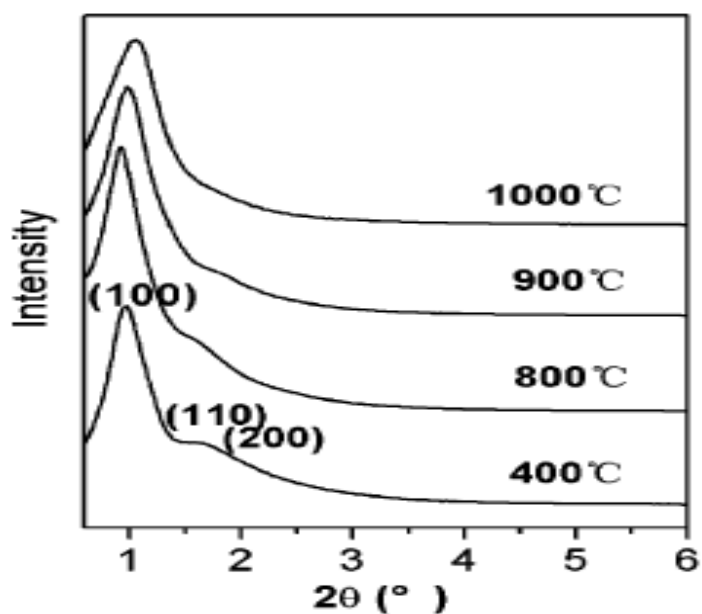


**Figure 4.3.** Typical small-angle XRD patterns of mesoporous alumina calcined at different temperatures [69]



As shown in Figure 4.3, mesoporous alumina shows a very strong diffraction peak around  $1.0^\circ$  and relatively weak reflection peak around  $1.7^\circ$ . Additionally, it is obvious that ordered mesostructure of mesoporous alumina is conserved even at elevated temperatures indicating a high thermal stability of the material.

Mesostructure formation can also be proved by transmission electron microscopy (TEM) technique. Highly ordered hexagonal arrangement of pores along [001] direction and the alignment of cylindrical pores along [110] direction can be observed in TEM images of mesoporous alumina.

$N_2$  physisorption technique can also be applied in order to analyze the porosity characteristic of the material. According to the study conducted by Yuan et al. [69], mesoporous alumina type materials treated at different temperatures all yield type IV curves with H1-shaped hysteresis loops indicating their uniform mesoporous cylindrical pores. Synthesized material calcined at  $400^\circ\text{C}$  has quite a large BET surface area of around  $400\text{ m}^2/\text{g}$ . It was concluded that the large surface areas and narrow pore-size distributions combined with excellent thermal stability can be achieved and these properties of mesoporous alumina are expected to enhance the potential applications of these ordered mesoporous aluminas as catalysts.

#### **4.4. Active Metal Component of the Mesoporous Alumina (MA) Supported Catalyst**

Mesoporous alumina (MA) type materials have taken great attention due to their unique physical properties, such as relatively high surface area, large pore diameter, high pore volume, narrow pore size distribution and very high thermal and hydrothermal stability up to  $1000^\circ\text{C}$ , which are the important characteristics of a good catalyst support material. However, in terms of catalytic activity, MA itself is not considered as an active catalyst. Catalytic functions can be introduced to MA framework by incorporation of active sites. Mesoporous structures are good supports for acids, bases, metals or metal oxides. Incorporation can be achieved by several methods; common ones are impregnation and direct synthesis methods. Schematic

representation of the products obtained following impregnation and direct synthesis methods is given in Figure 4.4.

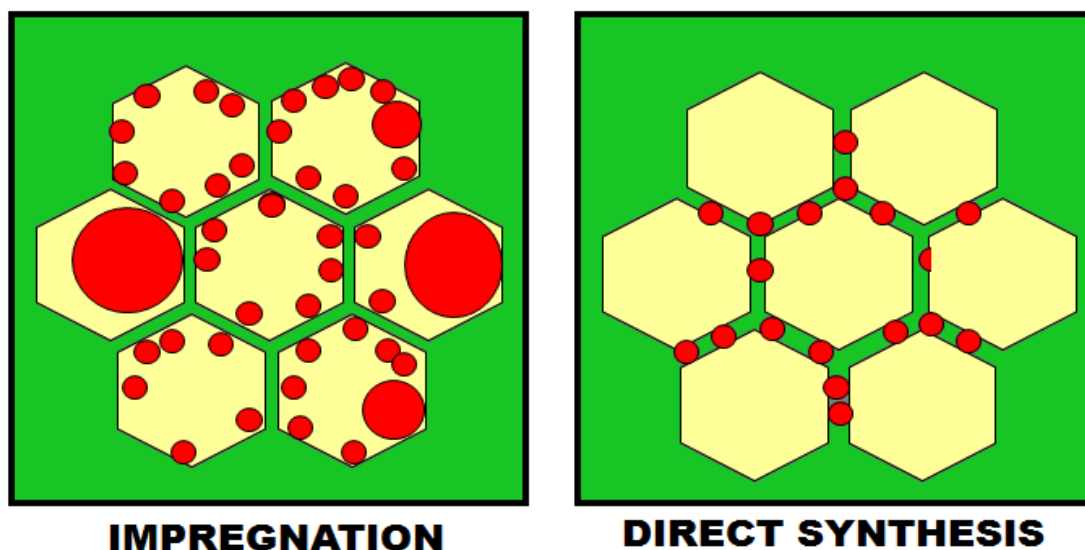


**Figure 4.4.** Schematic representation of the products obtained by impregnation and direct synthesis methods [13]

In the extent of the present study, cobalt and nickel incorporated mesoporous alumina (MA) type catalysts synthesized by both direct synthesis and impregnation methods were investigated.

Cobalt-based catalysts have been widely applied for hydrogenation reactions and reforming reactions [73]. To obtain a high metal dispersion, Co is generally incorporated into a high surface area support. Various supports have been used for Co incorporation, such as MgO [74, 75], ZrO<sub>2</sub> [74, 76], Al<sub>2</sub>O<sub>3</sub> [74, 75, 77], CeO<sub>2</sub> [75, 76, 78], TiO<sub>2</sub> [75] and SiO<sub>2</sub> [74, 75]. Although recent researches have focused on Co incorporated novel mesoporous materials, in order to achieve high surface area and superior dispersion of Co metal, synthesis and application of Co incorporated mesoporous alumina type catalysts attracted the attention of researcher in recent years.. There are few applications of Co incorporated mesoporous alumina type materials such as catalytic oxidation and acetaldehyde adsorption reported in literature [79, 80]. To the best of our knowledge, there is no study focused on steam

reforming of ethanol over Co incorporated mesoporous alumina type catalysts, in the literature. From this perspective, our study can be accepted as a pioneer for hydrogen production by steam reforming of ethanol process over Co incorporated mesoporous alumina type catalysts.

Supported Ni catalysts have been widely studied due to their high activity towards hydrogenation, hydrotreating and steam-reforming reactions [81]. Ni-Mg incorporated mesoporous alumina type catalysts synthesized by Shen and co-workers showed very high catalytic activity towards steam reforming of methane reaction. In literature, there is no study about the application of Ni incorporated mesoporous alumina type materials in steam reforming of ethanol process. However results obtained in the study conducted by Shen et al. towards steam reforming of methane reaction, which is very similar with SRE reaction, are highly encouraging.



## CHAPTER 5

### MICROWAVE ASSISTED STEAM REFORMING OF ETHANOL

Steam reforming of ethanol (SRE) reaction is a highly endothermic process. In order to make this process economically feasible, high temperatures should be achieved with low energy input. In recent years, the application of microwave energy has been intensively investigated as a potential way to enhance chemical reactions.

In this part of the report, general information about microwave energy and microwave-assisted processes are given and potential of microwave-assisted SRE reaction to produce hydrogen with lower energy input is analyzed in detail.

#### 5.1 History of Microwave

The development of microwave finds its origin in the research of radio waves. In 19<sup>th</sup> century, Heinrich Hertz discovered that radio waves are reflected off metals but transmitted through other materials [82]. With this discovery, radio wave technology developed rapidly during World War II. During a RADAR (Radio Detection and Ranging) related research project, it was accidentally discovered by Dr. Percy LeBaron Spencer that microwaves can cook food. The first commercial microwave oven was developed in 1952 by the Raytheon Company [83]. In 20<sup>th</sup> century, investigation of microwave energy for industrial application started and still today many new applications are discovered.

#### 5.2 Characteristics of Microwave Radiation

Microwaves are a form of electromagnetic waves which are located between radio waves and infrared radiation (Figure 5.1).

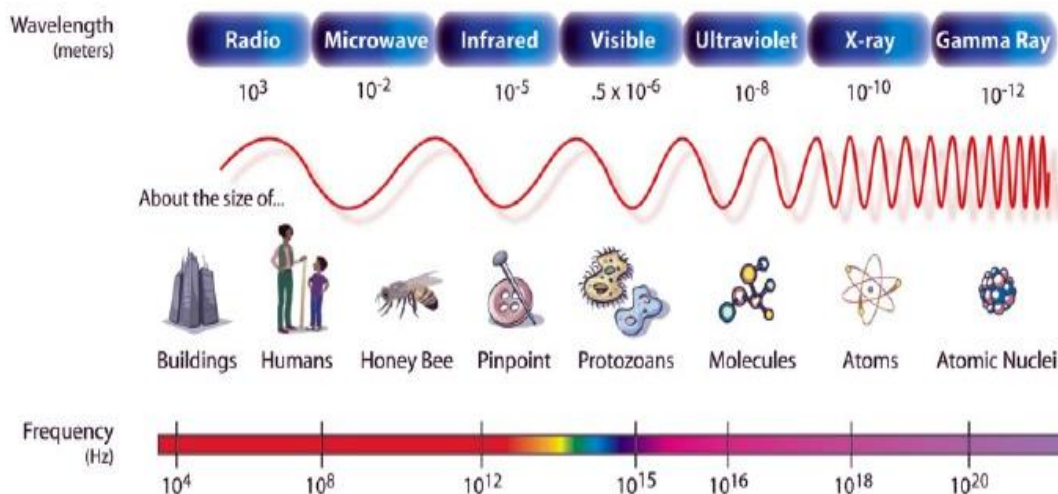


**Figure 5.1.** The electromagnetic spectrum [84]

Microwaves wavelengths range from 1 mm to 1 m with corresponding frequencies in the range from 300 to 300,000 megahertz [85]. Microwaves, similar to visible light, propagate the speed of light and carry energy as well as light does.

Applications of microwave radiation can be classified into communication and chemical field. When microwaves are used for communication purposes, they typically use an adjusted wave in terms of frequency, phase and amplitude in order to carry information [86]. Application of microwaves in the chemical field are now rather common in such areas as organic chemistry, analytical chemistry, biochemistry, polymer chemistry, catalysis, photochemistry and the inorganic chemistry of materials [87]. In order to avoid interference with civilian telecommunication, military and naval equipment, a precisely defined set of frequencies (ISM-frequencies), were specified for use by industrial, research and medical equipment. The most predominantly used frequencies are 915 MHz (33.3 cm) in the industrial sector and 2.45 GHz (12.2 cm) in household microwave ovens and laboratory research purposes [88].

The role of microwave radiation and its beneficial effects in chemical field can be investigated under four sub-groups which are;

- **Operating:** In microwave heating, a substance is heated directly by the microwaves so that the chemical synthesis can be coupled to some automated robot technology [89].
- **Green Chemistry:** The use of microwaves is a beneficial technique in green chemistry since it shortens the reaction times even in synthesis involving no solvent and no catalyst [89].
- **Chemical Reactions:** Microwave heating enhances many chemical reactions due to both thermal and non-thermal effects [86, 89].
- **Specific Heating**

### 5.3 Microwave Heating

Generally, in chemical processes, energy needed for the reaction is supplied by conventional heating. Major drawbacks of this type of heating can be listed as;

- Heat conductivity of the vessel (reactor) material should be high since heating ability of conventional heating strongly depends on the heat conductivity of the vessel material.
- Response time of a conductively heated system is very slow which causes difficulty in thermal control of the reaction system.
- Temperature gradients are unavoidable in conventionally heated systems. Higher temperature is observed near the heat source and depending on the size of the system to be heated and heat conductivity of the vessel material, it can take a long time before a homogeneous temperature is achieved [90]. Additionally, temperature gradients cause differences in reaction rates at different locations on the catalyst due to the Arrhenius like behaviour (Eqn. 5.1) of reaction rates.

$$k = A \times \exp(E_a/RT) \quad (5.1)$$

Microwave heating eliminates most of the drawbacks of conventional heating mentioned above. Advantages of microwave heating can be summarized as;

- Microwave heating is a very fast process due to the direct interaction of microwaves with molecules.
- Temperature gradients are eliminated or reduced in microwave heating since all the molecules of the same specie are samely affected by the microwave radiation. Figure 5.2 shows the temperature gradient difference between the conventional heating and microwave heating.

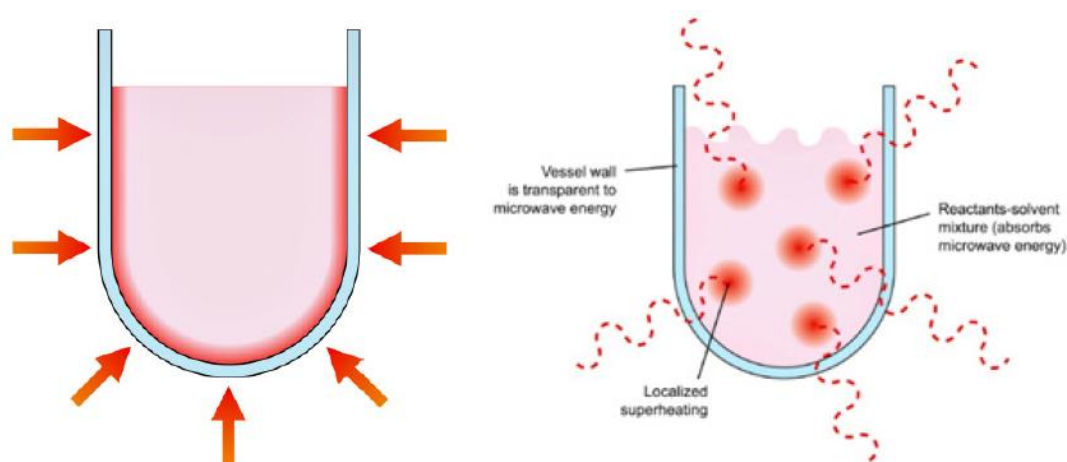


**Figure 5.2.** Comparison of conventional heating and microwave heating wrt temperature gradients [90]

- Localized superheating occurs due to the rapid heating of certain types of molecules [91].
- Microwave heating is an instant-on/instant-off application which means that when microwave power is reduced/switched off, only latent heat remains. This behaviour of microwave heating enhances the thermal control of the process.



### 5.3.1. Microwave Radiation-Material Interaction

All of the materials present in the universe are not samely affected by the microwave radiation. Materials can be studied under three groups according to their behaviour under microwave radiation as illustrated in Figure 5.3.

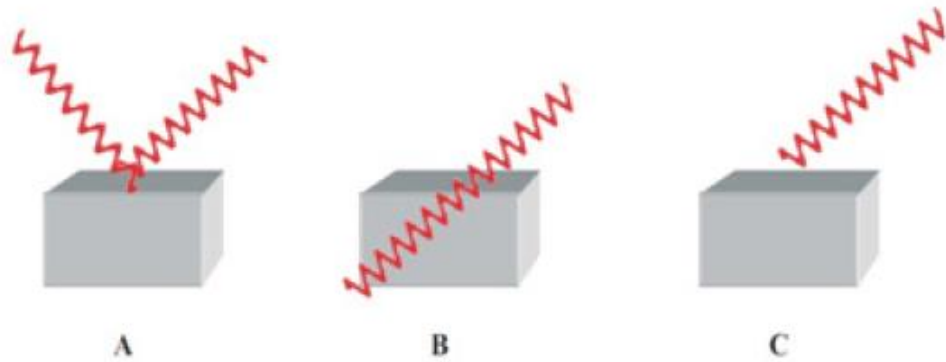


**Figure 5.3.** Interaction of molecules with (A) conductive, (B) insulating, (C) absorbing materials [90]

Conductive materials (conductors) reflect microwaves from their surface therefore they are not heated under microwave radiation. Insulating materials (insulators) are transparent to microwave radiation. On the other hand, absorbing materials (absorbers or dielectrics) can interact with microwave radiation and produce heat.

Complex permittivity  $\varepsilon^*$  [-] (Eqn. 5.2) and complex permeability  $\mu^*$  [-] (Eqn 5.3) both of which are described by a real part and an imaginary part are the two parameters which describes the microwave propagation and ability of materials to absorb microwave radiation [84, 85, 90].

$$\varepsilon^* = \varepsilon' - i\varepsilon'' \quad (5.2)$$

$$\mu^* = \mu' - i\mu'' \quad (5.3)$$

The real part ( $\epsilon'[-]$ ) of the complex permittivity (i.e., dielectric constant) shows the ability to propagate microwaves into the material and the imaginary part ( $\epsilon''[-]$ ) is named as loss factor and represents the ability of material to dissipate the energy in the form of heat [84, 85]. The real part of the complex permeability ( $\mu'[-]$ ) reflects the amount of magnetic energy stored in the material and the imaginary part ( $\mu''[-]$ ) shows the amount of magnetic energy that can be converted into thermal energy. Since most of the materials used for catalytic purposes are non-magnetic, magnetic losses can be neglected [85]. Although real and imaginary parts of the complex permittivity can give information about the ability of material to dissipate the energy under microwave radiation, for more convenient characterization of materials, another term has been introduced; loss tangent ( $\tan\delta$ ) which is the ratio of loss factor ( $\epsilon''[-]$ ) and dielectric constant ( $\epsilon'[-]$ ) as shown in Eqn 5.4.

$$\tan\delta = \frac{\epsilon''}{\epsilon'} \quad (5.4)$$

The dielectric constant, loss factor and loss tangent of common materials at room temperature are listed in Table 5.1.

**Table 5.1.** The dielectric constant, loss factor and loss tangent of common materials at room temperature [85]

<b>Material</b>	<b>Dielectric constant (<math>\epsilon'</math>)</b>	<b>Dielectric loss (<math>\epsilon''</math>)</b>	<b>Loss tangent (<math>\tan \delta</math>)</b>
Vacuum	1.00	0	0
Air	1.0006	0	0
Water	80.4	9.89	0.123
Methanol	32.6	21.48	0.659
Ethanol	24.3	22.86	0.941
Glass (Pyrex)	4.82	0.026	0.0054
Magnesium Oxide	9	0.0045	0.0005
Aluminum Oxide	9	0.0063	0.0007

Table 5.1 clearly shows that both water and ethanol (reactants of SRE reaction) are good microwave absorbers with high dielectric loss and loss tangent values. On the contrary, glass especially quartz, and polymeric species have very low loss tangent and dielectric constants which indicates that when these materials are used as constructive material for a reactor, only very little microwave power will be lost through the reactor wall.

### 5.3.2. Microwave Heating Mechanism

Microwave heating (dielectric heating) is a type of heating caused by high frequency electromagnetic radiation. The interaction of charged particles in microwave absorbing materials with the electric field component of electromagnetic radiation causes these materials to heat up [92, 93]. The heat produced by the interaction of material and electromagnetic radiation is mainly due to two different effects which are *Dipolar Polarization* and *Maxwell-Wagner Effect (Space Charge Polarization)*. Schematic representation of these two principal dielectric polarizations resulted in heating of the materials under microwave radiation is illustrated in Figure 5.4.

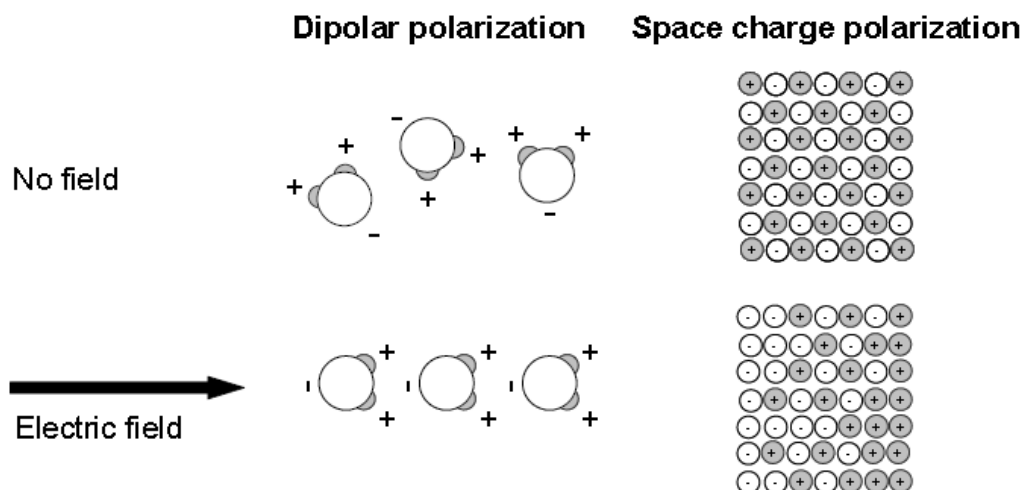


**Figure 5.4.** Types of dielectric polarization under microwave heating [90]

Dipolar Polarization: Dipolar polarization is observed in the case of polar molecules which have induced or permanent dipoles. The electric field component of the microwaves causes these dipoles to rotate as they try to align themselves with the alternating field (2450 million times per second). This molecular rotation movement cause friction among the molecules which releases energy in the form of heat [92].

Maxwell-Wagner Polarization: Maxwell-Wagner polarization, in other words space charge polarization, is observed in dielectric solid materials. In the case of these dielectric solid materials with charged particles in their structure which are free to move in a delimited region of the material, a current travelling with the electromagnetic current is induced. Since the electrons can not couple to the changes of phase of the electric field, energy is dissipated in the form of heat due to the Maxwell-Wagner effect [94].

#### **5.4 Microwave Applicators**

Currently, two types of microwave ovens are available for the application of microwave radiation in chemistry field which are multimode microwave and single mode microwave. Schematic representation of multimode microwave oven and its working principle is illustrated in Figure 5.5.

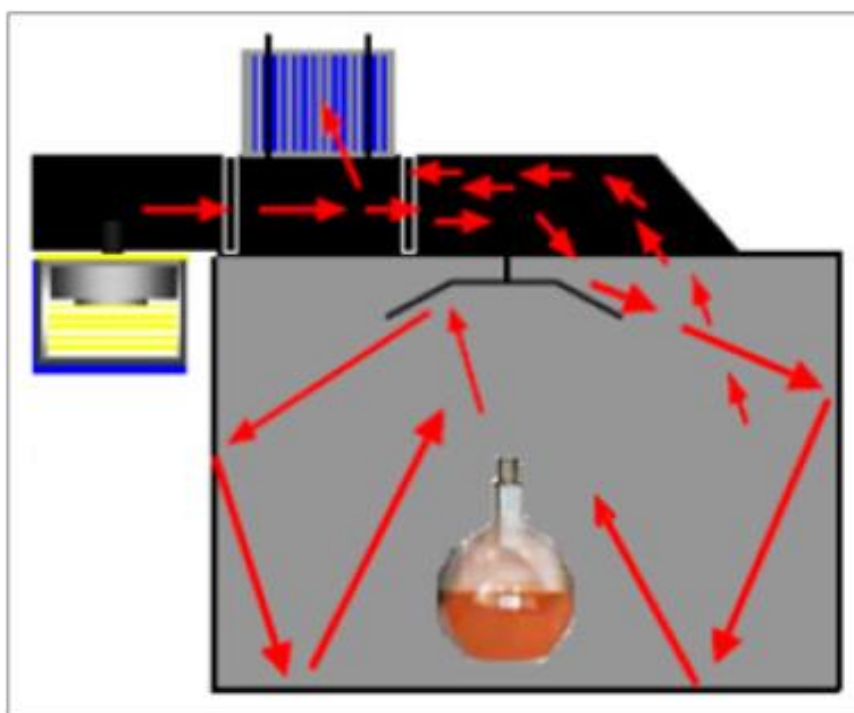


**Figure 5.5.** Multimode microwave oven and its working principle [91]

Multimode microwave applicators are mostly used in domestic microwave ovens due to their large capacity which is necessary for the heating of meals. Although they are not designed for laboratory applications, multimode microwave applicators were the first to be used in laboratories. However it was realized that due to the multiple modes which interact with each other inside the microwave cavity, hot and cold spots occurred resulting in non-homogeneous heating. This non-homogeneous heating observed in multimode microwave applicators cause non-reproducible results in laboratory experiments.

In order to improve the energy distribution in the microwave cavity and facilitating the reproducibility of the experiments, single-mode (monomode) microwave applicators were developed. Schematic representation and working principle of single-mode microwave applicator is shown in Figure 5.6.

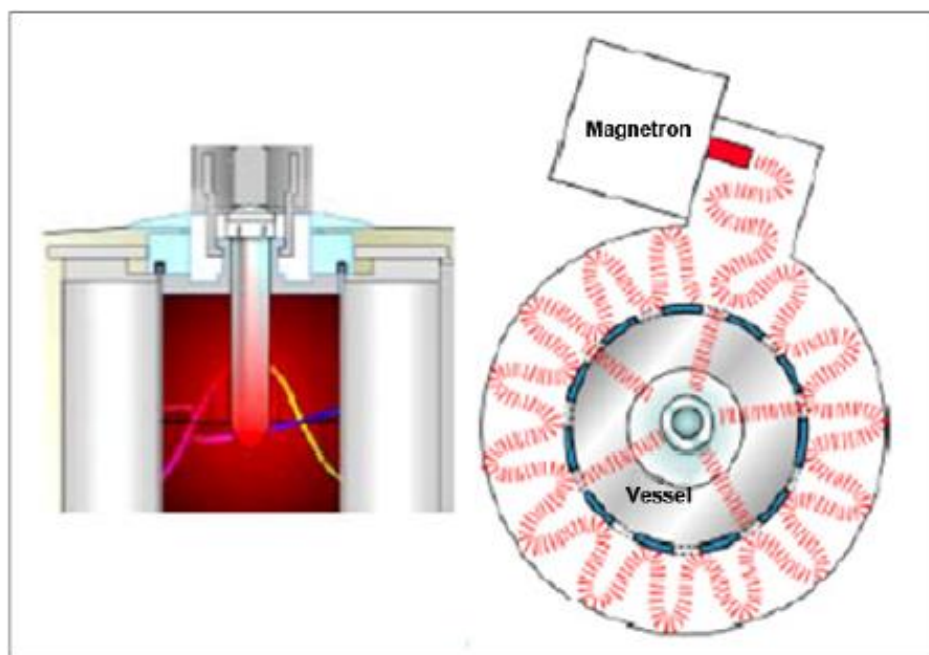


**Figure 5.6.** Single-mode microwave applicator and its working principle [91]

In single-mode microwave applicators, the microwave pattern is well defined and the chance of focusing the microwave radiation directly to the target point provides more effective and homogeneous heating.

### **5.5 Application of Microwave Heating in Heterogeneous Catalyzed Reactions**

Nowadays, intensive studies were carried out to investigate the effect of microwave heating on catalytic systems, involving solid catalysts (heterogeneous catalytic systems). There have been many studies in the literature, suggesting that reaction rate is accelerated and/or product selectivity is changed in the presence of microwave heating [95-97].

The temperature of the active sites is generally lower or equal to the bulk temperature in conductively heated systems, since active sites are heated by the bulk. However in the case of microwave heating, active sites in the catalyst are heated rapidly due to the direct interaction of microwave radiation with the nano-size metallic particles (active sites) in the catalyst framework. This rapid heating provides perfect conditions at which the active sites could have a higher temperature

than the bulk. Since the temperature at the active sites of the catalyst determines the reaction rate, reaction rates obtained under microwave heating are generally higher than the ones obtained in conventional heating. As mentioned before, the difference in heating also affects the product selectivity. Most of the conductively heated reactions are kinetically controlled, because the heat is provided in small amounts at a time. Due to the slow heating in conductively heated systems, the thermodynamic activation energy can not be applied before the reactants have taken the kinetic route. However in the case of microwave assisted heterogeneous reactions, a large amount of heat can be provided instantly, and thermodynamic control of the reaction is achievable giving products with lower energy than the kinetically controlled reaction [91].

For the time being, two models have been proposed for the microwave-assisted heterogeneous catalytic systems in order to clarify the reasons of activity enhancement achieved under microwave heating, namely *thermal effects* and *non-thermal effects (microwave effects)*. The origin of thermal effects is the different temperature regime that may be observed in the catalyst bed due to the dielectric heating characteristics. Non-thermal effects are the specific effects which can not be simply explained by the occurrence of different temperature regimes resulting from thermal interactions between the materials and microwave radiation in the catalyst bed. [90]. In order to understand whether the reason of the activity enhancement observed under microwave heating is purely thermal or non-thermal effects (microwave effects) are present, an accurate temperature measurement inside the reactor is essential. Since there is no such technology that can measure the temperature of the hot-spots formed in the catalyst bed, '*non-thermal effect*' is still questionable.

A brief literature survey was done and some of the results are discussed below in order to illustrate the effect of microwave heating on heterogeneous catalytic systems.

Zhang et al. [98] studied H<sub>2</sub>S decomposition in the presence of microwave heating and observed an increase in conversion compared to that of the conventionally heated experiment. Researchers explained this conversion enhancement by the formation of hot-spots on the catalyst surface. According to them, hot-spots formed on the catalyst surface provided a higher reaction temperature and thus a higher conversion, although it is not possible to prove this hypothesis with the temperature measurement techniques available right now. However, when they studied the used catalyst in microwave-assisted experiments, they realized that a high temperature phase change of the catalytic support ( $\gamma$ -Al<sub>2</sub>O<sub>3</sub> to  $\alpha$ -Al<sub>2</sub>O<sub>3</sub>) was observed proving that the catalyst had a higher temperature than the average reaction temperature, which is in accordance with the hot-spot theory.

In the study conducted by Perry et al. [99], CO oxidation was studied over Pt and Pd/Al<sub>2</sub>O<sub>3</sub> catalysts in a focused-microwave reactor system. In the case of microwave heating, a higher reaction rate was observed. Authors came to a conclusion that the higher reaction rate observed under microwave heating was not related to ‘specific microwave effect’ but related to inadequate temperature measurement under microwave irradiation. Furthermore, the theoretical analysis on possible hot-spot formation showed that local overheating of the catalyst active sites is approximately 10 K which is far below detection limit of any temperature measuring technique.

Will et al. [100] investigated oxidation of propane over LaCoO<sub>2</sub>, LaMnO<sub>3</sub> and La<sub>x</sub>Sr<sub>1-x</sub>MnO<sub>3</sub> catalysts under microwave and classical heating. To minimize temperature differences between the catalyst surface and the catalyst bed, the reactor was thermally isolated. Very small differences in conversion and selectivity were observed between experiments under the microwave and classical conditions.

Different from the study conducted by Will et al. [100], Beckers et al. [101] showed that propane oxidation performed with La<sub>0.9</sub>Sr<sub>0.1</sub>MnO<sub>3</sub> catalyst was strongly enhanced by microwave irradiation. In both conventionally heated and microwave



heating systems, same conversion was reached; however, this conversion was reached at a temperature 200°C lower when microwave heating was applied.

In the study conducted by Koch et al. [102], hydrogen cyanide (HCN) synthesis was investigated through two competitive routes which were production of HCN from ammonia over solid carbon and the reaction of ammonia and methane over Pt/Al<sub>2</sub>O<sub>3</sub> catalyst. In both routes, the selectivity to HCN was close to 95% which was slightly higher than the HCN selectivity obtained in the conventional process. Observed higher selectivity was explained by existence of a thermal gradient between the surface of the catalyst which was at a higher temperature, and the gas phase at lower temperature.

Recent study conducted by Sinev et al. [103] focused on the dehydrogenation of ethane over vanadium-based catalysts in both conventionally heated and microwave heated reaction systems. The results suggested that depending on the composition of the catalyst, different conclusions regarding influence of microwave irradiation could be drawn. It was shown that for some catalysts the conversion of ethane was not affected by the application of dielectric (microwave) heating, while for other catalysts the conversion of ethane under the microwave heating was higher than for conventional heating. It was also observed that the increased conversion was affected by the phase transition of catalysts, which occurred only when the microwave heating was applied.

### **5.6 Application of Microwave Heating in Catalytic Hydrogen Production**

Microwave-assisted production of hydrogen and synthesis gas is a far less documented field of microwave-assisted catalysis. This field of microwave-assisted catalysis hasn't received much attention so far. However, growing interest in the hydrogen production and the great number of reports describing potential of microwave energy application to chemical reactions attracts more and more attention from research groups. [84]

Research groups of Cooney and Xi [104] were the one of the first groups investigating microwave-assisted hydrogen production. In 1996, group of Cooney and Xi [104] studied both the decomposition of methane and methane steam reforming reactions. Although, methane decomposition reaction was not very successful, since obtained conversions were very low and the production of hydrogen sharply decreased with reaction time, these experiments showed great potential of microwaves as an alternative source of heat for the reaction. On the contrary, methane conversion was very high and remained stable over the reaction time in steam reforming of methane reaction experiments. Moreover, the results clearly showed that higher conversion of methane was achieved when microwave heating was applied. It was reported that the temperature of the conventional process had to be 30- 50 K higher than under microwave conditions to produce the same methane conversion. In this work, thermocouples were used in temperature measurement of the catalyst bed under microwave heating. Authors claimed that they were aware of the possible interaction of the thermocouple with the electro-magnetic field and certain modifications of the thermocouple were applied to minimize undesired effect. Despite of all effort, the researchers could not find an explanation for achieving same methane conversion at a lower temperature under microwave heating, and admitted that exact mechanism for the microwave effects is not known.

Bi and coworkers [105] studied the oxidation of methane for hydrogen production under microwave heating conditions, in 1999. The reaction was performed over Ni and Co incorporated  $ZrO_2$  and  $La_2O_3$  catalysts. Results from microwave and conventional heating were compared in terms of methane conversion and selectivity to the reaction products ( $H_2$ , CO,  $CO_2$ ). For all catalysts, higher conversion of methane and higher selectivity to hydrogen were observed under microwave heating. It was also observed that at the same conversion, the temperature of the catalytic bed under microwave conditions was almost 200 K lower than for the conventional heating. Authors postulated the occurrence of hot-spots on the catalyst surface under microwave heating as a possible explanation of the observed results. Although the authors were sensitive to correct temperature measurements of the catalytic bed, it is

not possible to prove the formation of hot-spots on the catalyst surface with the temperature measurement techniques available. Moreover, the temperature of the potential hot-spots can not be determined by the authors.

Another research group investigating microwave-assisted hydrogen production is Menendez and coworkers. They examined methane decomposition over activated carbon under both conventional and microwave heating modes [106]. The experimental results showed that the methane conversion obtained under microwave heated experiments is significantly higher at the beginning of the process and decreases in time to eventually drop below the methanol conversion obtained in conventionally heated system after 100 min of experiment. Based on the experimental data and visual observation (small sparks were observed during microwave heating experiment), the authors claimed that microwave heating gives rise to higher conversions than conventional heating due to the formation of hot spots inside the catalyst bed, which favors  $\text{CH}_4$  decomposition but at the same time decreases activity of the catalyst and enhances carbon deposit formation by reducing a porosity of the catalytic bed.

The group of Menendez and co-workers also conducted experiments on microwave-assisted dry reforming of methane using an activated carbon as a catalyst and microwave receptor [107]. It was found that conversion of both reagents,  $\text{CO}_2$  and  $\text{CH}_4$ , was up to 40% higher under microwave heating than for reaction carried out at the same conditions but under conventional heating (electric furnace). Similar to their previous work, authors proposed micro-plasma arcing (hot-spot formation) as a mechanism responsible for observed enhancement of conversion of both reagents.

The hot-spot formation hypothesis was abandoned by Perry [108] in his research on microwave heated methanol steam reforming on  $\text{Cu}/\text{ZnO}$  catalyst. The experimental study on the reaction kinetic showed no significant differences in kinetic expression for two heating modes – conventional and microwave. However, it was found that the microwave-enhanced methanol reforming could be carried out at temperature

around 20 K lower than in the conventional equivalent maintaining similar kinetics for both processes. The theoretical study revealed that when the catalytic bed is exposed to microwave irradiation, the spatial temperature gradients are mitigated resulting in better performance of the reaction and less heat is required to maintain the process.

Chen and co-workers carried out also a research work on hydrogen generation from a catalytic water gas shift reaction under microwave irradiation [109]. This research demonstrated that the microwave energy can be successfully implemented to WGSR resulting in higher CO conversions than the conversion obtained in conventionally heated reactor.

Beside thermal effects of microwave heating, the group of Xin-Rong Zhang [110] claims that microwave irradiation (3 – 10 minutes) of the oxide precursor of the Cu/ZnO/Al<sub>2</sub>O<sub>3</sub> catalyst, used for the steam reforming of methanol, has an effect on the structural modification of the catalyst surface. It was shown that the catalysts with modified surface characteristics displayed an enhanced performance in the conversion for steam reforming of methanol. This was acclaimed to be due to the creation of highly strained copper nanocrystals. It was observed that the specific copper surface area decreased for increased duration of microwave treatment, however the conversion increased significantly and showed an optimum at 8 minutes of treatment. Further investigation of the catalyst showed that the conversion was directly proportional to the measured microstrain of the copper crystals. To the best of our knowledge, there is no published work in the literature for the ethanol reforming reaction in a microwave reactor.

## CHAPTER 6

### EXPERIMENTAL

Experimental work of the present study has five major steps;

- 1) design & synthesis of the catalysts
- 2) characterization of the catalysts
- 3) catalytic activity tests in conventionally heated reactor system
- 4) installation of focused-microwave reactor system & catalytic activity tests
- 5) characterization of used catalysts

#### 6.1. Design and Synthesis of Catalysts

##### 6.1.1. Mesoporous Alumina (MA) Synthesis

In the scope of this study, mesoporous alumina type catalyst support material was synthesized due to its excellent hydrothermal stability and highly ordered pore structure, following a route named ‘Evaporation Induced Self-Assembly’ [69]. In this procedure, aluminum isopropoxide ( $\text{Al}[\text{OCH}(\text{CH}_3)_2]_3$ ) was used as Al source and triblock copolymer Pluronic P123 ((Poly(ethylene glycol)-*block*-poly(propylene glycol)-*block*-poly(ethylene glycol))) as the surfactant (Figure 6.1). In a typical synthesis route, a clear surfactant solution was prepared by dissolving 1.0 g of triblock copolymer Pluronic P123 in 20 ml of anhydrous ethanol at room temperature. Then the solution containing 1.6 ml of 67 wt% nitric acid ( $\text{HNO}_3$ ), 2.04 g of aluminum isopropoxide and 10 ml of anhydrous ethanol was added into this solution with vigorous stirring. Resulting mixture was covered with PE film, stirred at room temperature for 5 h and solvent evaporation process was performed in a 60°C drying oven for 2 days. Solid product was then calcined in a flow of dry air by heating from room temperature to 700°C at a rate of 1°C/min and keeping at this temperature for 6 h.

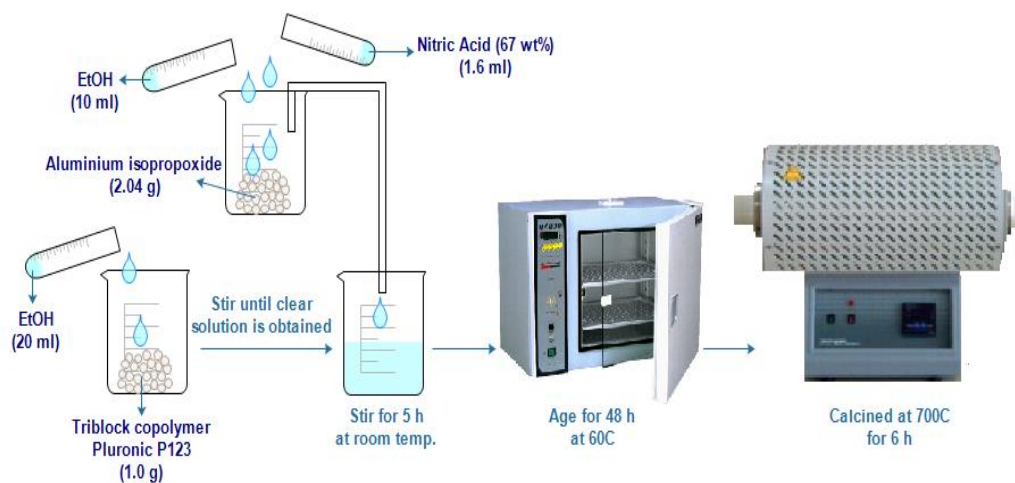


**Figure 6.1.** Schematic representation of mesoporous alumina (MA) synthesis

### 6.1.2. Mesoporous Alumina (MA) Supported Catalyst Synthesis

A set of cobalt and nickel incorporated mesoporous alumina (MA) catalysts, which were modified with Mg were synthesized by two different routes, namely direct synthesis and impregnation.

#### 6.1.2.1. Synthesis of Cobalt Incorporated Mesoporous Alumina (MA) Catalysts

In this set of materials, four Co incorporated catalysts were synthesized by both direct synthesis (Co-Mg-MA), impregnation (Co@MA, Co-Mg@MA) and combination of direct synthesis and impregnation (Co@Mg-MA) methods.

##### 6.1.2.1.1. Synthesis of Co-Mg-MA

Surfactant solution was prepared by dissolving 1.0 g of triblock copolymer (Pluronic P123) in 20 ml of unhydrous ethanol at room temperature. Then the solution containing 1.6 ml of 67 wt% nitric acid ( $\text{HNO}_3$ ), 2.04 g of aluminum isopropoxide and 10 ml of unhydrous ethanol was added into the above solution with vigorous stirring. Resulting mixture was covered with PE film and allowed to stir at room temperature. Meanwhile, a solution containing desired amount of Co-acetylacetonate,  $\text{MgCl}_2 \cdot 6\text{H}_2\text{O}$  and 10 ml unhydrous ethanol was prepared and added to the above solution and stirred for 5 h. After 2 days of aging at 60°C, solid product

was calcined in a flow of dry air at 700°C for 6 h and reduced under H<sub>2</sub> flow at 650°C for 4 h. Resulting catalyst was named as *Co-Mg-MA*. Co/Al and Mg/Al ratios were adjusted as 0.1 and 0.25, respectively, during the synthesis of this material.

#### ***6.1.2.1.2. Synthesis of Co-Mg@MA***

Co-Mg@MA catalyst was prepared by impregnation of Co and Mg into the MA support material. Support material MA was suspended in deionized water. Two solutions containing desired amount of Co and Mg were prepared and added dropwise into the above suspension, stirred for 24 h and evaporated to dryness. Solid product was calcined and reduced at same conditions. Resulting catalyst was named as *Co-Mg@MA*. Co/Al and Mg/Al ratios were again adjusted as 0.1 and 0.25, respectively, during the synthesis of this material.

#### ***6.1.2.1.3. Synthesis of Co@MA***

Co@MA catalyst was prepared by impregnation of Co into the MA support material. Support material MA was suspended in deionized water. A solution containing desired amount of Co was prepared and added dropwise into the above suspension, stirred for 24 h and evaporated to dryness. Solid product was calcined and reduced at same conditions. Resulting catalyst was named as *Co@MA*. Co/Al ratio was adjusted as 0.1 during the synthesis of this material.

#### ***6.1.2.1.4. Synthesis of Co@Mg-MA***

In order to investigate the effect of Mg incorporation procedure on the catalytic performance of the synthesized materials, Co@Mg-MA was synthesized following direct addition of Mg into the MA structure (Mg-MA) and impregnation of Co into this Mg-MA type support material. Co/Al and Mg/Al ratios were again adjusted as 0.1 and 0.25, respectively, during the synthesis of this material.

### **6.1.2.2. Synthesis of Nickel Incorporated Mesoporous Alumina (MA) Catalysts**

In this set of materials, three nickel incorporated catalysts were synthesized by both direct synthesis (Ni-Mg-MA), impregnation (Ni-Mg@MA) and combination of

direct synthesis and impregnation (Ni@Mg-MA) methods. Synthesis procedures of Ni-Mg-MA, Ni-Mg@MA and Ni@Mg-MA were quite similar to the synthesis procedures of Co-Mg-MA, Co-Mg@MA and Co@Mg-MA, respectively, In the synthesis of these catalysts, Ni-acetylacetonate was used as the Ni source.

## **6.2. Characterization of the Catalysts**

Synthesized materials were characterized by X-Ray Diffraction (XRD), Nitrogen Physisorption, X-Ray Photoelectron Spectroscopy (XPS), Diffuse Reflectance FTIR Spectroscopy (DRIFTS), Scanning Electron Microscopy (SEM) and Transmission Electron Microscopy (TEM) techniques.

### **6.2.1. X-Ray Diffraction (XRD)**

X-ray diffraction (XRD) is a widely used technique in order to identify the crystalline phases in the materials and to measure the structural properties of these phases. XRD technique is also used to get information about the pore architecture of the mesoporous materials. XRD analysis of synthesized materials were performed with a Rigaku Ultima-IV diffractometer in METU Central Laboratory. For low angle analysis of the synthesized materials, the scanning range was set between  $2\theta$  of  $0.3^\circ$  and  $10^\circ$  and for high angle analysis it was set between  $10^\circ$  and  $90^\circ$ .

### **6.2.2. Nitrogen Physisorption**

Nitrogen physisorption is an adsorption technique applied to identify the specific surface area and porosity of the catalytic materials.  $N_2$  physisorption analysis of synthesized materials were performed by a Quantachrome Autosorb-6 device in METU Central Laboratory. Before the analysis, catalysts were degassed at  $110^\circ\text{C}$  for 6 hours and analysis was performed at a relative pressure ( $P/P_0$ ) range of  $5 \times 10^{-2}$  and 0.99 at 77 K (liquid nitrogen temperature).

### **6.2.3. X-Ray Photoelectron Spectroscopy (XPS)**

XPS is the most broadly applicable general surface analysis technique used to get information about surface composition and chemical states of the elements present



on the materials. XPS analysis of the synthesized catalysts were performed with the PHI 5000 Versa Probe instrument equipped with a monochromatized Al K $\alpha$  X-ray source at METU Central Laboratory. Collected XPS data were corrected for charge shifting using standard C 1s binding energy of 284.5 eV and curve fitting was performed with XPSPeak 4.1 software package. Since the materials are inorganic, Shirley-type background fitting was used to determine spectra baselines and deconvolution was done using 80% Lorentzian-20% Gaussian combination peaks.

#### **6.2.4. Diffuse Reflectance Infrared Fourier Transform Spectroscopy (DRIFTS)**

Diffuse reflectance FT-IR spectroscopic (DRIFTS) analysis of pyridine adsorbed materials is a technique which give information about the surface acidity of these materials. DRIFTS analysis of the pyridine adsorbed samples were carried out by a Perkin Elmer Spectrum One instrument available in the Kinetic Laboratory of METU Chemical Engineering Department. Before the analysis, catalysts were dried at 110°C for 12 hours and then pyridine was adsorbed on them. A reference spectrum was recorded with pure KBr at room temperature. In order to analyze the acidic nature of the samples, the spectra of the clean samples were subtracted from the spectra of the pyridine adsorbed samples.

#### **6.2.5. Scanning Electron Microscopy (SEM)**

Scanning Electron Microscopy (SEM) is a technique which provides a highly magnified image of the surface of a material [111]. SEM analysis of the materials were performed with Jeol JSM-6400 instrument at the METU Central Laboratory.

#### **6.2.6. Transmission Electron Microscopy (TEM)**

TEM analysis of the synthesized materials were performed with Jem Jeol 2100F 200 kV HRTEM instrument available in METU Central Laboratory.

### 6.3. Catalytic Activity Tests in Conventionally Heated Reactor System

Catalytic activity tests of the synthesized materials were conducted in the conventionally heated flow reactor set-up, which was schematically shown in Figure 6.2.

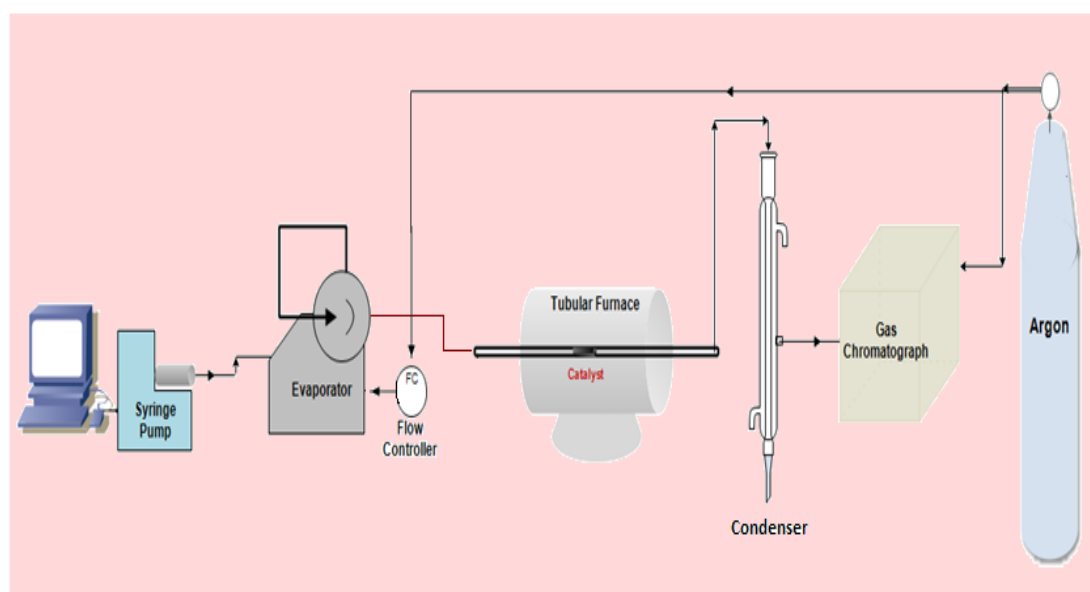


**Figure 6.2.** Schematic representation of conventionally heated reactor system

The reaction system consists of a syringe pump, preheater, electrically heated tubular furnace, fixed bed flow reactor, condenser and gas chromatograph (Agilent Technologies 6850). Fixed bed flow reactor is a  $\frac{1}{4}$  in diameter quartz tube which has a porous quartz filter (porosity: 2) in the middle of it in order to fix the catalyst bed. The catalyst (0.15 g) was placed in this quartz tube and put into electrically heated tubular furnace. Reaction temperature was adjusted by the temperature controller of the furnace. Liquid feed was prepared with a  $\text{H}_2\text{O}/\text{C}_2\text{H}_5\text{OH}$  volumetric ratio of 1.0 which corresponds to a molar ratio of 3.2. Prepared liquid feed was introduced to the system by a Cole Parmer liquid injection pump, with a volumetric flow rate of 0.9 ml/h. Liquid feed was then evaporated in the preheater ( $130^\circ\text{C} - 150^\circ\text{C}$ ). Water-ethanol vapor which was mixed with carrier gas argon (20 ml/min water-ethanol vapor and 30 ml/min Ar) was then sent to the reactor (space time: 0.18 s g/l). Ar gas flow rate was adjusted by a gas mass flow controller placed at the entrance of the

preheater. A condenser was placed between the reactor and gas chromatograph (GC). The liquified products were collected in condenser and the gaseous products were sent to GC and analyzed there. Chemical analysis of the liquid effluent of the reactor was also determined at certain intervals. Thermal conductivity detector and Porapak S column were used in the chromatograph and Ar was selected as the reference gas.

#### 6.4. Installation of Focused-Microwave Reactor System & Activity Tests

A photograph of the reaction system installed with a focused-microwave heating unit is shown in Figure 6.3. Selection and design of the components of microwave reactor (Appendix B) was performed with the help of SAIREM Co.

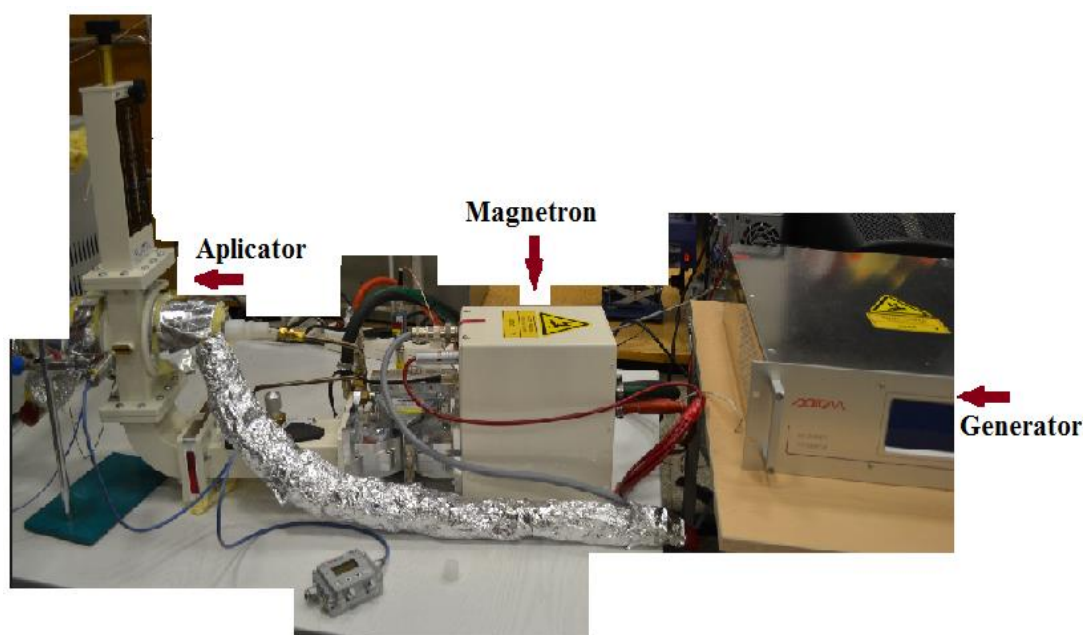


**Figure 6.3.** Reaction system with focused-microwave

Microwave reactor system is composed of 3 main parts; which are generator, magnetron and applicator. Power is regulated by the generator. Maximum power that can be sent from the generator is 2000 W in our system. Magnetron switches the direct current, which comes from the generator, to microwave energy. Tuner, which is composed of reflected paddles and located between the magnetron and applicator, focuses the microwave directly onto the catalyst bed inserted into the quartz reactor.

Unabsorbed microwavel is reflected back by the help of a piston located on the applicator and reabsorbed by the catalyst bed. Water recirculater installed between the magnetron and regulator absorbs the microwave which is not absorbed by the material, in order to protect the sensitive filaments of the magnetron. Temperature measurement of the catalyst bed was achieved with an infrared pyrometer, which was fixed in front of the window, looking directly to the catalyst bed from a distance of 2 cm.

### **6.5. Characterization of Used Catalysts**

Catalysts were characterized by Thermal Gravimetric Analysis method (TGA) after the reaction tests, in order to investigate the amount and type of coke deposited on the catalyst during reaction period. Thermal gravimetric analysis of the used catalysts were carried out using a Perkin-Elmer Pyris 1 TGA Thermal Analyzer instrument in METU Chemical Engineering Department.

## CHAPTER 7

### RESULTS AND DISCUSSIONS

In the scope of this study, Co-Mg and Ni-Mg incorporated mesoporous alumina (MA) type catalysts were synthesized, characterized and tested for their activity towards steam reforming of ethanol (SRE) reaction in both conventionally heated and focused-microwave reactor systems.

In this chapter, the results of characterization and activity tests of synthesized materials are illustrated and discussed in two parts. **Part 1** focuses on the characterization and activity test results of Co-Mg incorporated catalysts and **Part 2** focuses on the Ni-Mg incorporated catalysts.

#### **PART 1: Co-Mg Incorporated MA Type Catalysts**

In this part, characterization and activity test results of Co-Mg incorporated MA type catalysts synthesized by both direct synthesis and impregnation methods are given and discussed.

##### **7.1. Results of Co-Mg Incorporated MA Type Catalysts**

Firstly, synthesized Co-Mg-MA, Co-Mg@MA, Co@Mg-MA and Co@MA catalysts were characterized by several methods in order to understand their nature. Then, synthesized materials were tested for SRE reaction in conventionally heated reactor system and activity test results of the catalysts were collected and analyzed. In order to analyze coke deposition during reaction period, thermal gravimetric analysis

(TGA) method was applied to used catalysts. Finally, the best catalyst towards SRE reaction was tested in focused-microwave reactor system.

### 7.1.1. Characterization Results of Mesoporous Alumina (MA)-type Support Material

Synthesized mesoporous alumina (MA) type catalyst support material was characterized by X-ray diffraction (XRD) and N<sub>2</sub> physisorption (BET) methods.

Evidence for the formation of mesostructures is provided by small-angle X-ray diffraction (XRD) pattern of MA shown in Figure 7.1. MA type support material showed a very strong diffraction peak around 0.85° and two weak peaks around 1.2° and 1.8° which can be attributed to *p6mm* hexagonal symmetry [69].

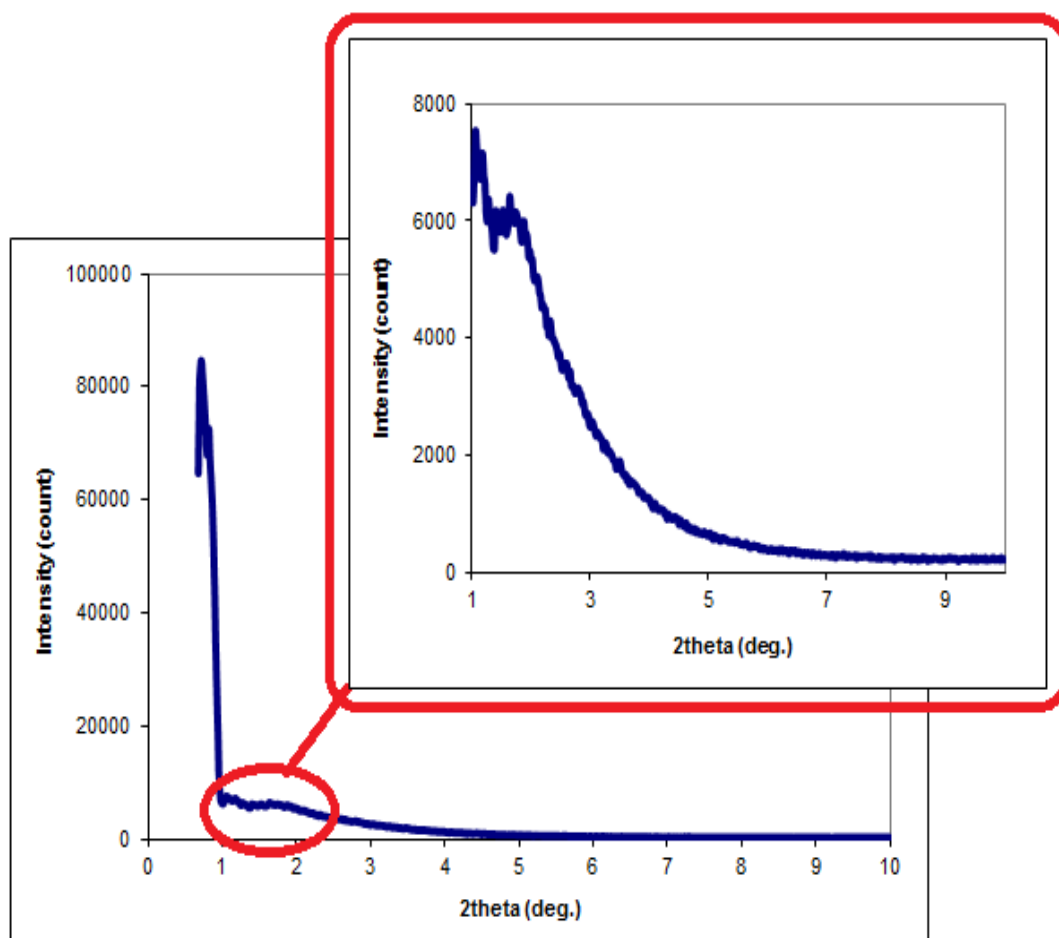


**Figure 7.1.** XRD pattern of MA type support material

The nitrogen adsorption-desorption isotherms (Figure 7.2) of mesoporous alumina (MA) type support material yields type IV curve with H1-shaped hysteresis loop, suggesting its uniform cylindrical pores. MA type material has a BET surface area of 172 m<sup>2</sup>/g, a BJH desorption pore volume of 0.63 cc/g and BJH desorption pore diameter of 9.5 nm.

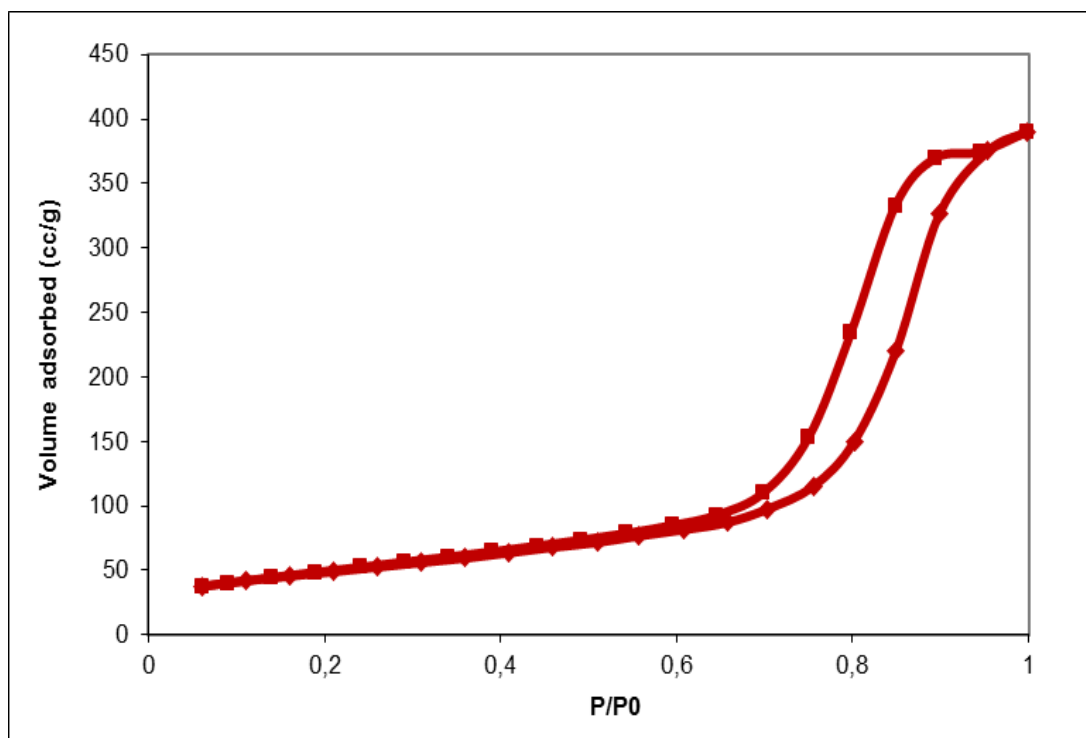


**Figure 7.2.** N<sub>2</sub> physisorption curve of MA type support material

It is believed that the relatively large surface areas and narrow pore-size distributions combined with excellent thermal and hydrothermal stability enhance the potential applications of these ordered mesoporous aluminas in catalysis.

### 7.1.2. Characterization Results of Co-Mg Incorporated Catalysts

In order to analyze physical and chemical properties of Co-Mg incorporated MA type catalysts, N<sub>2</sub> physisorption, X-ray diffraction (XRD), X-ray photoelectron spectroscopy (XPS), Diffuse reflectance infrared fourier transform spectroscopy (DRIFTS) of pyridine adsorbed samples and transmission electron microscopy

(TEM) type characterization methods were applied and the results of these characterization studies were given and discussed in this section.

#### 7.1.2.1. N<sub>2</sub> Physisorption Analysis Results of Co-Mg Incorporated Catalysts

In order to investigate the textural properties of the synthesized catalysts, nitrogen physisorption characterization method was applied. Surface area values, pore diameters and pore volumes of the synthesized catalysts are shown in Table 7.1. Both surface area and pore volume values decreased by the impregnation of Mg and Co. Some decrease in the pore diameter was also observed as a result of impregnation, indicating blocking of some of the pores by the impregnated metals. On the contrary, direct addition of Mg into the MA structure enhanced both the surface area and pore volume.

**Table 7.1.** Textural properties of synthesized materials

Material	BET Surface Area (m <sup>2</sup> /g)	BJH Pore Volume (cc/g)	BJH Pore Diameter (nm)
Co-Mg-MA	384.3	0.56	3.8
Co-Mg@MA	129.4	0.39	4.3
Co@Mg-MA	123.1	0.57	9.7
Co@MA	192.7	0.42	5.6
MA	212.0	0.51	5.1

Nitrogen adsorption-desorption isotherm curves of Co based catalysts are shown in Figure 7.3. Well-defined and steep hysteresis loops with parallel adsorption-desorption branches is the characteristic of formation of ordered mesopores with a narrow pore size distribution. Such hysteresis loops were observed for Co-Mg-MA and Co@Mg-MA catalysts synthesized by direct addition of Mg. However in the case of Co and Mg impregnated materials (Co-Mg@MA and Co@MA), this



characteristic behavior was essentially lost, indicating deformations in the long-range order of mesopores.

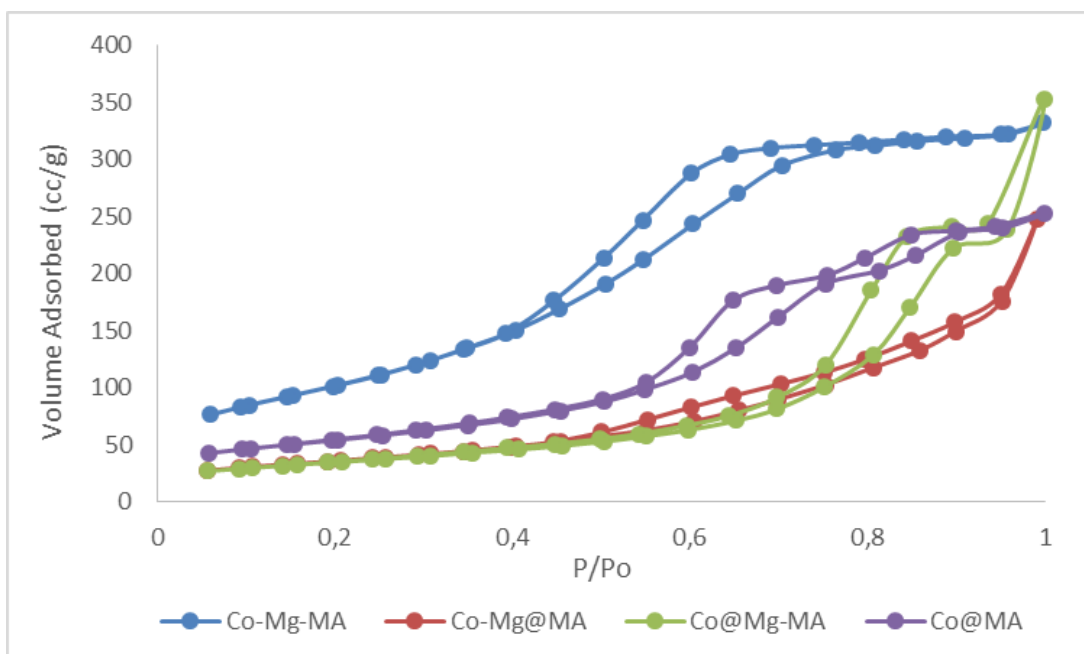


**Figure 7.3.** Nitrogen physisorption isotherms of Co-Mg incorporated catalysts

Pore size distribution curves of Co-Mg incorporated MA type catalysts are given in Figure 7.4.

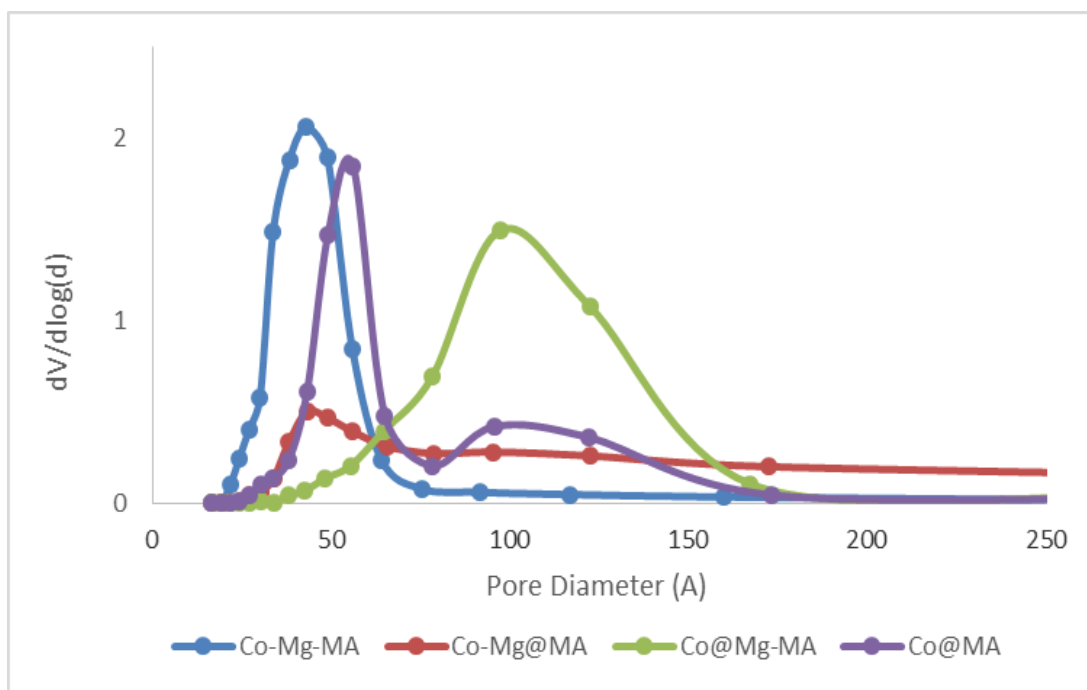


**Figure 7.4.** Pore size distribution of Co-Mg incorporated catalysts

### 7.1.2.2. X-Ray Diffraction (XRD) Analysis Results of Co-Mg Incorporated Catalysts

In the XRD patterns of Co-Mg-MA and Co@Mg-MA (Figure 7.5) eight diffraction peaks were observed at  $2\theta$  values of  $19^\circ$ ,  $31^\circ$ ,  $37^\circ$ ,  $44^\circ$ ,  $55^\circ$ ,  $59^\circ$ ,  $65^\circ$  and  $78^\circ$ , correspond to  $\text{Co}_3\text{O}_4$  (black antiferromagnetic solid;  $\text{CoO}\cdot\text{Co}_2\text{O}_3$ ) [112]. For pure  $\text{Co}_3\text{O}_4$ , the ratio of intensities of [311] plane peak (at  $37^\circ$ ) and [400] plane peak (at  $44^\circ$ ) should be nearly 4.0 [112]. However, this ratio was about 2 and 1.5 in the XRD patterns of Co-Mg-MA and Co@Mg-MA, respectively. These results indicated that  $\text{Co}_3\text{O}_4$  was not the only cobalt form in these two catalysts. The main [111] plane peak of metallic Co is also expected at  $44^\circ$ . However, metallic Co does not have a characteristic peak at  $37^\circ$ . These results indicated the presence of metallic Co, as well as  $\text{Co}_3\text{O}_4$  in Co-Mg-MA and Co@Mg-MA catalysts. Another small peak observed in the XRD patterns of these catalysts (Figure 7.5) was at a  $2\theta$  value of  $42.4$ , which indicated that CoO was also present in these catalysts [113]. Cluster sizes of  $\text{Co}_3\text{O}_4$  were estimated from the characteristic peak at the  $2\theta$  value of  $19.01$  as 11 and 6 nm

for Co-Mg-MA and Co@Mg-MA, respectively, using Scherrer equation (Appendix C).

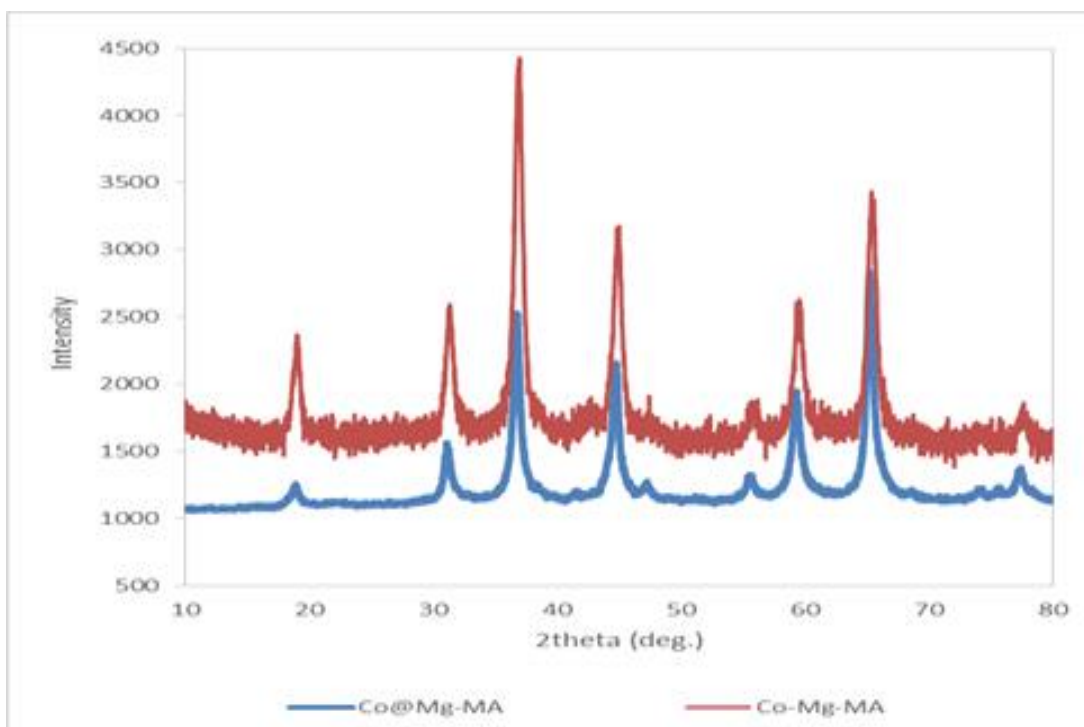


**Figure 7.5.** XRD patterns of Co-Mg-MA and Co@Mg-MA

XRD patterns of Co@MA and Co-Mg@MA indicated that these materials were less crystalline (Figure 7.6). The main difference of XRD patterns shown in Figure 7.5 and Figure 7.6 is the peak observed at the  $2\theta$  value of  $19^\circ$  observed in XRD patterns of Co-Mg-MA and Co@Mg-MA, which corresponds to  $\text{Co}_3\text{O}_4$ . Absence of this peak in the XRD patterns of Co@MA and Co-Mg@MA catalysts is an indication of presence of  $\text{CoAl}_2\text{O}_4$  instead of  $\text{Co}_3\text{O}_4$  as the main phase in these materials.

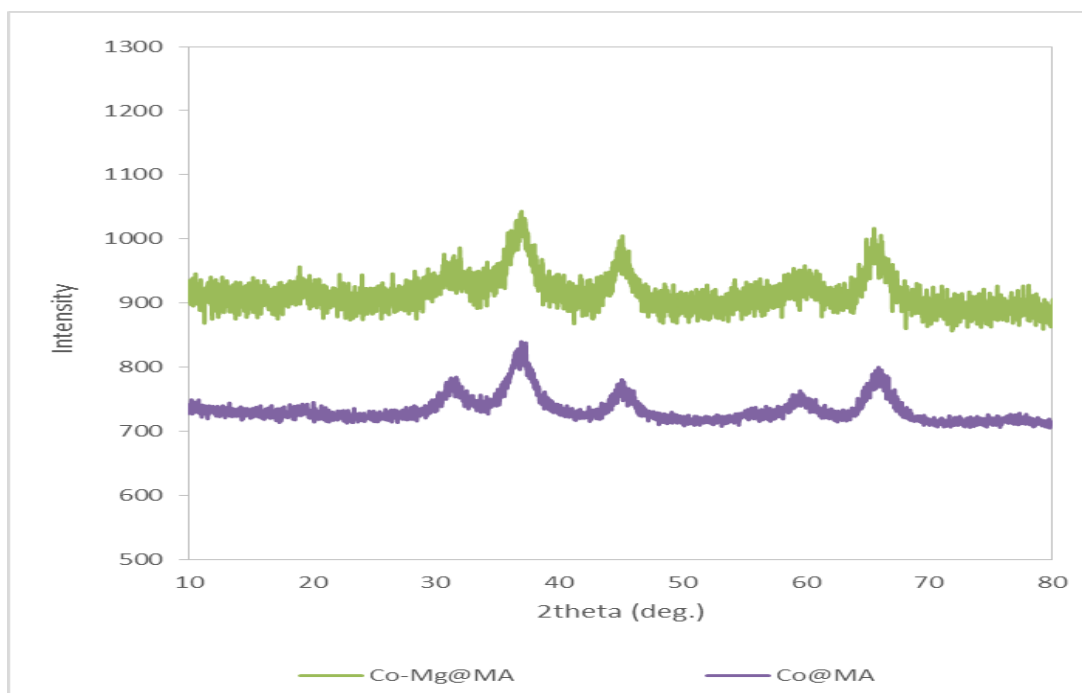


**Figure 7.6.** XRD patterns of Co-Mg@MA and Co@MA

As a summary, XRD patterns of the synthesized Co-Mg incorporated mesoporous alumina type catalysts suggested that catalysts synthesized by the direct addition of Mg had  $\text{Co}^0$  and CoO phases in their structure which are known as the active sites for SRE reaction. However in the case of Co-Mg@MA and Co@MA,  $\text{Co}^0$  and CoO phases were not observed that may result in inactive catalysts for SRE reaction.

The color of the synthesized materials also gives a clear indication of the catalyst composition (Figure 7.7).  $\text{CoAl}_2\text{O}_4$  is well known as Thenard's blue [114]. Blue color of Co@MA and Co-Mg@MA catalysts also indicated the presence of  $\text{CoAl}_2\text{O}_4$  phase in these materials. Black color of Co-Mg-MA and Co@Mg-MA catalysts indicated that these catalysts had no  $\text{CoAl}_2\text{O}_4$  form in their structure but they most probably had  $\text{Co}_3\text{O}_4$  and/or CoO in their framework since the colors of  $\text{Co}_3\text{O}_4$  and CoO are both black according to their MSDS.

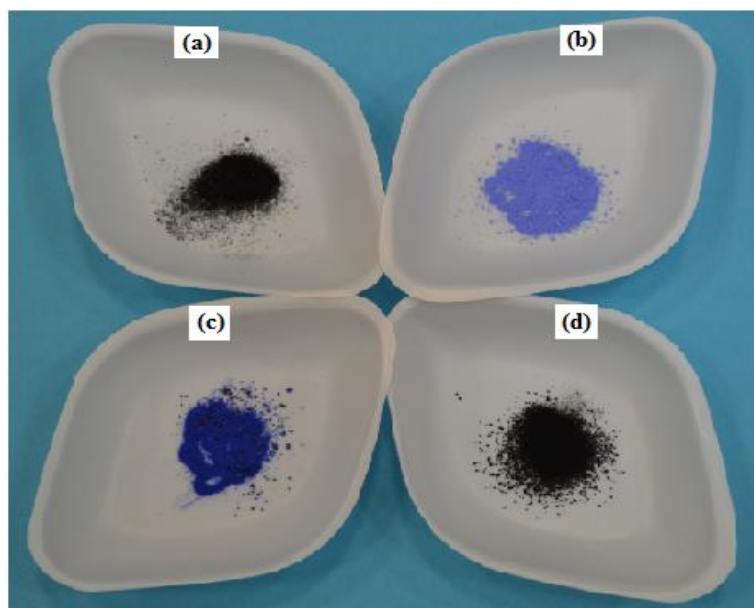


**Figure 7.7.** Color analysis of catalysts (a: Co-Mg-MA, b: Co-Mg@MA, c: Co@MA, d: Co@Mg-MA)

### 7.1.2.3. X-Ray Photoelectron Spectroscopy (XPS) Analysis Results of Co-Mg Incorporated Catalysts

**Figure 7.8** shows the X-ray photoelectron spectra of the synthesized materials in the Co2p region. XPS results supported the conclusions reached from XRD and color analysis. In agreement with the assignments in the literature [113], curve fitting in the Co 2p<sub>3/2</sub> region suggested the presence of three features assigned to Co<sup>0</sup> (779 eV), Co<sup>+2</sup> (781.4 eV) and a shake-up component associated with Co<sup>+2</sup> species over Co-Mg-MA and Co@Mg-MA catalysts. These results indicated that the surface of Co-Mg-MA and Co@Mg-MA catalysts were composed of metallic cobalt and cobalt oxide (CoO).

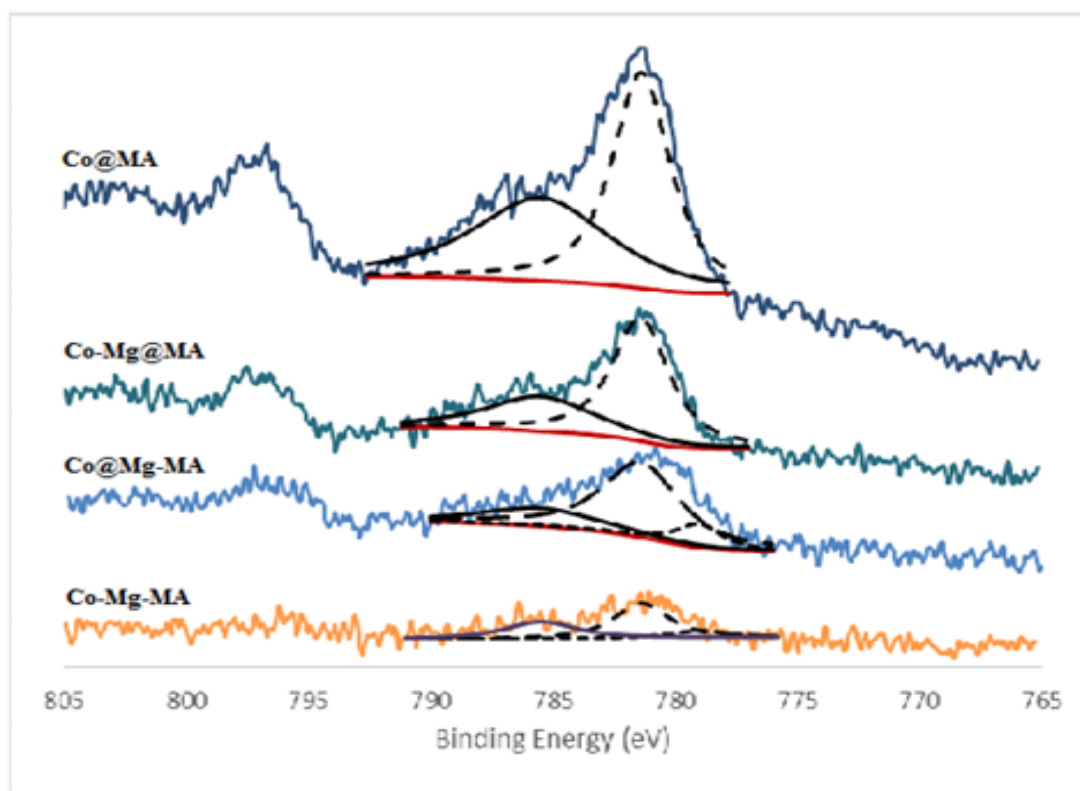


**Figure 7.8.** X-ray photoelectron spectra of catalysts

Curve fitting of XPS of Co-Mg@MA and Co@MA catalysts indicated the presence of two features, which are assigned to  $\text{Co}^{+2}$  main peak and  $\text{Co}^{+2}$  shake-up component. It is shown that metallic Co was not present on the surface of Co@MA and Co-Mg@MA catalysts. In agreement with the literature [115, 116], approximately 0.2 eV increase of the spin-orbital splitting peak of  $\text{Co}2p_{1/2}$  (at about 797 eV) of Co-Mg@MA and Co@MA catalysts supported the conclusion that  $\text{Co}^{+2}$  was in cobalt aluminate ( $\text{CoAl}_2\text{O}_4$ ) form on these materials.

#### **7.1.2.5. DRIFT Spectra (DRIFTS) Analysis Results of Pyridine Adsorbed Co-Mg Incorporated Catalysts**

Figure 7.9 illustrates the DRIFT spectra of pyridine adsorbed catalysts. Transmission bands observed at 1445 and 1590  $\text{cm}^{-1}$  corresponds to Lewis acid sites. Results indicated that, while the Lewis acid intensity of the Co-Mg@MA catalyst prepared

with impregnation of Co and Mg was very high, it was very low in Co-Mg-MA synthesized by direct addition of Co and Mg.

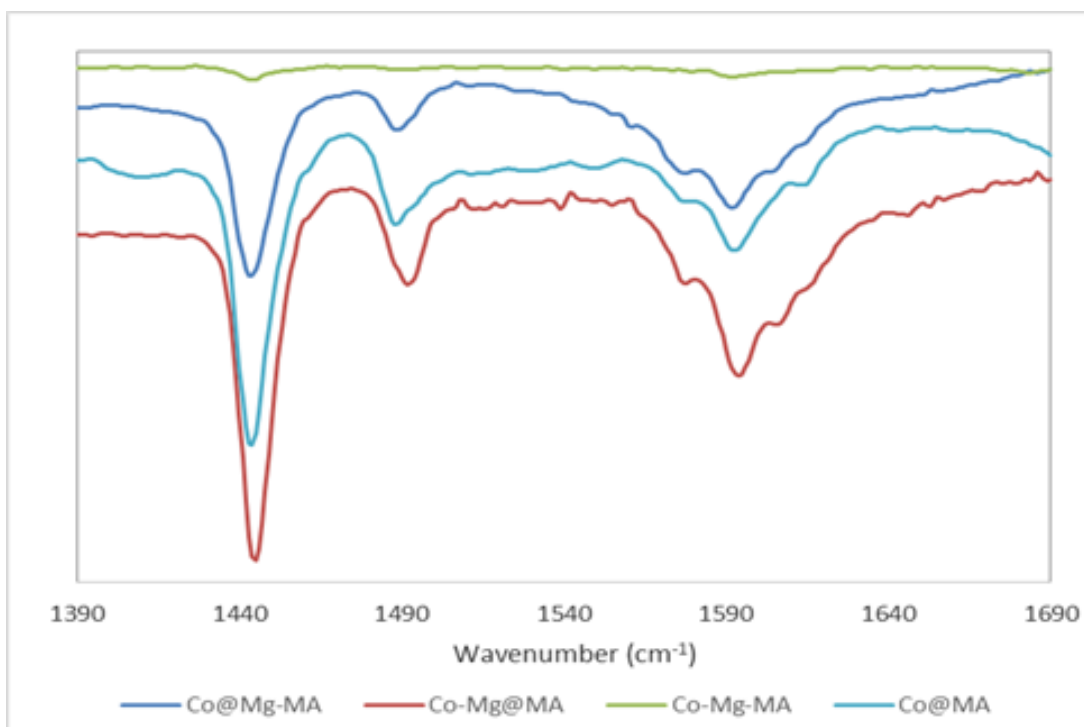


**Figure 7.9.** DRIFT spectra of Co-Mg incorporated catalysts

#### **7.1.2.5. Transmission Electron Microscopy (TEM) Analysis Results of Co-Mg Incorporated Catalysts**

TEM images of Co-Mg-MA, Co-Mg@MA and Co@Mg-MA catalysts are shown in Figure 7.10, 7.11 and 7.12, respectively. Additionally, mapping analysis of Co-Mg@MA and Co@Mg-MA catalysts are shown in Figure 7.13.

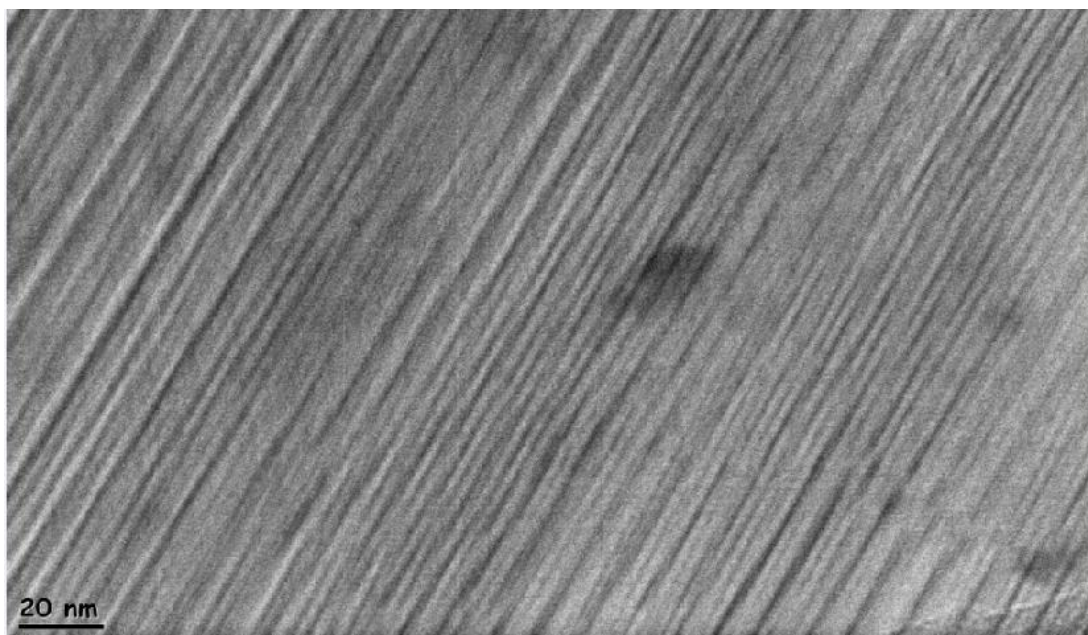


**Figure 7.10.** TEM image of Co-Mg-MA catalyst

TEM image of Co-Mg-MA shown in Figure 7.10 indicated that highly ordered alignment of cylindrical pores along [110] direction formed in the catalyst structure.

TEM images of Co-Mg@MA catalyst are given in Figure 7.11. As shown, rod-like structures were formed in the catalyst framework.



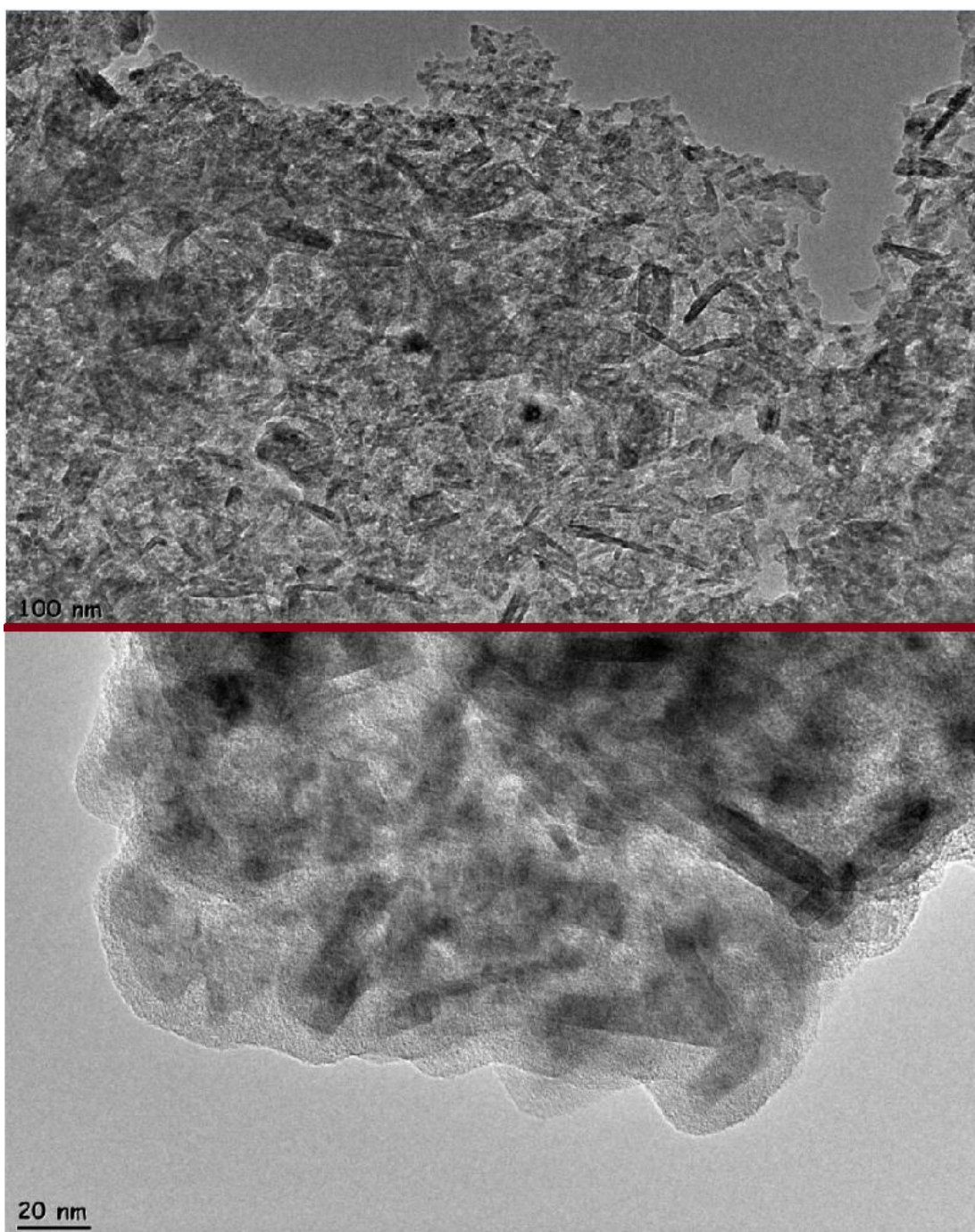


**Figure 7.11.** TEM images of Co-Mg@MA catalyst

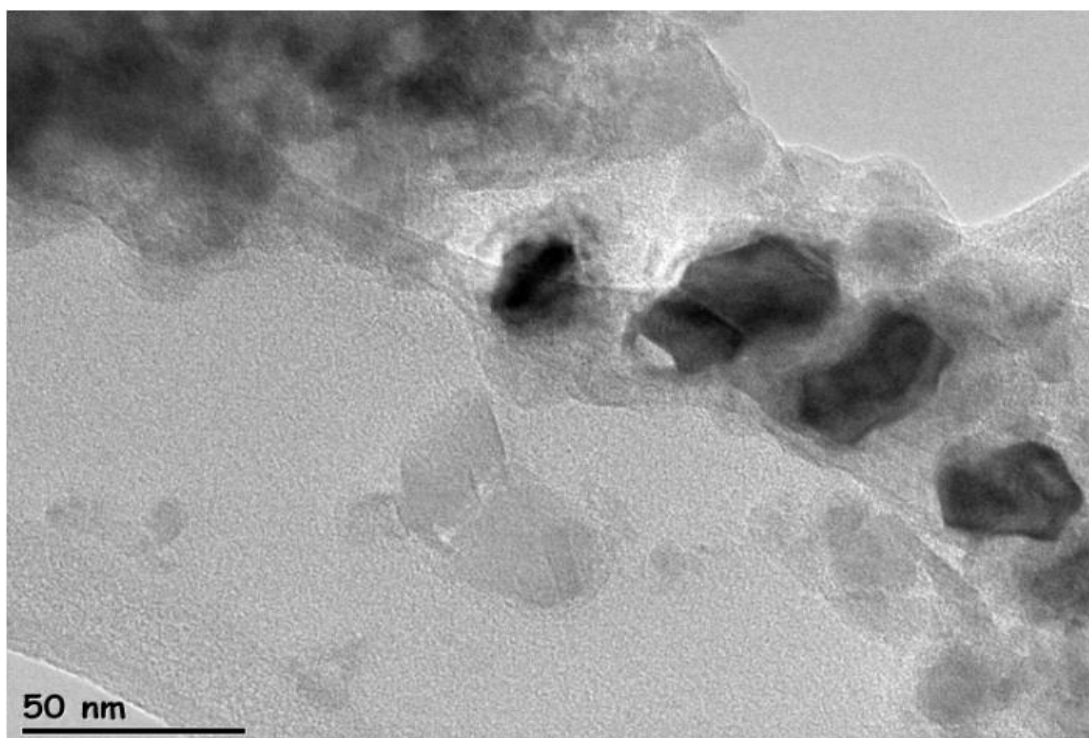


**Figure 7.12.** TEM image of Co@Mg-MA catalyst

Mapping analysis of Co-Mg@MA and Co@Mg-MA catalysts indicated that direct addition of Mg in MA (Co@Mg-MA) resulted in a uniform distribution of Mg in the catalyst framework (Figure 7.13b). In the case of Mg impregnated catalyst (Co-Mg@MA) distribution of Mg was not uniform, but accumulated at certain location (Figure 7.13a).

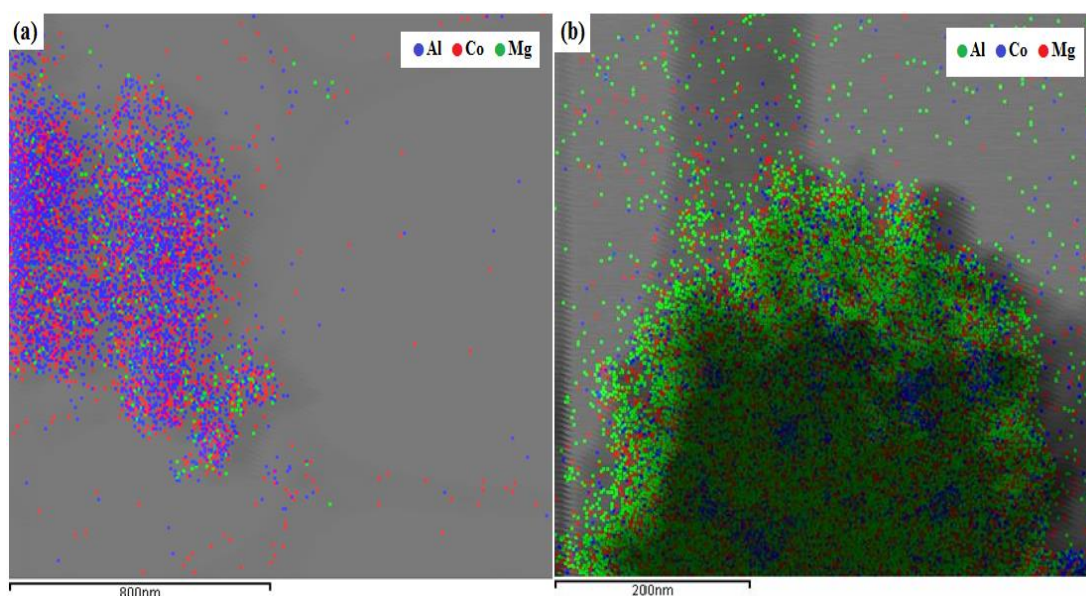


**Figure 7.13.** Mapping analysis of (a) Co-Mg@MA and (b) Co@Mg-MA

### 7.1.3. Activity Test Results of Co-Mg Incorporated Catalysts in Conventionally Heated Reactor System

The synthesized Co-Mg incorporated MA type catalysts (Co-Mg-MA, Co-Mg@MA, Co@Mg-MA and Co@MA) were tested for SRE reaction (GC calibration is given in Appendix D) and the results are given and discussed in this section. Catalytic tests were performed at atmospheric pressure at 550°C. In each experiment, 0.15 g of catalyst was used. Catalytic activities of the materials were evaluated according to their ethanol conversion, hydrogen yield and product distributions which are defined as follows (sample calculation is given in Appendix E) ;

$$\text{Ethanol Conversion: } X_{\text{EtOH}} = \frac{\text{Moles of EtOH converted}}{\text{Moles of EtOH fed to the reactor}} * 100$$

$$\text{Hydrogen Yield: } Y_{\text{H}_2} = \frac{\text{Moles of H}_2 \text{ produced}}{\text{Moles of EtOH fed to the reactor}}$$

$$\text{Distribution of product 'i': } i\% = \frac{(\text{Moles of i produced})}{(\text{Total moles of all products})} * 100$$

Complete conversion of ethanol was achieved with all four catalysts, at a space time less than a second, which indicated very high activity of all of the synthesized materials. As shown in Figure 7.14, a drastic difference was observed in the hydrogen yield values obtained with the materials prepared by the impregnation of Co or Co-Mg into MA (Co@MA and Co-Mg@MA) and the materials prepared by the one-pot route for the incorporation of Mg into MA (Co@Mg-MA and Co-Mg-MA). Co-Mg-MA and Co@Mg-MA gave very high H<sub>2</sub> yield values, while the H<sub>2</sub> yield values obtained with Co@MA and Co-Mg@MA were close to zero. Co@Mg-MA gave the highest hydrogen yield value of about 5.2 per mole of ethanol reacted which corresponds to 90% of the maximum hydrogen yield value of 6.0. This result indicated that steam reforming of ethanol reaction dominated the reaction pathway over Co@Mg-MA catalyst. In the case of Co-Mg@MA and Co@MA catalysts, hydrogen yield values were close to zero indicated that a reaction or reactions other than SRE dominated the reaction pathway over these catalysts. In order to get information about the dominated reactions over Co-Mg incorporated catalysts, their product distribution data should be analyzed.

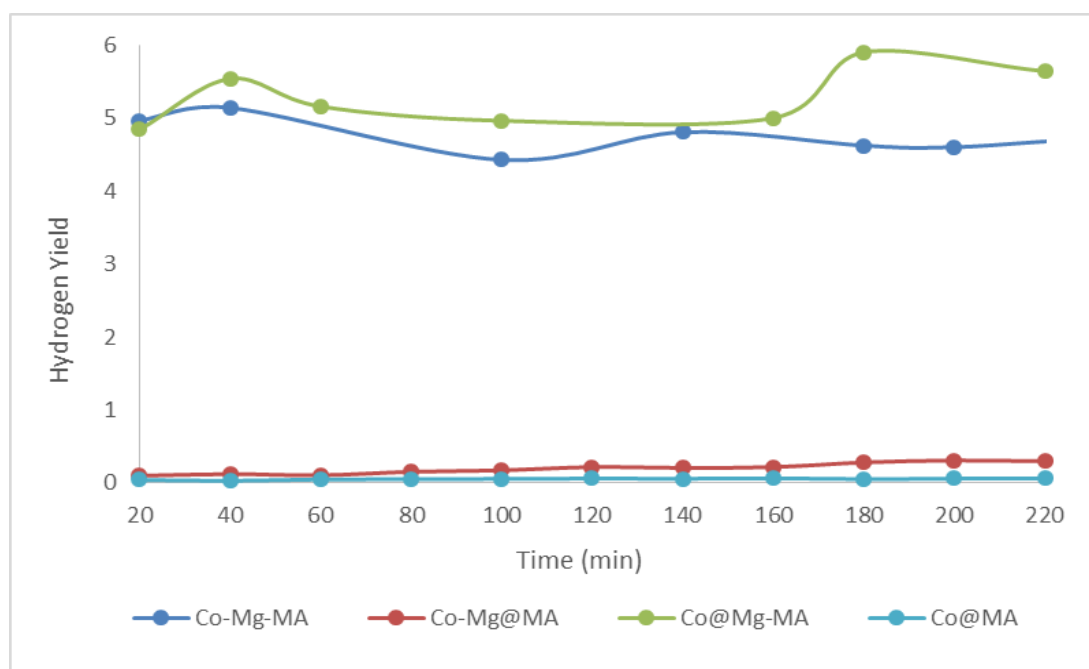


**Figure 7.14.** Hydrogen yield with respect to time data of Co-Mg incorporated catalysts obtained at 550°C

Differences of the catalytic performances of these four catalysts are more clearly seen in the product distributions. Product distributions of Co@Mg-MA, Co-Mg-MA, Co-Mg@MA and Co@MA with respect to time are shown in Figure 7.15, 7.16, 7.17 and 7.18, respectively. As illustrated in Figure 7.2 and Figure 7.3, the main product was H<sub>2</sub> (70-74% of the product stream) over Co@Mg-MA and Co-Mg-MA catalysts.

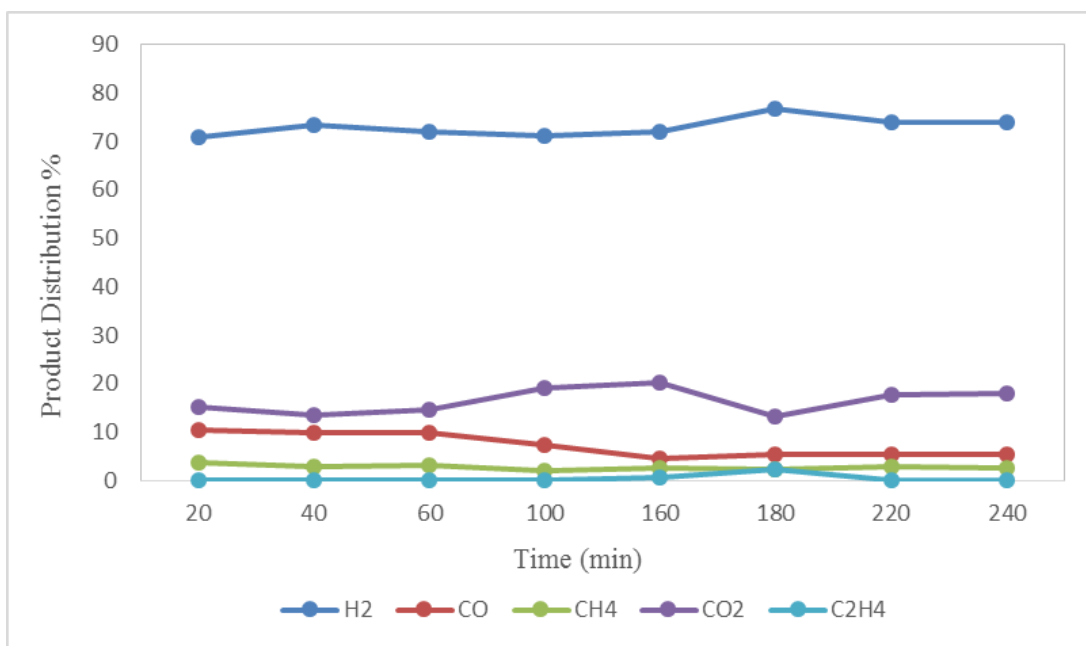


**Figure 7.15.** Product distribution of Co@Mg-MA catalyst

CO and CO<sub>2</sub> were the main side products and almost negligible amount of CH<sub>4</sub> and C<sub>2</sub>H<sub>4</sub> were produced. High amount of H<sub>2</sub> and CO<sub>2</sub> formation indicated that SRE reaction dominated the reaction pathway over Co@Mg-MA and Co-Mg-MA catalysts which is in agreement with the results reached by analyzing H<sub>2</sub> yield curves. Negligible amount of C<sub>2</sub>H<sub>4</sub> proved the negligible contribution of ethanol dehydration reaction over these Co@Mg-MA and Co-Mg-MA catalysts. Activity results of Co-Mg-MA and Co@Mg-MA catalysts are in agreement with the characterization results of these catalysts. According to XRD and XPS analysis, Co-Mg-MA and Co@Mg-MA catalysts had Co<sup>0</sup> and CoO phases in their structure which are known as the active phases in steam reforming of ethanol process. Therefore, high activity and high hydrogen yield observed with these catalysts can be attributed



to the presence of active  $\text{Co}^0$  and  $\text{CoO}$  phases in their structure. Additionally, according to DRIFTS analysis, presence of relatively low amount of Lewis acidity in the structure of these catalysts was not enough to dominate the reaction pathway through ethanol dehydration reaction. Lack of ethylene and high amount of hydrogen in the product stream of Co-Mg-MA and Co@Mg-MA catalysts suggested that while the selectivity of ethanol dehydration reaction over these catalysts was almost negligible, the selectivity of ethanol steam reforming reaction was extremely high.

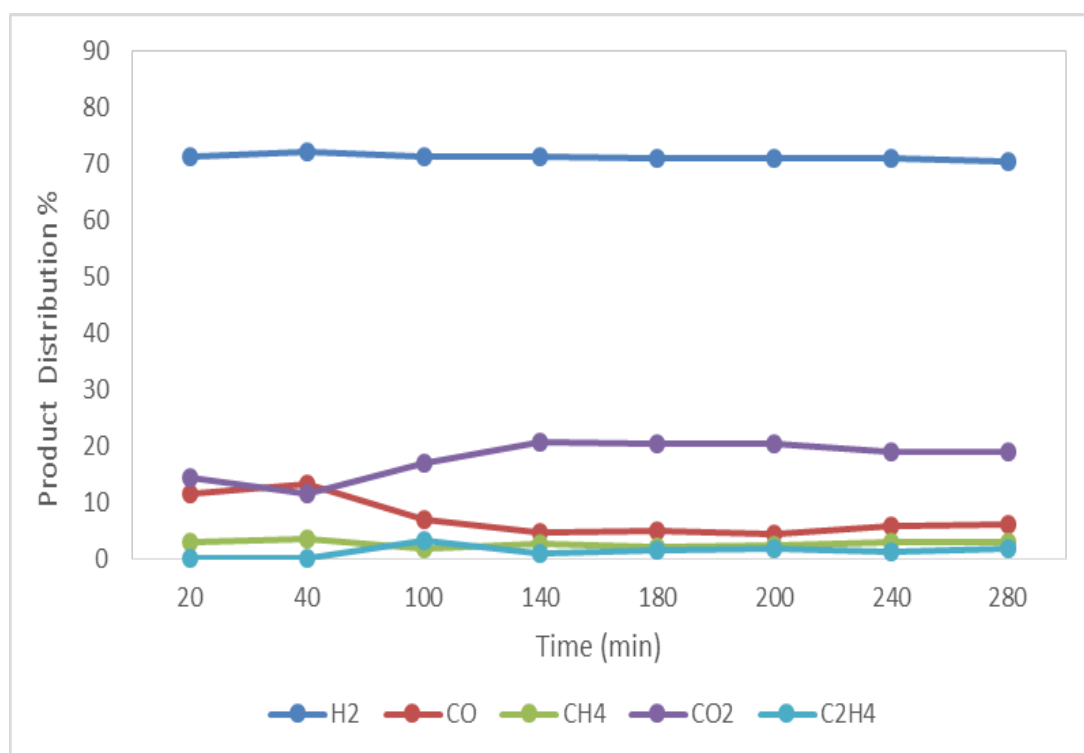


**Figure 7.16.** Product distribution of Co-Mg-MA catalyst

The main C-containing product was  $\text{C}_2\text{H}_4$  over Co-Mg@MA and Co@MA catalysts (Figure 7.17 and 7.18). High amount of  $\text{C}_2\text{H}_4$  in the product stream indicated that ethanol dehydration reaction dominated the reaction pathway over these Co-Mg@MA and Co@MA catalysts. Low amount of  $\text{H}_2$  observed in the product stream of these catalysts was most probably due to the lack of  $\text{Co}^0$  and  $\text{CoO}$  phases (proved by XRD and XPS analysis) in their structure that are active phases for SRE reaction and relatively high amount of Lewis acidity (proved by DRIFTS analysis) present in

their structure. Co-Mg@MA and Co@MA having higher intensity values of Lewis acid sites mainly catalyzed ethanol dehydration reaction rather than SRE. Therefore, it can be concluded that Co-Mg@MA and Co@MA catalysts are not active towards SRE reaction. However, especially Co@MA catalyst can be used for production of C<sub>2</sub>H<sub>4</sub> which is a valuable chemical in petrochemical industry.

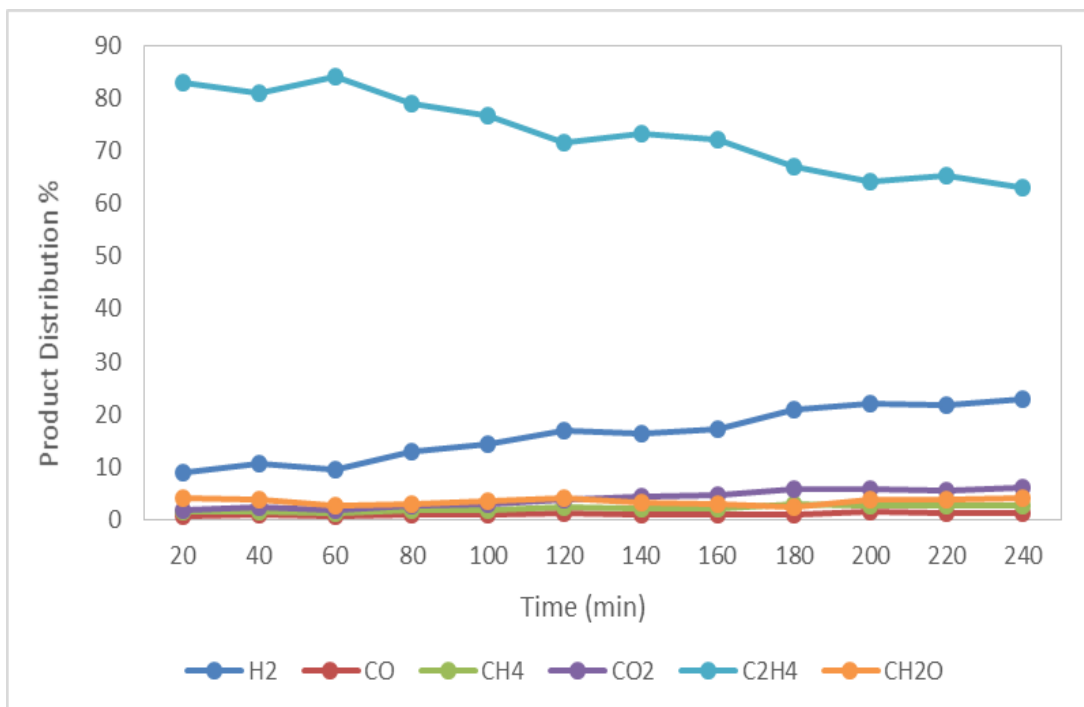


**Figure 7.17.** Product distribution of Co-Mg@MA catalyst

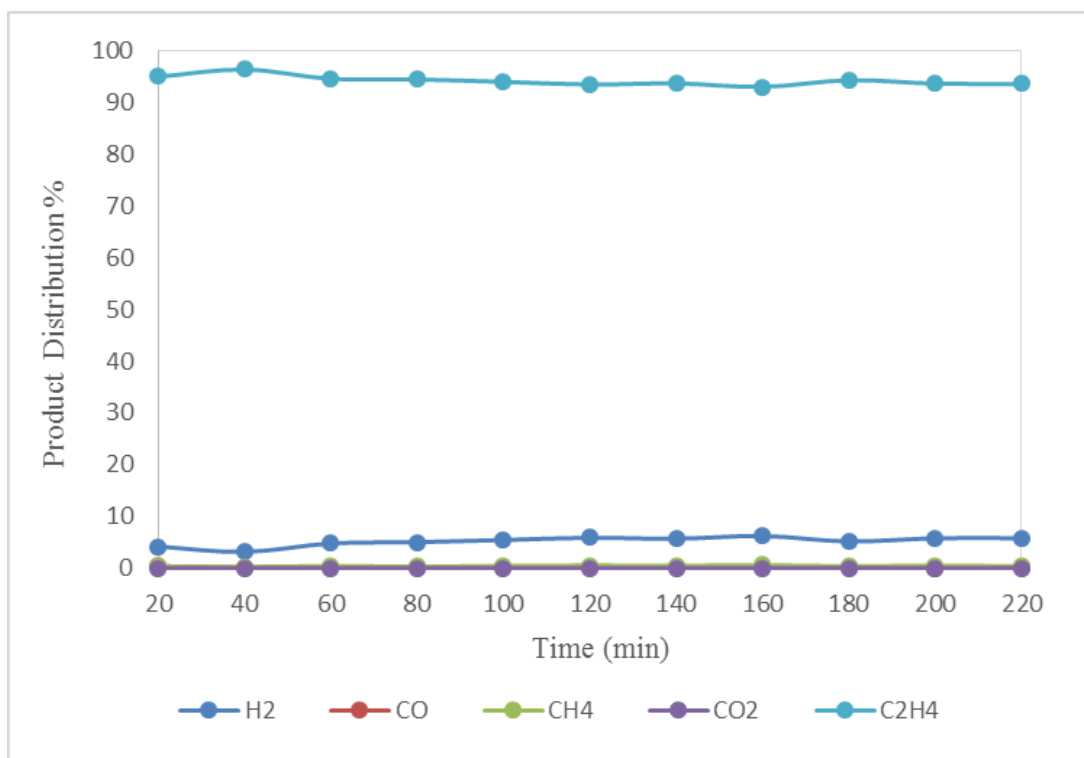


**Figure 7.18.** Product distribution of Co@MA catalyst

In order to analyze carbon deposition (coke formation) during reaction period, thermal gravimetric analysis (TGA) method was applied to used Co-Mg incorporated catalysts and the results are given in Figure 7.19.



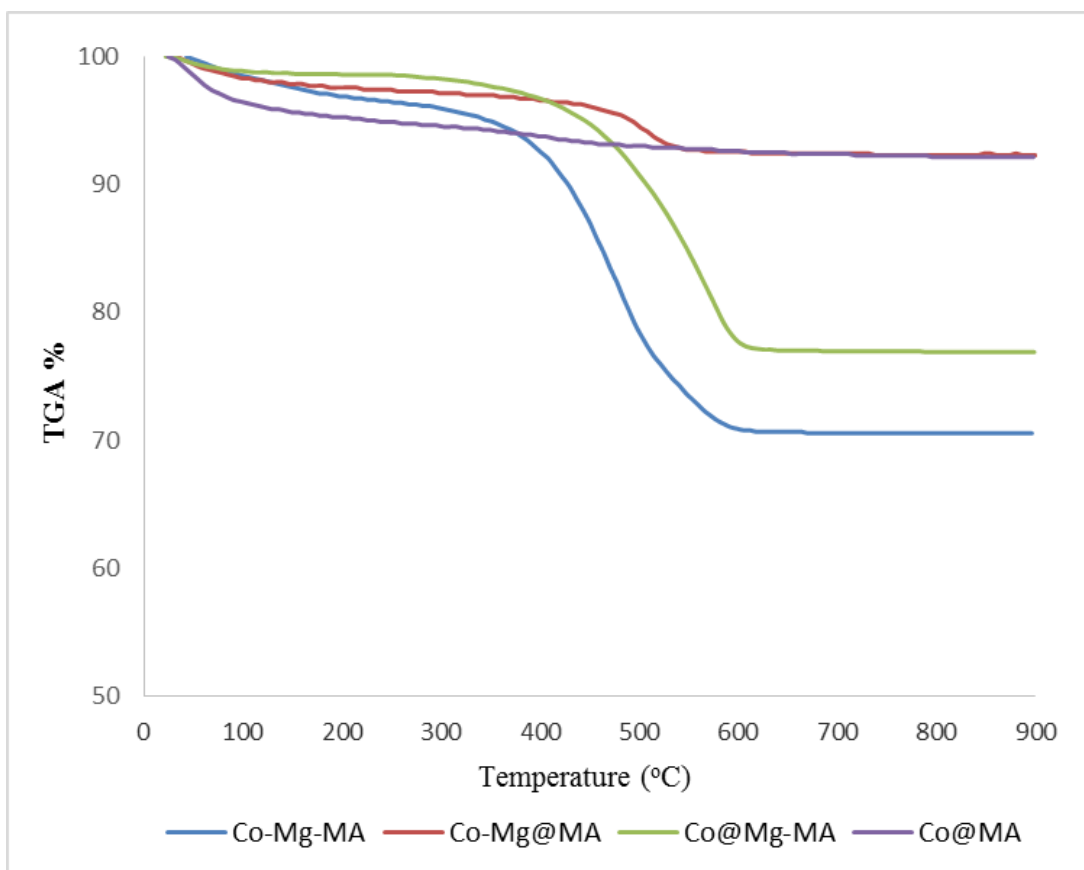


**Figure 7.19.** TGA curves of used Co-Mg incorporated catalysts

As shown in Figure 7.19, coke formation was negligible with the catalysts (Co-Mg@MA and Co@MA) that yield ethylene as the main product. However, about 20% coke formation was observed with the catalysts giving high hydrogen yields. This result indicated that coke formation mechanism over Co-Mg incorporated catalysts was not decomposition of ethylene to polymeric deposits (coke). The mechanism of the coke deposition over Co-Mg-MA and Co@Mg-MA catalysts was most probably Boudouard reaction which was supported by the high amount of CO<sub>2</sub> observed in their product stream.

#### **7.1.4. Activity Test Results of Co@Mg-MA Catalyst in the Focused-Microwave Reactor System**

In this part of the study, activity test result of the best catalyst among the Co-Mg incorporated catalysts (Co@Mg-MA) conducted in focused-microwave reactor system is presented and discussed.

In preliminary studies conducted in focused-microwave reactor system, it was realized that the catalyst itself can not be heated up to reaction temperature. In order to solve this problem, activated carbon was physically mixed with the catalyst to generate hot spots within the catalyst bed. Activated carbon used in focused-microwave reactor system is a product of Aldrich and has a density value of 0.25-0.60 g/cm<sup>3</sup>.

Co@Mg-MA catalyst was physically mixed with activated carbon at a ratio of 3 (0.15 g of catalyst and 0.05 g of activated carbon) and this mixture was charged to the reactor. Initially, generator power was set to 870 W and microwave was focused on the catalyst bed with the help of the piston, in order to create arcs to initiate microwave heating. The first moment that the arc appeared is shown in Figure 7.20.

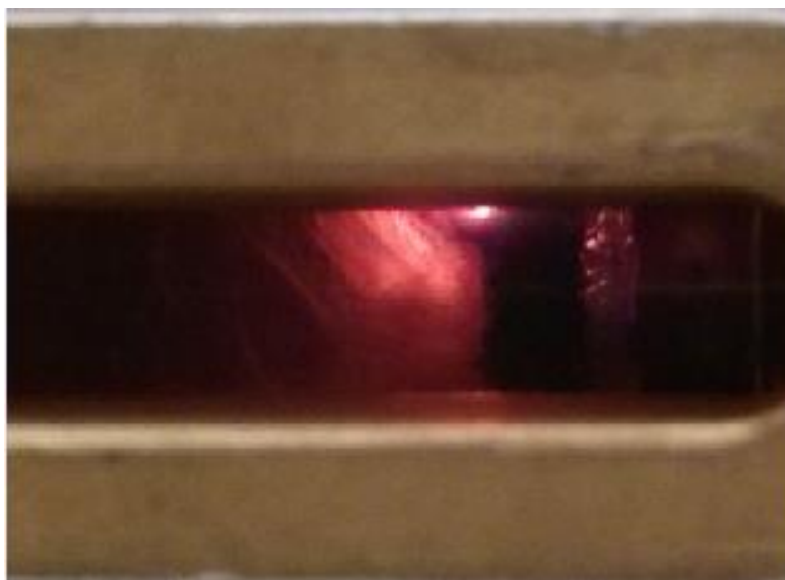


**Figure 7.20.** Picture of first moment of arc formation within the catalyst bed

Within 2-3 minutes after the start of the experiment, catalyst bed bulk temperature raised to 560°C, then the power was decreased and finally kept constant at 300 W in order to keep the temperature within the range of 550-560°C. Although 300 W microwave power sent to the system, catalyst-activated carbon mixture only absorbed 10 W of this power, while the remaining microwave was absorbed by cooling water in the recirculator placed between the magnetron and applicator.

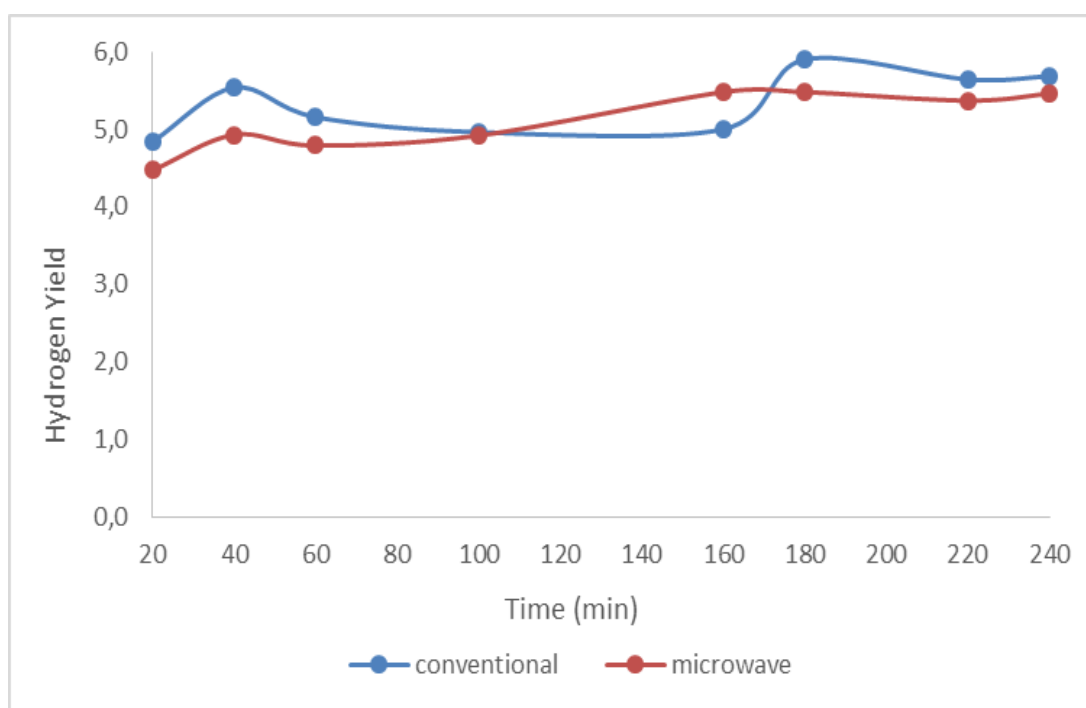


**Figure 7.21.** Hydrogen yield of Co@Mg-MA in conventionally heated and microwave reactors

Hydrogen yield values obtained in the reaction systems with both conventional heating and microwave heating are compared in Figure 7.21. Results indicated comparable H<sub>2</sub> yield values. However, time variation of product distributions showed were more stable in the microwave reactor.

A more important result is related to the coke formation. In the case of microwave heating, coke formation was much less than conventional heating (Figure 7.22).

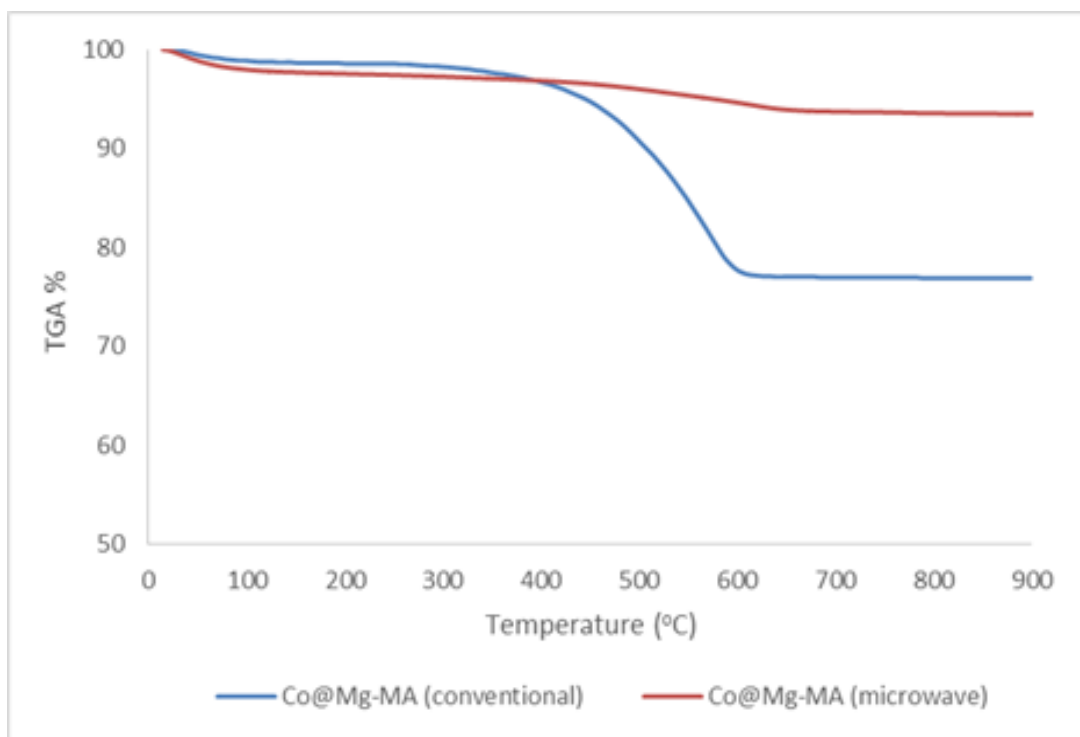


**Figure 7.22.** TGA curves of used Co@Mg-MA catalyst in conventionally heated and microwave reactors

These observations could be explained by the fact that temperature gradients were minimized in the microwave reactor and quite uniform temperature distribution were achieved. In the case of conventional heating, temperature gradients within the catalyst bed are inevitable for such an endothermic reaction.

Since the thermodynamics of coke formation by Boudouard reaction becomes more favorable at lower temperatures, such temperature gradients may cause coke formation at the lower temperature locations. Product distributions obtained in microwave and conductive heating reactors also justified this conclusion, giving more CO than CO<sub>2</sub> in the microwave reactor (20% CO and 6% CO<sub>2</sub> in product stream) illustrated in Figure 7.23, while Boudouard reaction yielded more CO<sub>2</sub> in the conductively heated reactor (19% CO<sub>2</sub> and 6% CO) shown in Figure 7.24.

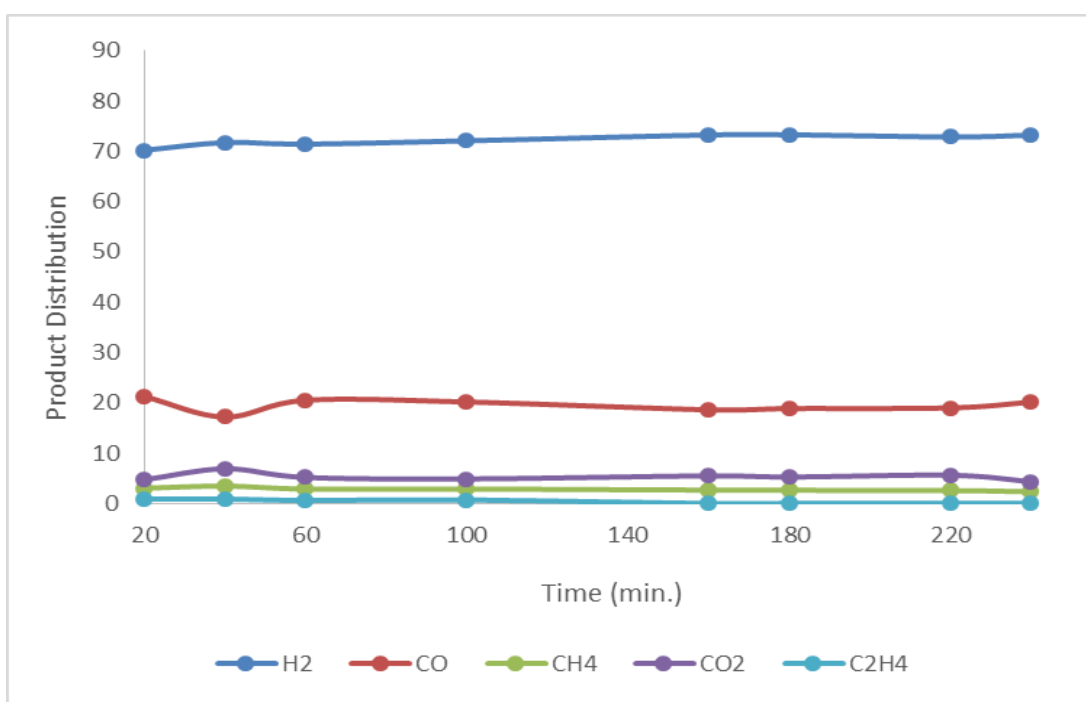


**Figure 7.23.** Product distribution of Co@Mg-MA catalyst in microwave reactor system

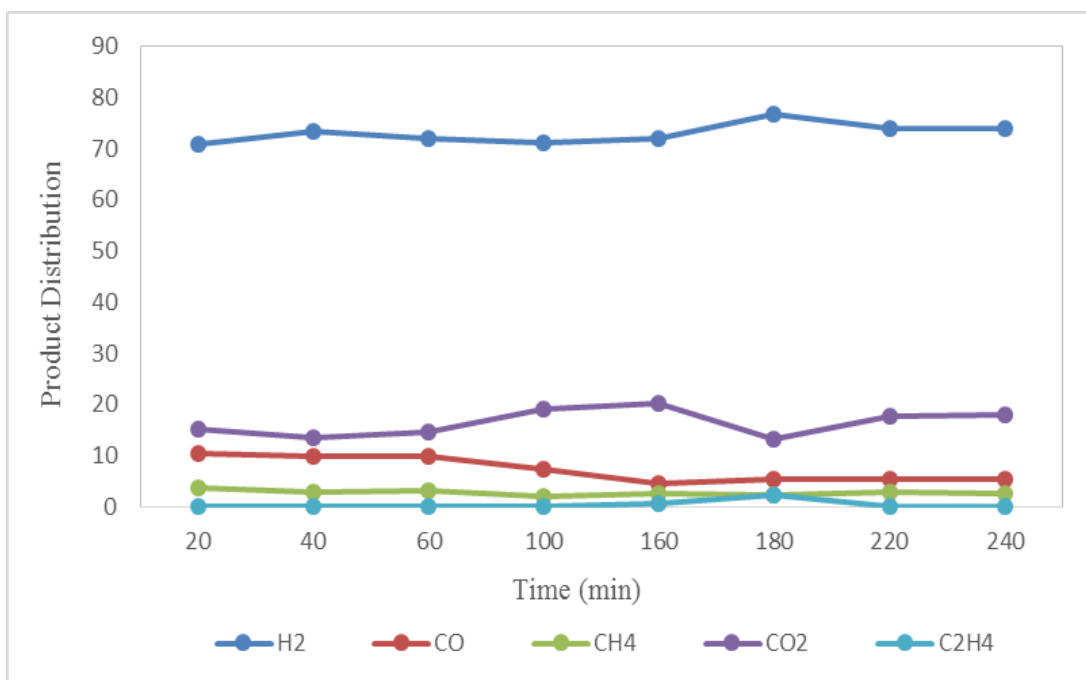


**Figure 7.24.** Product distribution of Co@Mg-MA catalyst in conventionally heated reactor

In order to investigate the catalyst stability and reliability of microwave reactor, time-on stream reaction test, extending upto 80 h, was performed in the focused-microwave reactor system. As shown in Figure 7.25, hydrogen yield curve indicated that Co@Mg-MA catalyst was highly stable up to 80 h in microwave reactor system. More importantly, according to TGA result, coke deposition was not high (about 14%) after 80 h of reaction in this system, which was only 0.2% in a one hour test. Product distribution of Co@Mg-MA catalyst is given in Figure 7.26 which also supports the stability of the catalyst during reaction period in focused-microwave reactor system.

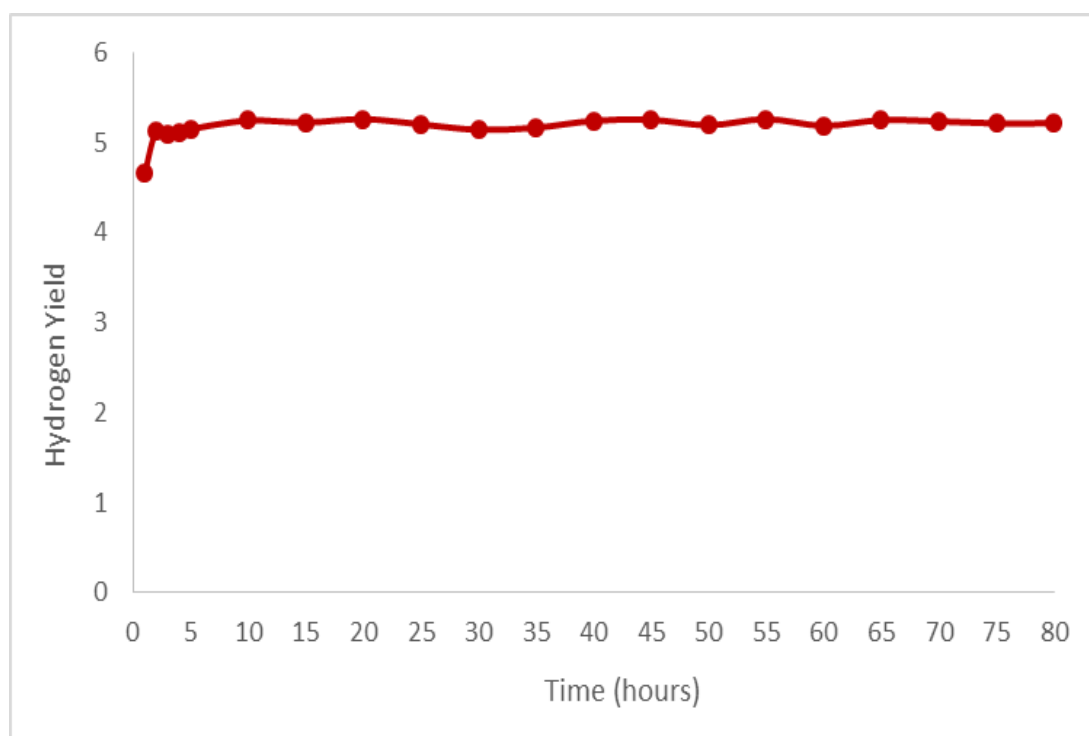


**Figure 7.25.** Hydrogen yield of Co@Mg-MA in microwave reactor (long-term stability test)

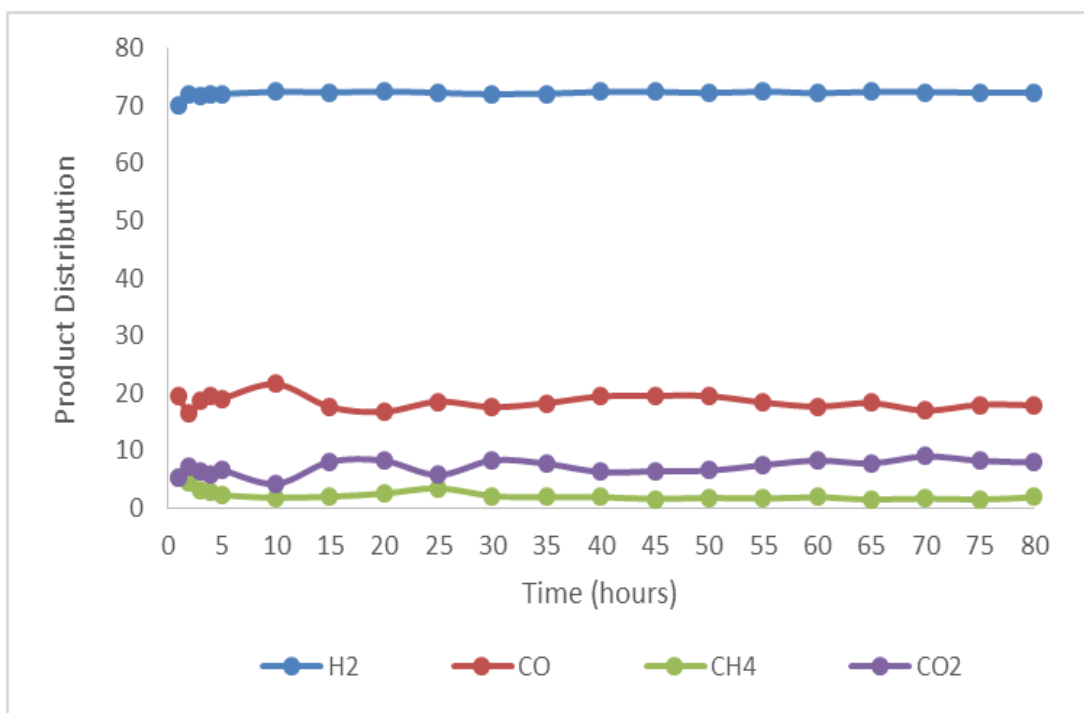


**Figure 7.26.** Product distribution of Co@Mg-MA in MW reactor (long-term stability test)

## PART 2: Ni-Mg Incorporated MA Type Catalysts

In this part, characterization and activity test results of Ni-Mg incorporated MA type catalysts synthesized by both direct synthesis and impregnation methods are given and discussed.

### 7.2. Results of Ni-Mg Incorporated MA Type Catalysts

Firstly, Ni-Mg-MA, Ni-Mg@MA and Ni@Mg-MA catalysts were characterized by N<sub>2</sub> physisorption, X-ray diffraction, DRIFTS analysis of pyridine adsorbed samples and scanning electron microscopy (SEM) techniques. Then, synthesized catalysts were tested for SRE reaction in conventionally heated reactor system and activity test results of the catalysts were collected and analyzed. In order to analyze coke deposition during reaction period, thermal gravimetric analysis (TGA) method was

applied to used catalysts. Finally, the best catalyst towards SRE reaction was tested in the focused-microwave reactor system.

### 7.2.1. Characterization Results of Ni-Mg Incorporated Catalysts

In order to investigate physical and chemical properties of Ni-Mg incorporated MA type catalysts, N<sub>2</sub> physisorption, X-ray diffraction (XRD), Diffuse reflectance infrared fourier transform spectroscopy (DRIFTS) of pyridine adsorbed samples and scanning electron microscopy (SEM) type characterization methods were applied and the results of these characterization studies are given and discussed in this section.

#### 7.2.1.1. N<sub>2</sub> Physisorption Analysis Results of Ni-Mg Incorporated Catalysts

In order to investigate the textural properties of the synthesized catalysts, nitrogen physisorption characterization method was applied. Surface area values, pore diameters and pore volumes of the synthesized catalysts are shown in Table 7. 2. Both surface area and pore volume values decreased by the impregnation of Mg and Ni. Some decrease in the pore diameter was also observed as a result of impregnation of Mg, indicating blocking of some of the pores by the impregnated Mg particles. On the contrary, direct addition of Mg into the MA structure enhanced both the surface area and pore volume.

**Table 7. 2.** Textural properties of synthesized materials

Material	BET Surface Area (m <sup>2</sup> /g)	BJH Pore Volume (cc/g)	BJH Pore Diameter (nm)
Ni-Mg-MA	213.1	0.69	9.7
Ni@Mg-MA	128.1	0.41	9.6
Ni-Mg@MA	116.8	0.27	5.6

Nitrogen adsorption-desorption isotherm curves of Ni based catalysts are shown in Figure 7.27. Steep and parallel hysteresis loops which are the characteristics of the formation of mesopores were observed for Ni-Mg-MA and Ni@Mg-MA catalysts



synthesized by direct addition of Mg. However in the case of Ni and Mg impregnated material (Ni-Mg@MA), this characteristic behavior was partially lost, indicating deformations in the long-range order of mesopores.

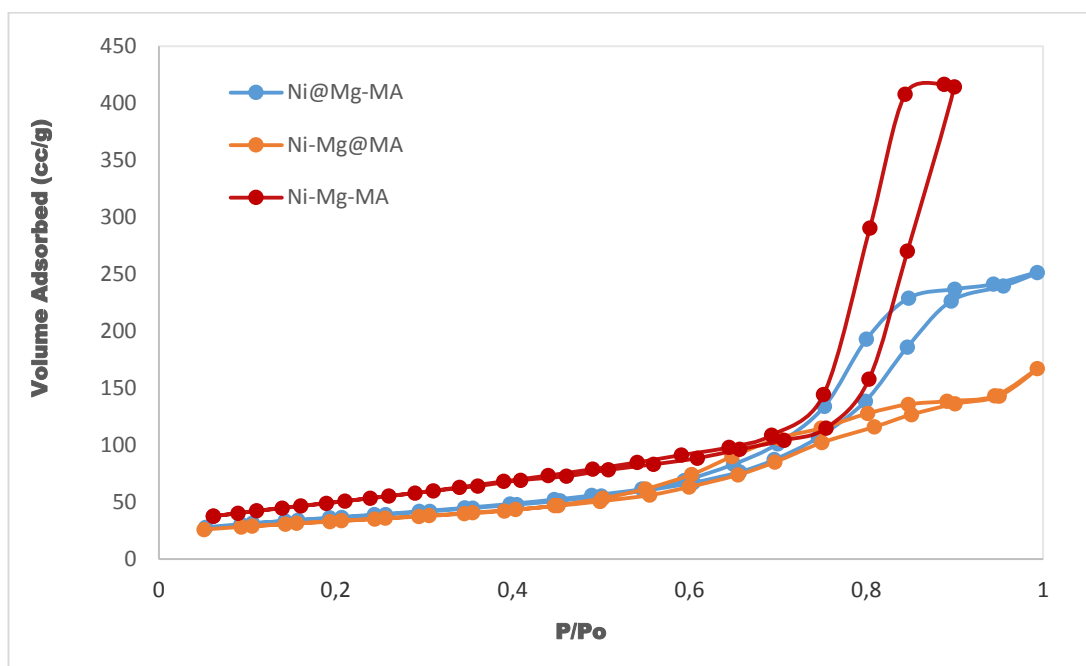


**Figure 7.27.** Nitrogen physisorption isotherms of Ni-Mg incorporated catalysts

Pore size distribution curves of Co-Mg incorporated MA type catalysts are given in Figure 7.28.

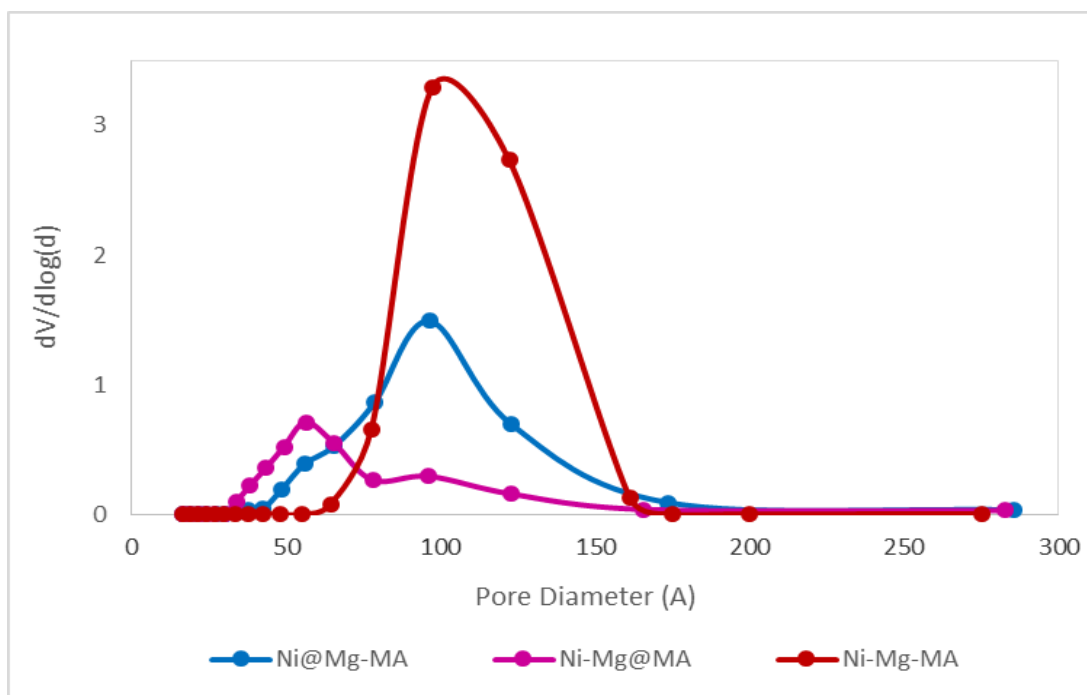


**Figure 7.28.** Pore size distribution of Ni-Mg incorporated catalyst

### 7.2.1.2. X-Ray Diffraction (XRD) Analysis Results of Ni-Mg Incorporated Catalysts

XRD patterns of Ni-Mg incorporated catalysts are illustrated in Figure 7.29. As shown in this figure, both catalysts had metallic Ni, NiO and NiAl<sub>2</sub>O<sub>4</sub> crystals in their framework. Metallic Ni crystal sizes of Ni-Mg-MA, Ni@Mg-MA and Ni-Mg@MA catalysts were calculated as 20 nm, 7 nm and 6 nm from the Scherrer equation, respectively.

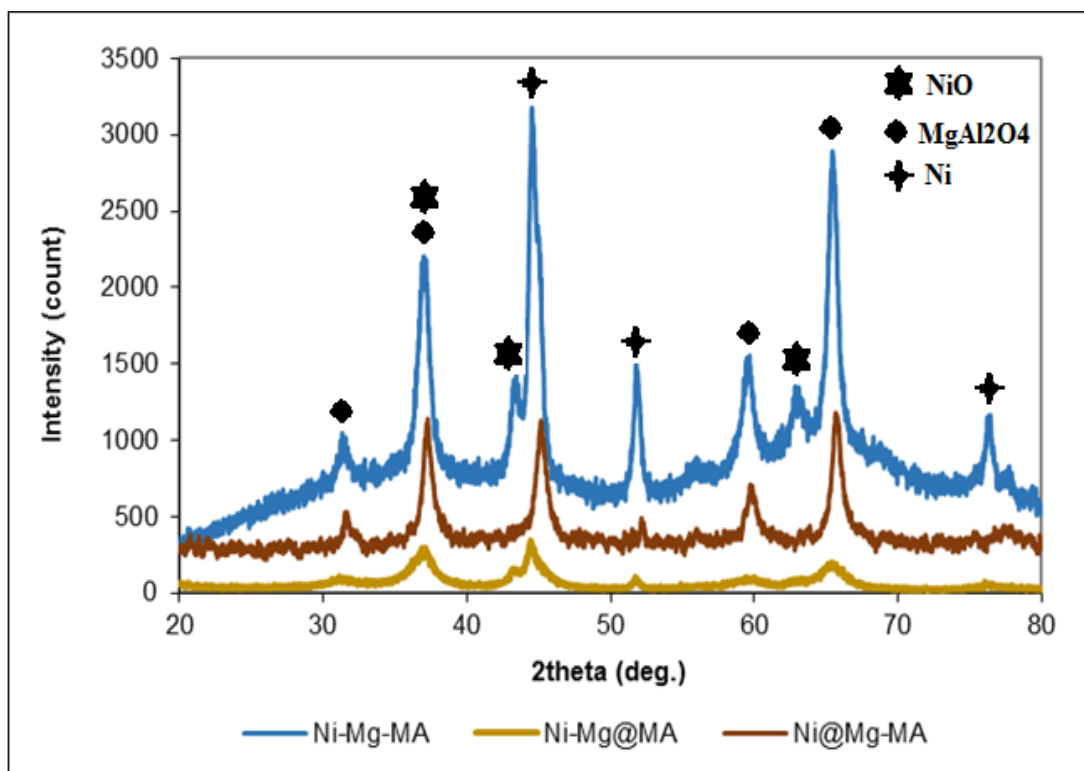


**Figure 7.29.** XRD patterns of Ni-Mg incorporated catalysts

### 7.2.1.3. DRIFT Spectra (DRIFTS) Analysis Results of Pyridine Adsorbed Ni-Mg Incorporated Catalysts

Figure 7.30 illustrates the DRIFT spectra of pyridine adsorbed Ni-Mg incorporated catalysts. Transmission bands observed at 1445 and 1592  $\text{cm}^{-1}$  corresponds to Lewis acid sites. Results indicated that, while the Lewis acid intensity of the Ni@Mg-MA catalyst prepared with impregnation of Ni and direct addition of Mg was very high, it was very low in Ni-Mg-MA synthesized by direct addition of both Ni and Mg.

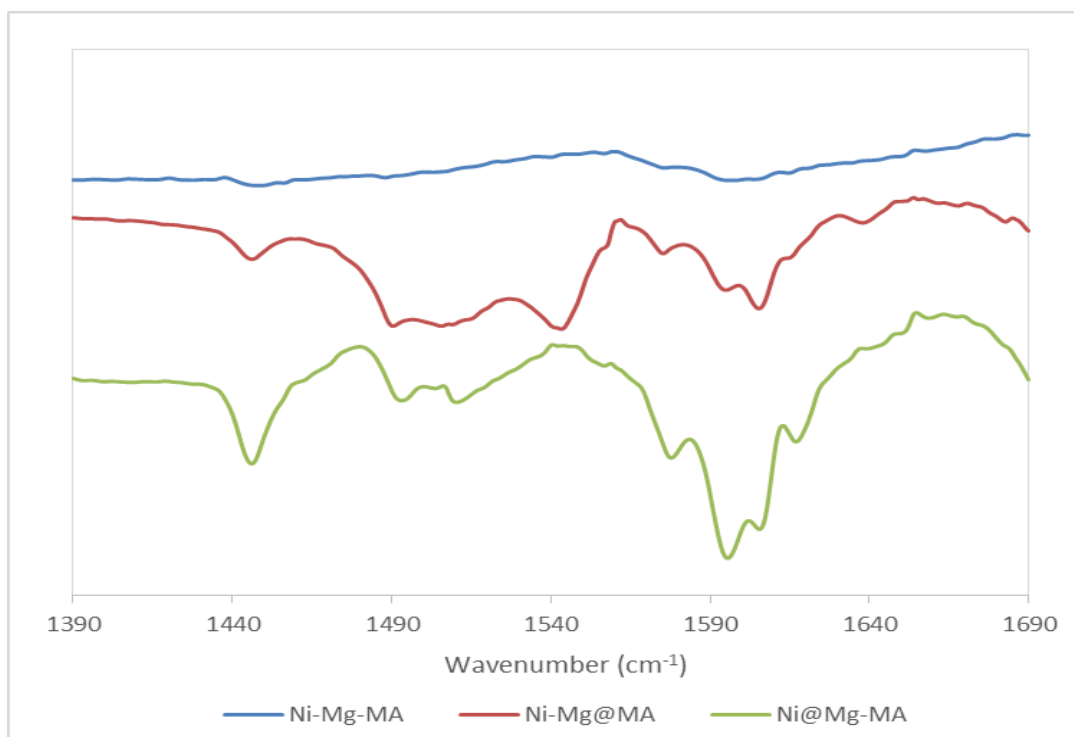


**Figure 7.30.** DRIFT spectra of Ni-Mg incorporated catalyst

#### **7.2.1.4. Scanning Electron Microscopy (SEM) Analysis of Ni-Mg Incorporated Catalysts**

SEM images of Ni-Mg-MA and Ni@Mg-MA catalysts are illustrated in Figure 7.31 and 7.32, respectively.

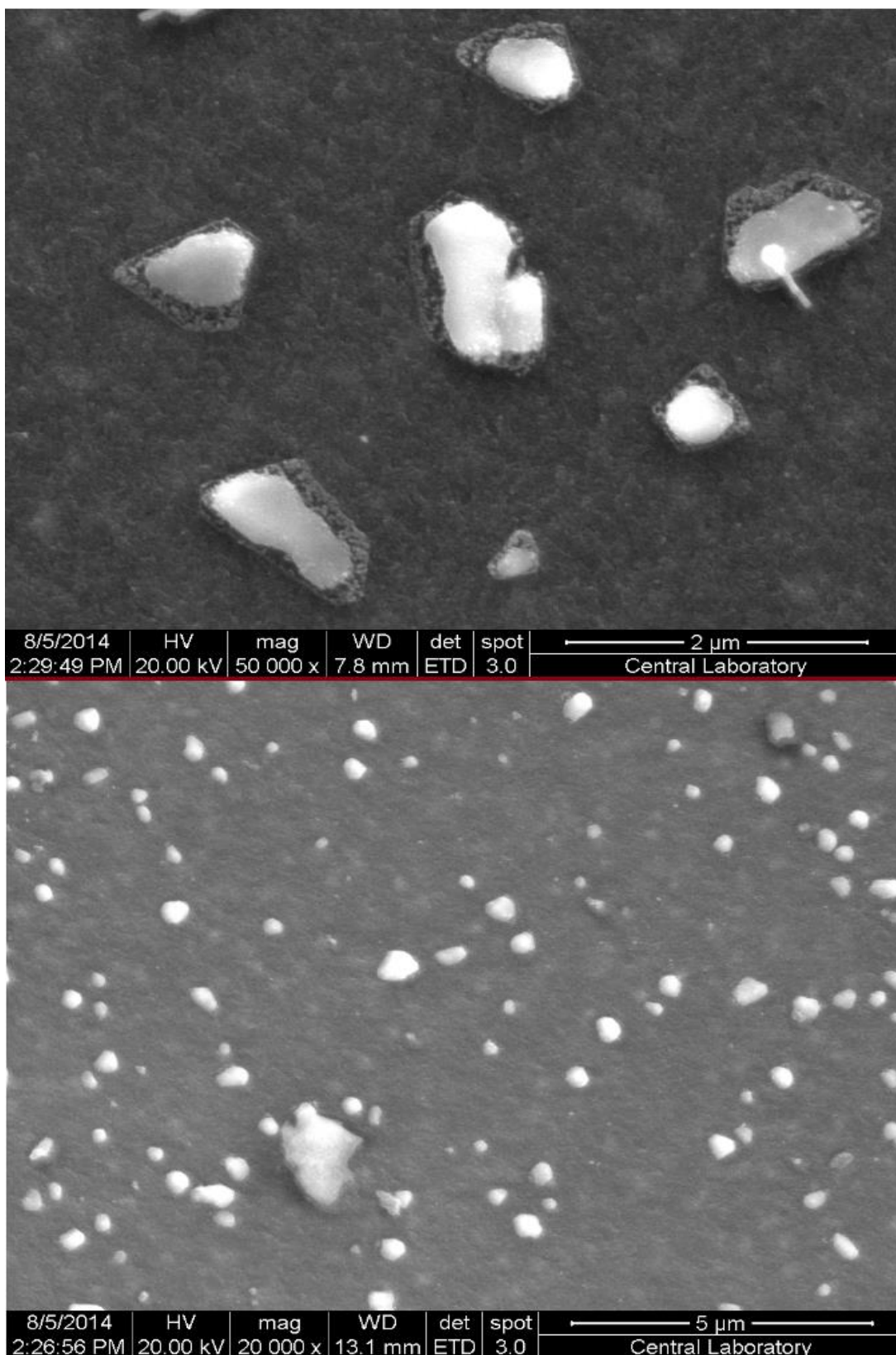


**Figure 7.31.** SEM images of Ni-Mg-MA catalyst

In SEM images of Ni-Mg-MA, large, cluster type structures, most probably Ni and/or NiO clusters, with an approximate diameter of 500 nm were observed over the catalyst surface.

Unlike Ni-Mg-MA catalyst, large cluster type structures were not observed in SEM image of Ni@Mg-MA catalyst.

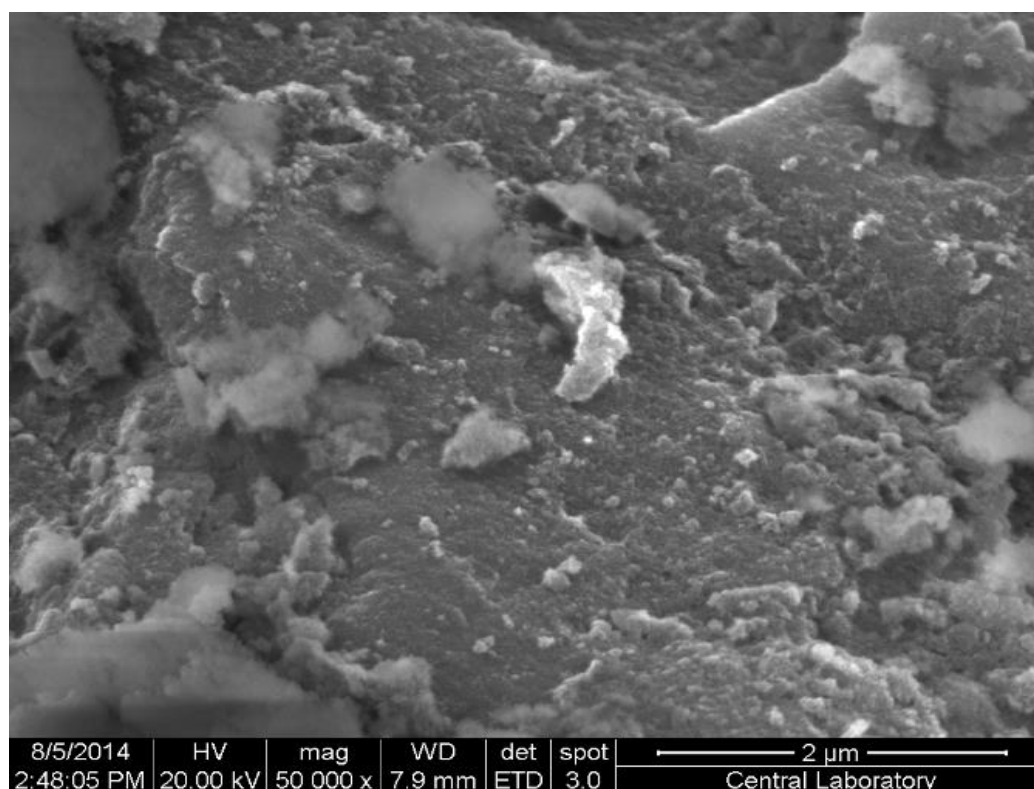


**Figure 7.32.** SEM image of Ni@Mg-MA catalyst

### **7.2.2. Activity Test Results of Ni-Mg Incorporated Catalysts in Conventionally Heated Reactor System**

The synthesized Ni-Mg incorporated MA type catalysts (Ni-Mg-MA, Ni-Mg@MA and Ni@Mg-MA) were tested for SRE reaction and the results are given and discussed in this section. Catalytic tests were performed at atmospheric pressure at 550°C. In each experiment, 0.15 g of catalyst was used. Catalytic activities of the synthesized materials were evaluated according to their ethanol conversion, hydrogen yield and product distributions.

Complete conversion of ethanol was achieved with all three catalysts, at a space time less than a second, which indicated very high activity of all of the synthesized materials. As shown in Figure 7.33, unlike Co-Mg based catalysts, a drastic difference was not observed between the hydrogen yield values of Ni-Mg incorporated catalysts. The average hydrogen yield values of Ni-Mg-MA, Ni-Mg@MA and Ni@Mg-MA catalysts were 4.0, 4.5 and 5.1, respectively. Hydrogen yield curves indicated that, catalyst prepared with direct addition of Mg and impregnation of Ni gave the best activity towards SRE reaction with a H<sub>2</sub> yield value of 5.1, which is 85% of the maximum hydrogen yield value of 6.0. However in the case of Ni-Mg-MA catalyst prepared with direct addition of Ni and Mg, hydrogen yield value was 4.0, which is about 67% of maximum hydrogen yield that can be achieved in SRE reaction. This result implied that impregnation of Ni resulted in a better catalyst for SRE reaction than direct addition of Ni. This is most probably due to higher availability of surface Ni sites in the case of impregnated material, than the material prepared by the one-pot route.

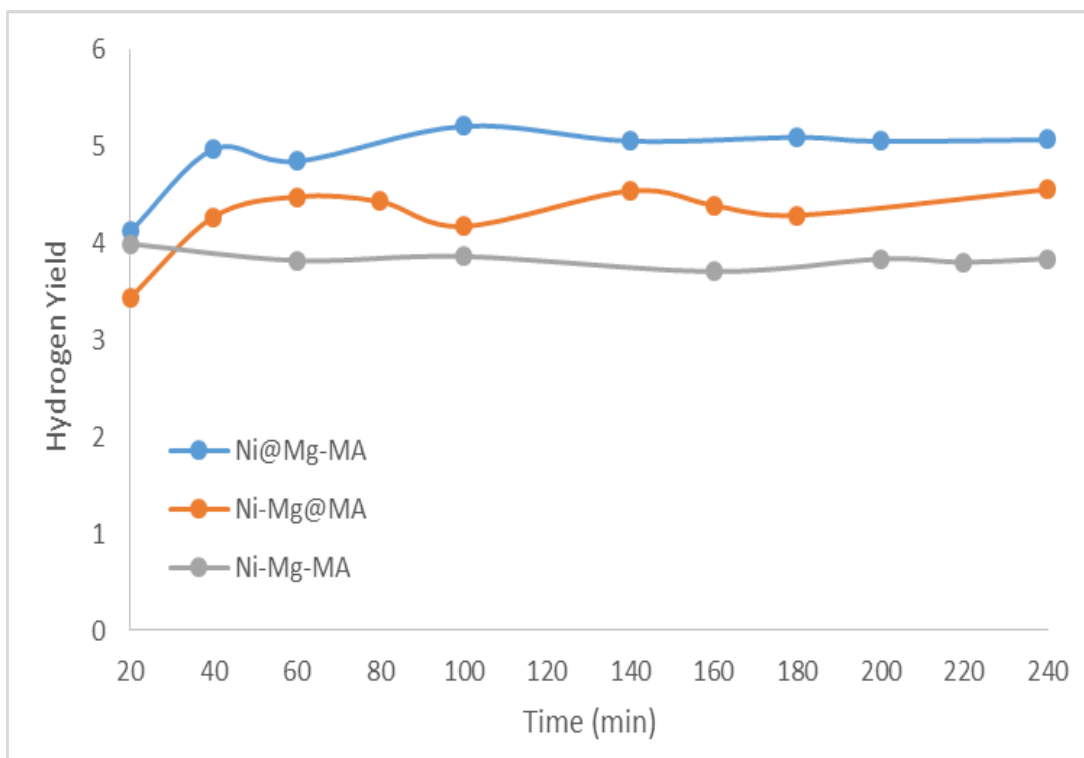


**Figure 7.33.** H<sub>2</sub> yield curves of Ni-Mg incorporated catalysts obtained at 550°C

Product distribution curves of Ni-Mg-MA, Ni-Mg@MA and Ni@Mg-MA catalysts are given in Figure 7.34, 7.35 and 7.36, respectively. The main carbon-containing side products were CO and CH<sub>4</sub> for all Ni-Mg incorporated catalysts.

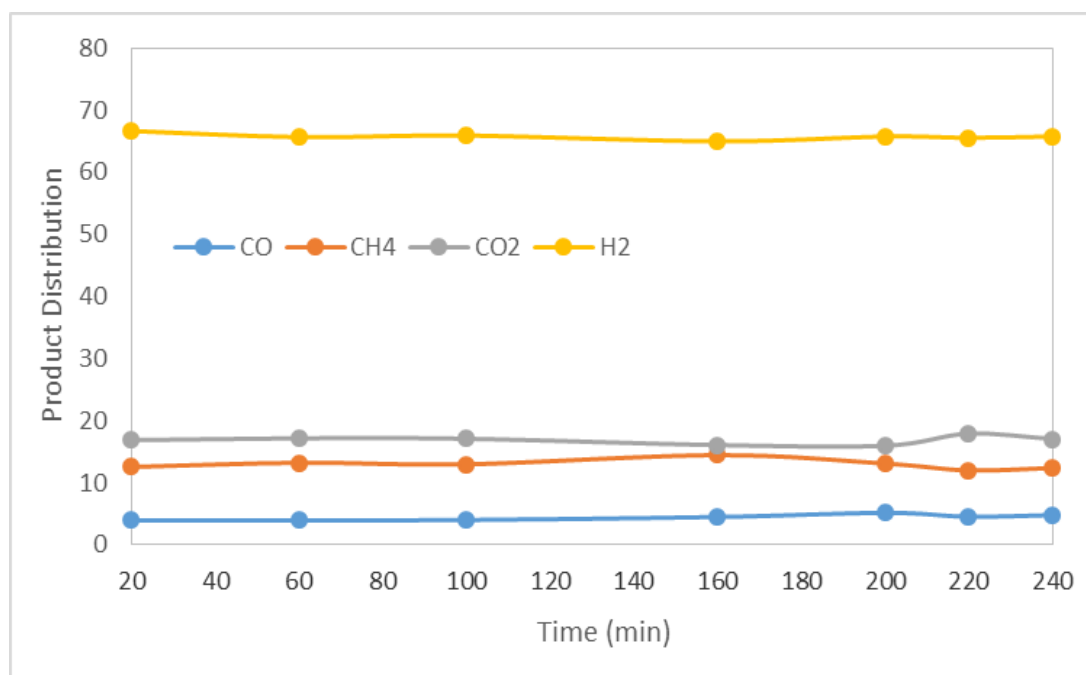


**Figure 7.34.** Product distribution of Ni-Mg-MA

The major difference between the product distributions of Ni-Mg incorporated catalysts was the amount of CH<sub>4</sub> in the product stream. Ni-Mg-MA catalyst produced by direct synthesis method yielded more CH<sub>4</sub> that resulted in lower hydrogen yield over this catalyst. Crystalline size of metallic nickel has significant impact on the catalytic activity of methanation. Takenaka et al. [117] have reported that Ni particles with relatively large diameters yielded a higher catalytic activity in the methanation of CO (Eqn. 7.1) over supported nickel catalysts.



Therefore, the higher CH<sub>4</sub> concentration and lower H<sub>2</sub> yield of Ni-Mg-MA catalyst can be explained by the larger Ni particles in the structure of this catalyst.



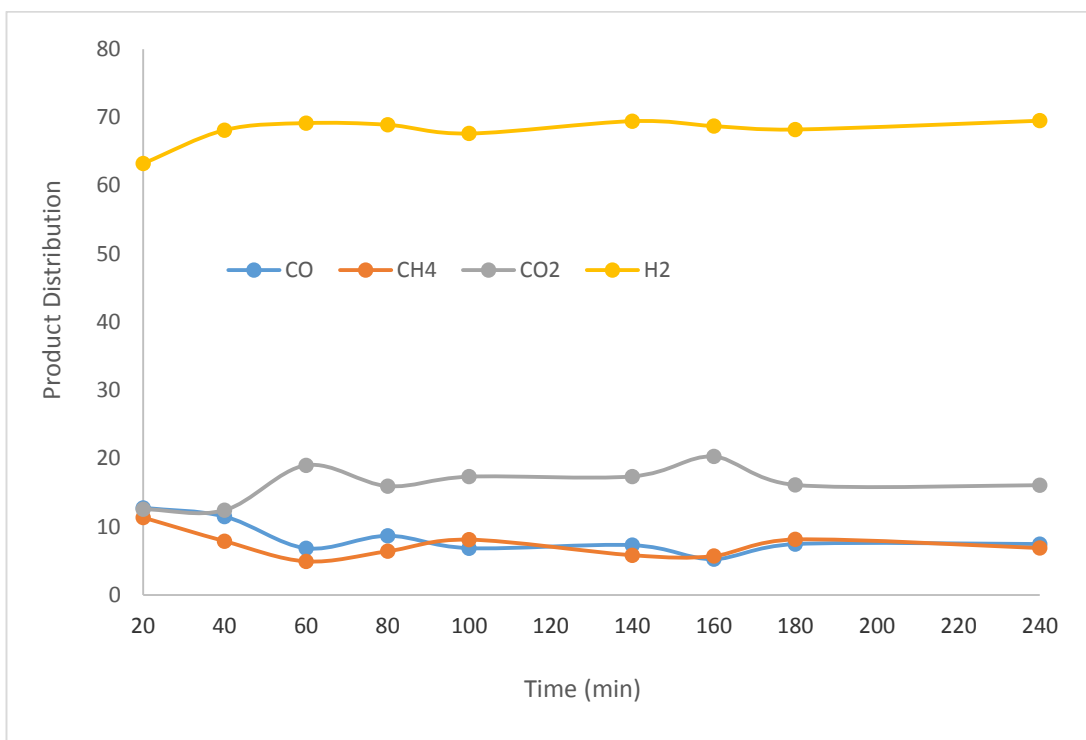


**Figure 7.35.** Product distribution of Ni-Mg@MA

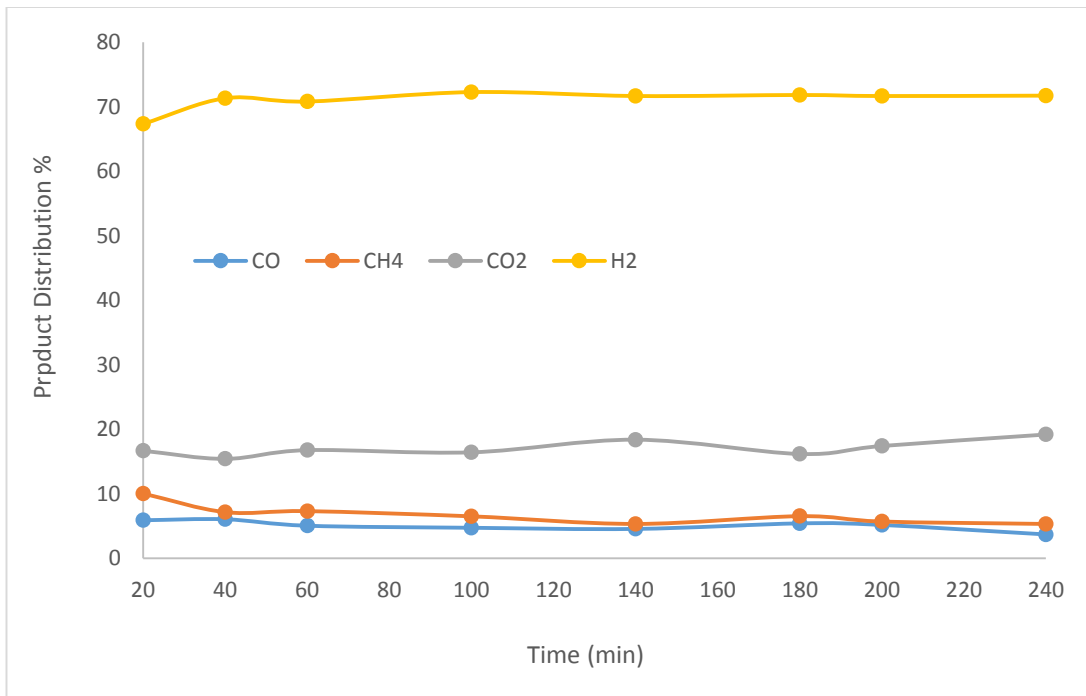


**Figure 7.36.** Product distribution of Ni@Mg-MA

In order to analyze carbon deposition (coke formation) during reaction period, thermal gravimetric analysis (TGA) method was applied to the used Ni-Mg incorporated catalysts and the results are given in Figure 7.37.

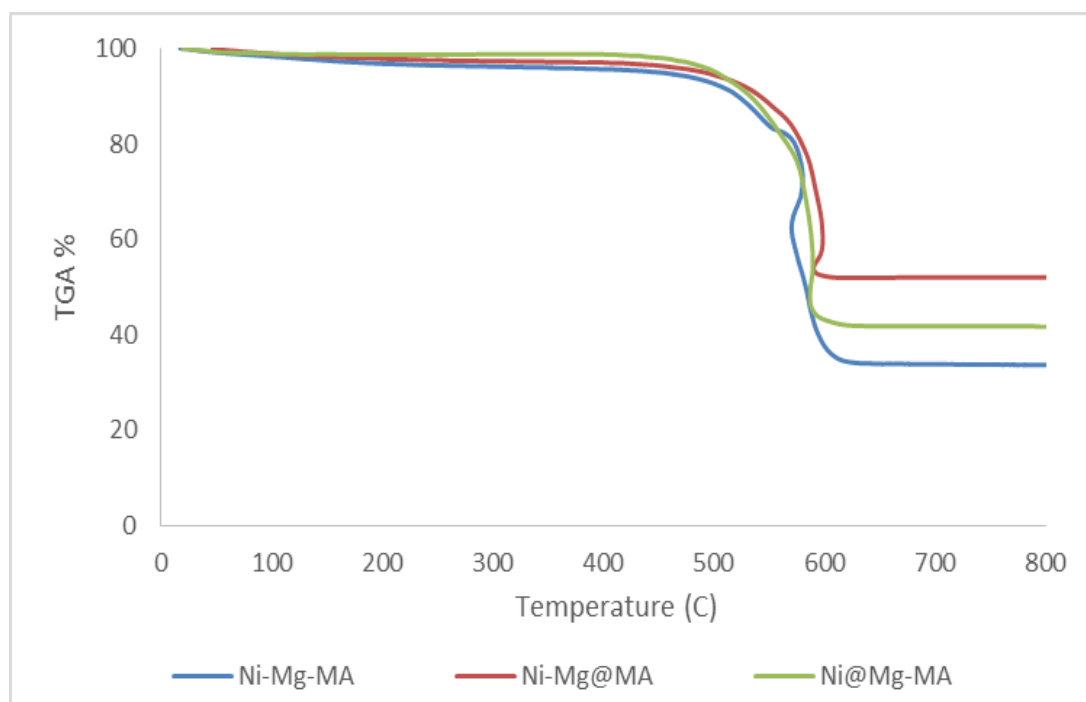


**Figure 7.37.** TGA curves of used Ni-Mg incorporated catalysts

As shown in Figure 7.37, coke deposition was very high in Ni incorporated catalysts. In fact, coke deposition was highest over Ni-Mg-MA.

Duprez et al. [118] who studied hydrogenolysis of cyclopentane over Ni@Al<sub>2</sub>O<sub>3</sub> catalyst reported that Ni particle size could affect both catalytic activity and coke formation. They discovered that a minimum metal particle diameter, 6 nm, was required to form filamentous carbon. In our case, all Ni-Mg incorporated catalysts had larger Ni particle sizes than the minimum value of 6 nm, therefore, coke formation was very high for all three catalysts. The catalyst with the highest Ni particle size (Ni-Mg-MA) gave the highest carbon yield and the catalyst including the smallest Ni particle size (Ni-Mg@MA) gave the lowest carbon yield.

### **7.2.3. Activity Test Results of Ni@Mg-MA Catalyst in the Focused-Microwave Reactor System**

Ni@Mg-MA catalyst was physically mixed with activated carbon at a ratio of 3 (0.15 g of catalyst and 0.05 g of activated carbon) and this mixture was charged to the reactor. Initially, generator power was set to 800 W and microwave was focused on the catalyst bed with the help of the piston, in order to create arcs to initiate microwave heating.

Within 2-3 minutes after the start of the experiment, catalyst bed bulk temperature raised to 560°C, then the power was decreased and finally kept constant at 220 W in order to keep the temperature within the range of 550-560°C. Although 220 W microwave power sent to the system, catalyst-activated carbon mixture only absorbed 10 W of this power, while the remaining microwave was absorbed by cooling water in the recirculator placed between the magnetron and applicator.

Hydrogen yield values obtained over Ni@Mg-MA catalyst in the reaction systems with both conventional heating and microwave heating are compared in Figure 7.38. Results indicated comparable H<sub>2</sub> yield values. However, time variation of hydrogen yield was more stable in the microwave reactor.

TGA curves of used Ni@Mg-MA catalyst obtained in both conventionally heated and microwave reactor systems (Figure 7.39) showed similar behavior with TGA curves of used Co@Mg-MA catalyst. As shown in Figure 7.39, while the coke deposition on the Ni@Mg-MA catalyst was about 60% in conventionally heated system, it was nearly zero in microwave reactor system.

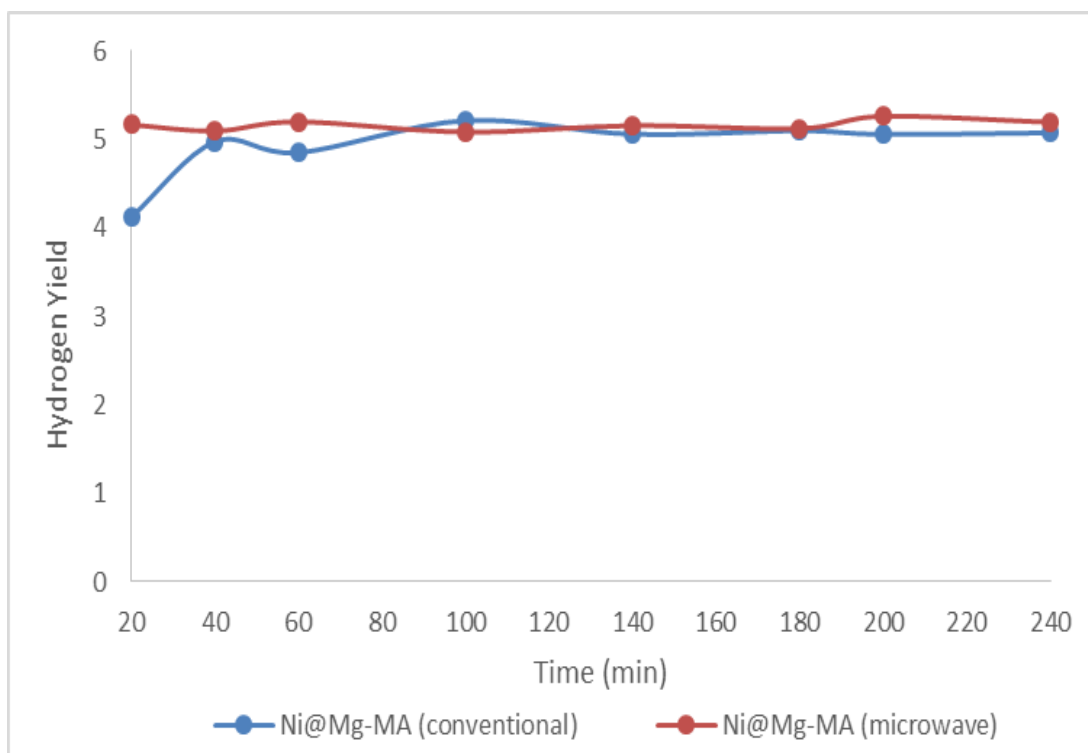


**Figure 7.38.** Hydrogen yield of Ni@Mg-MA in both conventionally heated and microwave reactors

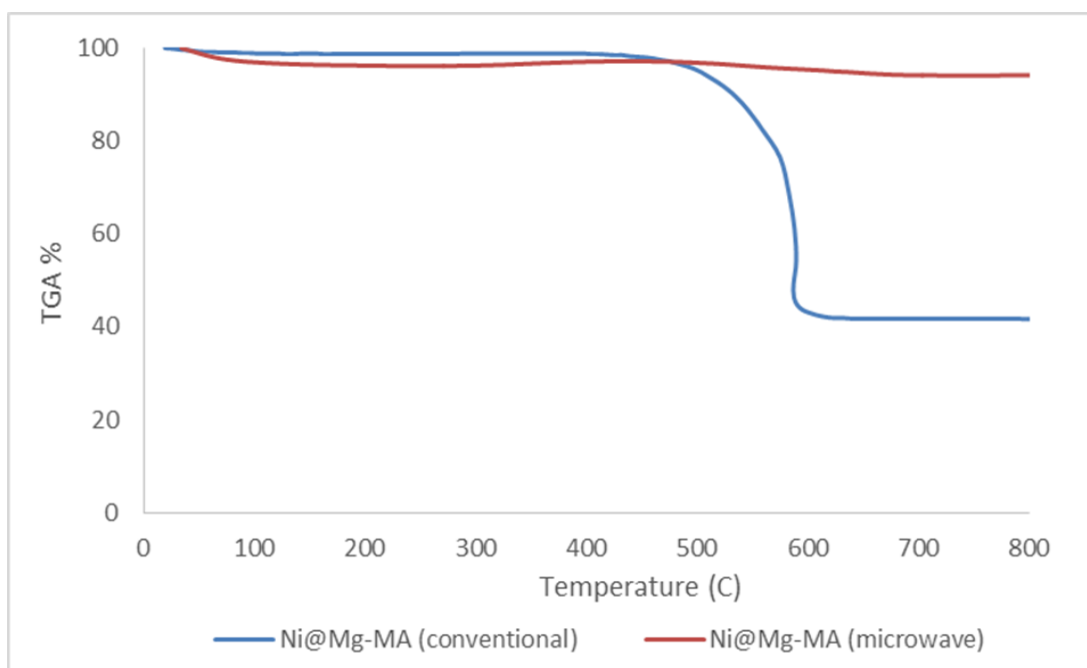


**Figure 7.39.** TGA curves of Ni@Mg-MA obtained in both conventionally heated and microwave reactors

The reason of the coke elimination over Ni@Mg-MA catalyst achieved in focused-microwave reactor system was that under microwave heating, Boudouard reaction is not favorable due to the elimination of temperature gradients that is inevitable in conventionally heated systems. Product distributions obtained in both conventionally heated (Figure 7.40) and microwave reactor (Figure 7.41) systems proved this hypothesis. The amount of CO<sub>2</sub> was higher than the amount of CO in the product stream of Ni@Mg-MA in the conventionally heated reactor which is an evidence of occurrence of Boudouard reaction. However in the focused-microwave reactor system, the amount of CO was higher than CO<sub>2</sub> which indicated that Boudouard reaction was not favored in this reaction system.

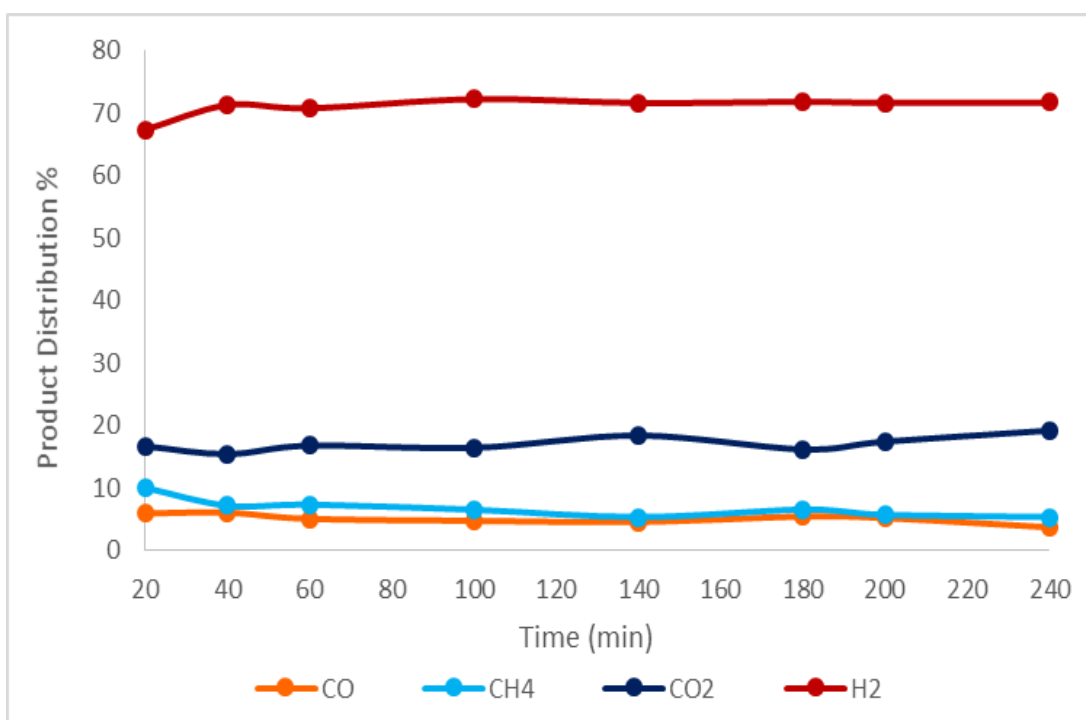


**Figure 7.40.** Product distribution of Ni@Mg-MA obtained in conventionally heated system

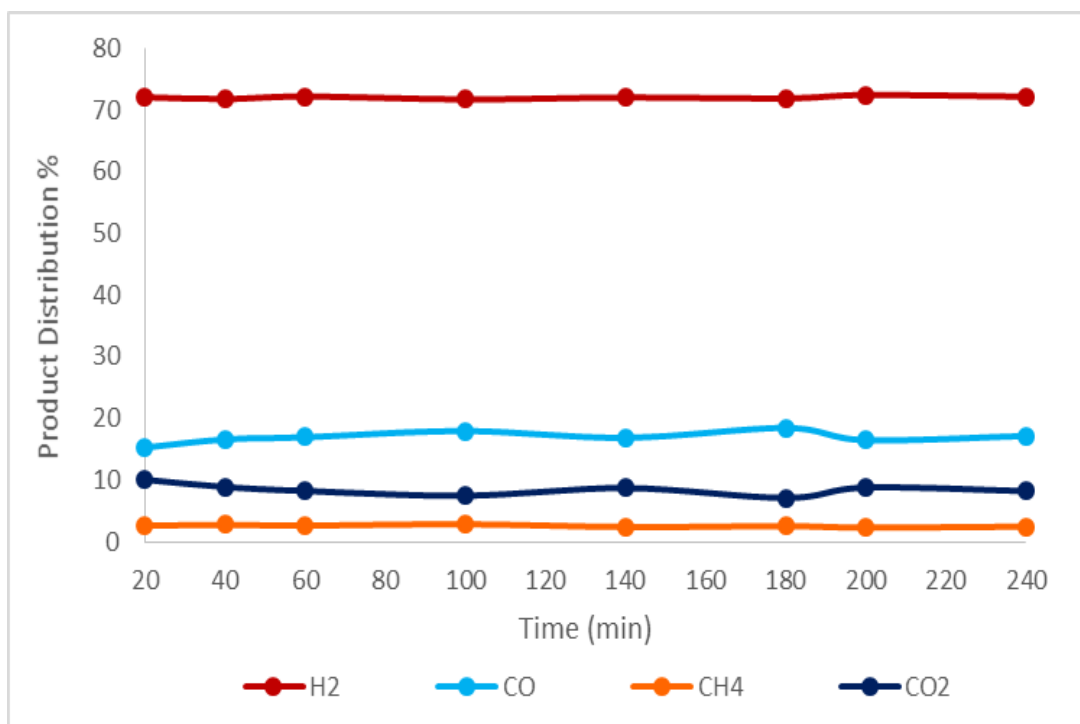


**Figure 7.41.** Product distribution of Ni@Mg-MA obtained in focused-microwave reactor system

In order to investigate the catalyst stability in focused-microwave reactor system, time-on stream reaction test extending upto 24 h was performed. As shown in Figure 7.42, hydrogen yield curve indicated that Ni@Mg-MA catalyst was highly stable up to 24 h in microwave reactor system.

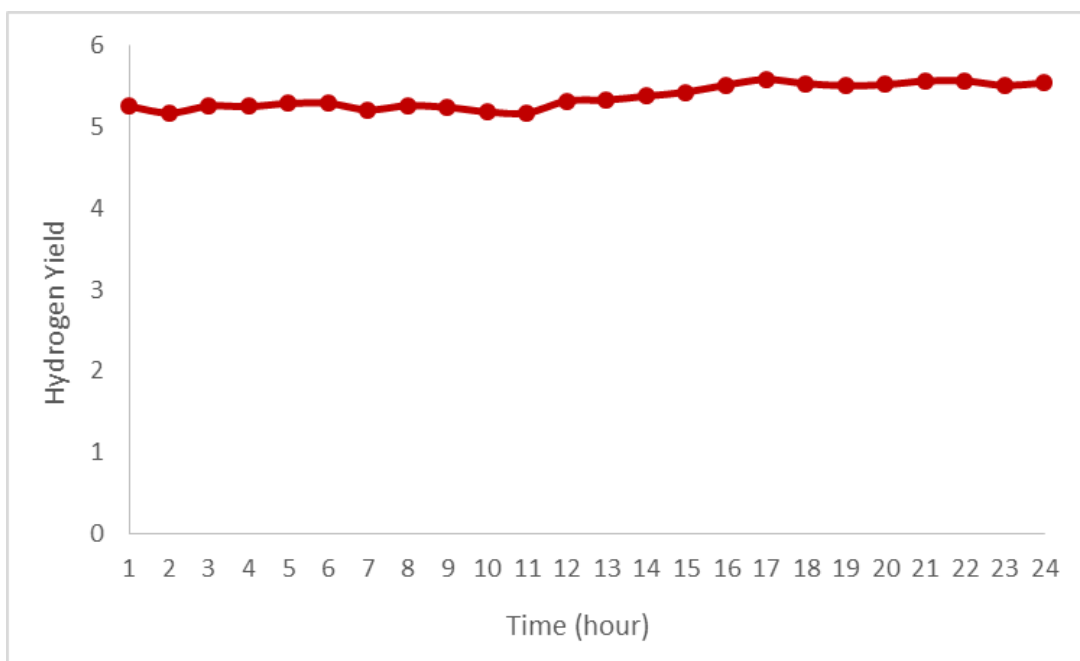


**Figure 7.42.** Hydrogen yield of Ni@Mg-MA in microwave reactor (long-term stability test)

More importantly, according to TGA result, coke deposition was quite low (about 6%) after 24 h of reaction in this system, which was only about 0.25% in the one hour test. Product distribution of Ni@Mg-MA catalyst is given in Figure 7.43 which also supports the stability of the catalyst during reaction period in focused-microwave reactor system.

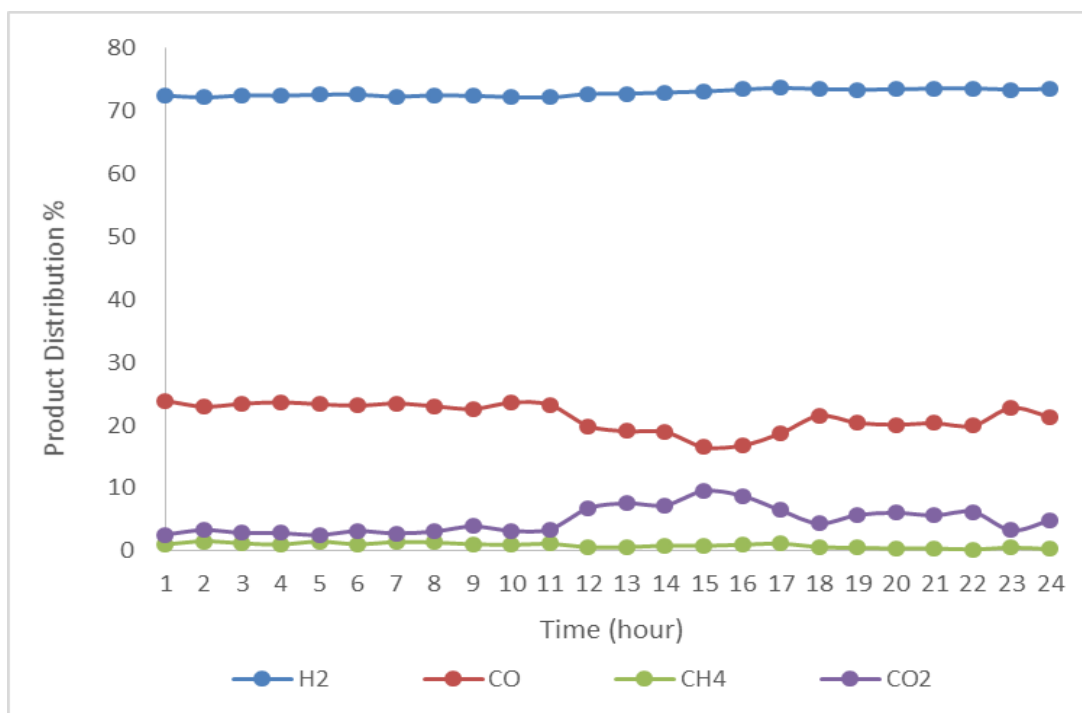


**Figure 7.43.** Product distribution of Ni@Mg-MA in MW reactor (long-term stability test)

#### 7.2.4. Scanning Electron Microscopy (SEM) Analysis of used Ni@Mg-MA Catalyst both in Conventionally Heated and Microwave Reactor Systems

SEM images of used Ni@Mg-MA catalyst in conventionally heated and microwave heating systems are illustrated in Figure 7.44 and 7.45, respectively.

SEM image of used Ni@Mg-MA catalyst obtained in conventionally heated reactor system indicates that high amount of filamentous coke was deposited on the catalyst. The shiny points observed in the SEM image may belong to the Ni particles pulled away from the catalyst surface by the growing filamentous coke.



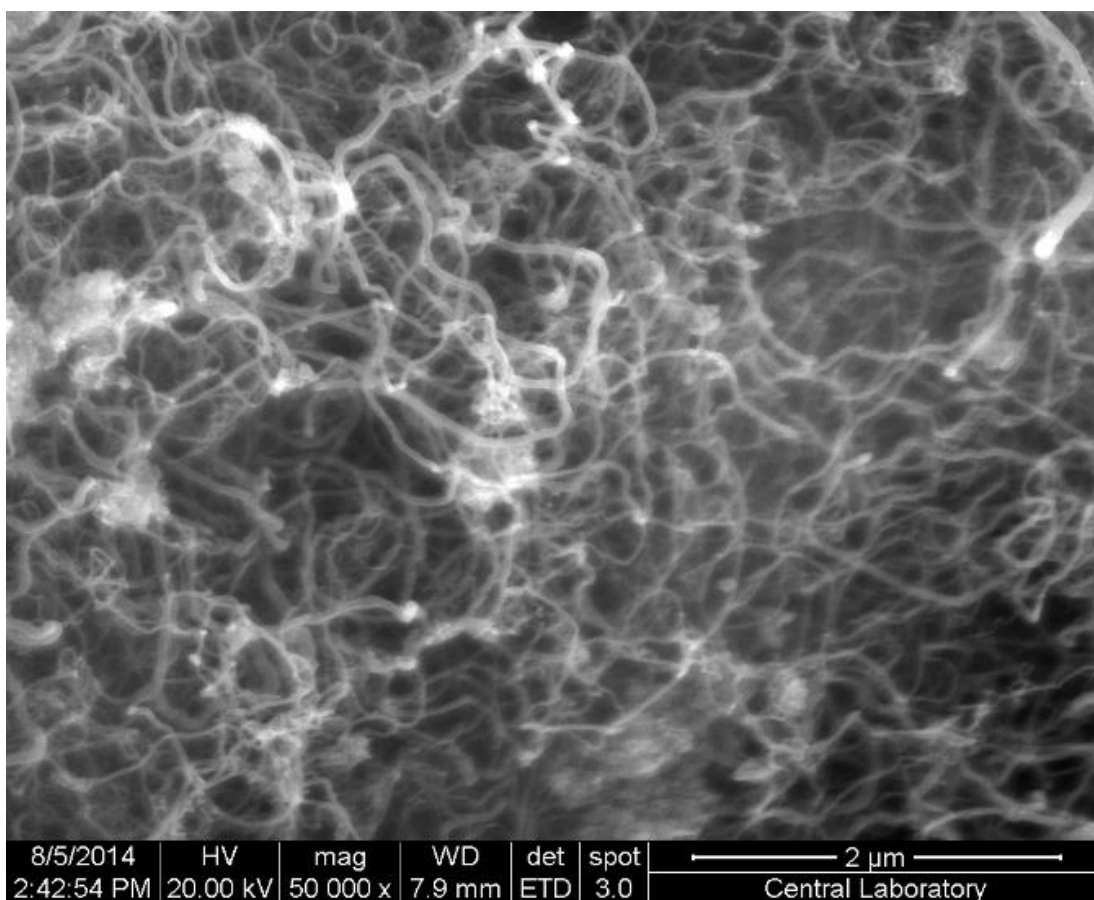


**Figure 7.44.** SEM image of used Ni@Mg-MA catalyst in conventionally heated reactor system

Filamentous carbon deposition was not observed on the used Ni@Mg-MA catalyst obtained in the microwave heating reactor system (Figure 7.45). This result is in agreement with the TGA result. Uniform distribution of temperature observed in microwave heating eliminates the cold-spots in the catalyst bed which is the main reason of coke formation following Boudouard reaction.

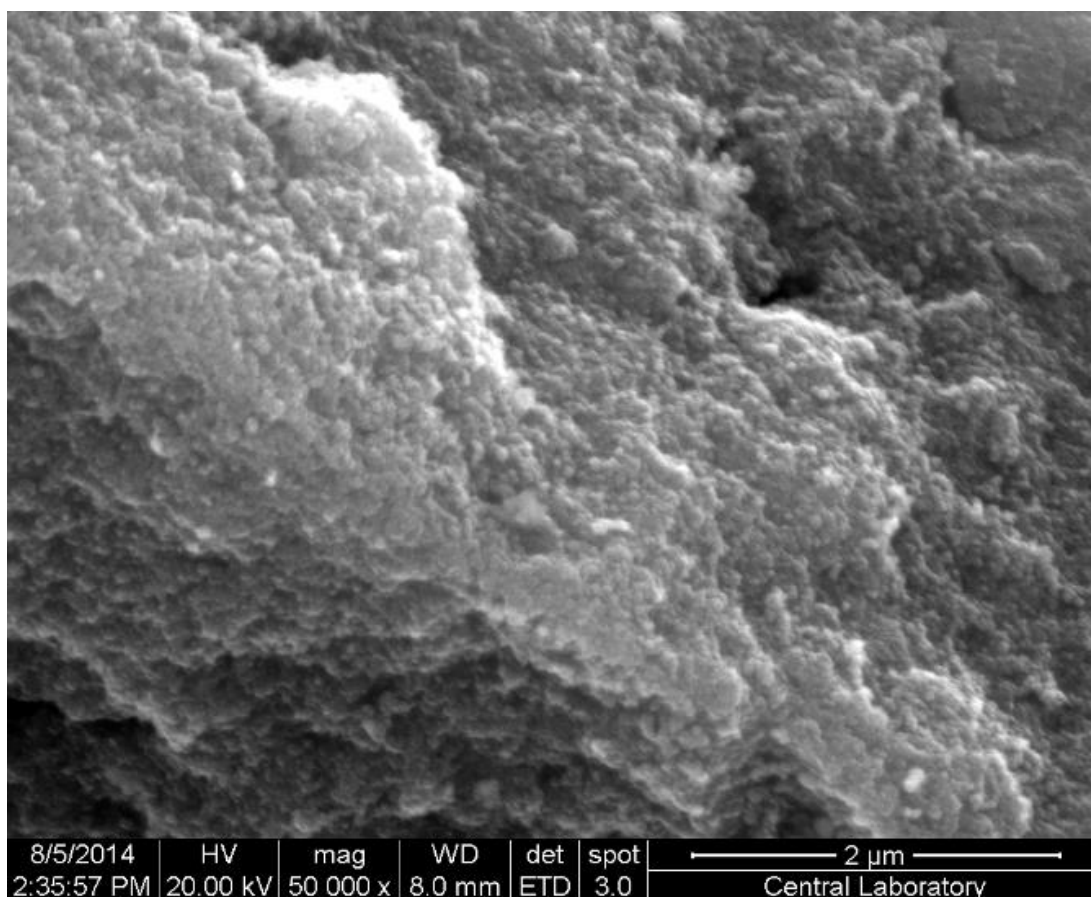


**Figure 7.45.** SEM image of used Ni@Mg-MA catalyst in microwave heating reactor system

## CHAPTER 8

### CONCLUSIONS

In the scope of the present study, Co-Mg and Ni-Mg incorporated mesoporous alumina type catalysts were synthesized, characterized and tested in steam reforming of ethanol reaction performed in both conventionally heated and focused-microwave reactor systems. Concluding remarks of the study is listed below;

- Co-Mg and Ni-Mg incorporated mesoporous alumina catalysts were successfully synthesized following one-pot (direct) and impregnation procedures. Well ordered mesoporous alumina materials were obtained even with the one-pot route.
- Complete conversion of ethanol was achieved with all four Co-Mg incorporated catalysts (Co-Mg-MA, Co-Mg@MA, Co@Mg-MA and Co@MA), at a space time less than a second, which indicated very high activity of all of the synthesized materials. While Co-Mg-MA and Co@Mg-MA (synthesized by direct addition of Mg) gave an average hydrogen yield of 5.3 which is almost 90% of the maximum hydrogen yield value of 6.0, Co-Mg@MA and Co@MA (synthesized by impregnation/lack of Mg) gave nearly zero hydrogen yield. Product distributions of the catalysts indicated that over Co-Mg-MA and Co@Mg-MA catalysts, the main reaction was steam reforming of ethanol; however over Co-Mg@MA and Co@MA catalysts, the dominated reaction was ethanol dehydration to ethylene reaction. This outcome was attributed to presence of  $\text{Co}^0$  and  $\text{CoO}$  phases (proved by XRD and XPS characterization techniques), that are very active for SRE reaction, in the structure of Co-Mg-MA and Co@Mg-MA catalysts. In the case of Co-

Mg@MA and Co@MA, the main phase was  $\text{CoAl}_2\text{O}_4$  which is not reported as an active phase for SRE reaction. Additionally, DRIFTS analysis of the pyridine adsorbed samples showed that the acidity of Co-Mg@MA and Co@MA catalysts was very high which could be another reason of high activity of these catalysts in ethanol dehydration reaction that dominates the reaction pathway in acidic environment.

- Experiments performed in focused microwave reactor system over Co@Mg-MA catalyst showed that hydrogen yield obtained under microwave heating was slightly higher and both hydrogen yield and product distributions were more stable. This outcome was attributed to the uniform temperature distribution in the catalyst bed provided by microwave heating. Additionally, thermal gravimetric analysis of the used catalysts in both reaction systems showed that while the coke deposition in conventionally heated system was nearly 30%, it was almost zero in focused-microwave reactor system after 5 h reaction periods. This coke elimination achieved under microwave heating was most probably due to the lack of cold-spots which is the main reason of carbon formation through Boudouard reaction in this type of heating. The long-term stability test (80 h) performed in focused-microwave reactor system concluded that Co@Mg-MA catalyst was highly stable under reaction conditions and the amount of coke after 80 h was 14% which is a very promising result considering catalyst stability and activity under microwave heating conditions.
- Complete conversion of ethanol was also achieved with all three Ni-Mg incorporated catalysts (Ni-Mg-MA, Ni-Mg@MA and Ni@Mg-MA), at a space time less than a second, which indicated very high activity of all of the synthesized materials. The hydrogen yields of Ni-Mg-MA, Ni-Mg@MA and Ni@Mg-MA catalysts were 4.0, 4.5 and 5.0, respectively. The slight difference of hydrogen yields was explained by the different Ni particle sizes observed in the structure of catalysts. Formation of higher Ni particles (approximately 20 nm, calculated by Scherrer's equation) enhanced methanation of CO reaction

resulted in higher amount of CH<sub>4</sub> in the product stream and lower hydrogen yield. Additionally, larger Ni particles observed in Ni-Mg-MA catalyst resulted in higher coke formation during reaction period.

- Experiments performed in the focused microwave reactor system using Ni@Mg-MA catalyst showed similar results with Co@Mg-MA catalyst. Microwave heating provided uniform temperature within the bed, resulting stable hydrogen yield and product distribution. Coke elimination was also observed over this catalyst under microwave heating.
- Consequently, among Co-Mg incorporated catalysts, Co@Mg-MA catalyst was recommended as the best catalyst and among Ni-Mg incorporated catalysts Ni@Mg-MA was chosen as the most active catalyst towards steam reforming of ethanol reaction for hydrogen production with its relatively high hydrogen yield and less coke deposition.
- In conclusion, focused-microwave reactor system was more preferable than conventionally heated system due to its energy efficiency, more stable product distribution and coke minimization.



## REFERENCES

1. Subramani, V., Song, C., Advances in catalysis and process for hydrogen production from ethanol reforming, *Catalysis*, 2007, 20, 65-106.
2. World Commission on Environment and Development (WCED), *Our Common Future*, Oxford University Press, Oxford, 1987.
3. International Energy Outlook 2013, Report # DOE/EIA-0484, 2013; release date: July 25, 2013.
4. EIA/IEA, *International Energy Annual*, Energy Information Administration, US Department of Energy, Washington DC, 2000.
5. EIA/AER, *Annual Energy Review 1998*, Energy Information Administration, US Department of Energy, Washington DC, 1999.
6. Demirbas, A., Progress and recent trends in biofuels, *Progress in Energy and Combustion Science*, 2006.
7. Haryanto, A., Fernando, S., Murali, N., Adhikari, S., Current status of hydrogen production techniques by steam reforming of ethanol : A review, *Energy & Fuels*, 2005, 19, 2098-2106.
8. Midilli, A., Ay, M., Dincer, I., Rosen, M. A., On hydrogen and hydrogen energy strategies I: current status and needs, *Renewable and Sustainable Energy Reviews*, 2005, 9, 255-271.
9. TUSIAD, *Evaluation of energy strategy of Turkey towards 21st century*, No. TUSIAD-T/98-12/239, Istanbul, 1998.

10. Statistical Review of World Energy 2003, Primary energy: consumption by fuel type Mtoe., <http://www.bp.com/centres/energy>, (accessed July 2014).
11. Pusz J., Alternative energy sources, <http://www.fuelcells.prv.pl>, 2001, 57–58 (accessed July 2014).
12. Veziroglu, T.N., Barbir, F., Hydrogen energy technologies, Emerging technology series, Vienna Austria, UNIDO, 1998.
13. Sener, C., Novel bimetallic mesoporous catalysts for hydrogen production through steam reforming of ethanol, PhD Thesis, METU, 2012.
14. Contreras, A., Yigit, S., Ozay, K., Veziroglu, T. N., Hydrogen as aviation fuel: a comparison with hydrocarbon fuels, *Int J Hydrogen Energy*, 1997, 22, 1053–1060.
15. P. Corbo et al., Hydrogen Fuel Cells for Road Vehicles, *Green Energy and Technology*, DOI: 10.1007/978-0-85729-136-3\_2, Springer-Verlag London Limited, 2011.
16. D.J. Wilhelm, D.R. Simbeck, A.D. Karp, R.L. Dickenson, Syngas production for gas-to-liquids applications: technologies, issues and outlook, *Fuel Processing Technology*, 2001, 71, 139–148.
17. Holladay, J., Jones, E., Palo, D. R., Phelps, M., Chin, Y. H., Dagle, R., Hu, J., Wang, Y., Baker, E., Miniature fuel processors for portable fuel cell power supplies, Materials Research Society, Boston United States, 2003, 429–434.
18. Navarro, R. M., Pena, M. A., Fierro, J. L. G., Hydrogen production reactions from carbon feedstocks: fossil fuels and biomass, *Chemical Reviews*, 2007, 107, 3952–3991.



19. Holladay, J. D., Hu, J., King, D. L., Wang, Y., An overview of hydrogen production technologies, *Catalysis Today*, 2009, 139, 244-260.
20. Ivy, J. Summary of Electrolytic Hydrogen Production, Report No. NREL/MP-560-36734, National Renewable Energy Laboratory, Golden, CO, September 2004.
21. Levin, D. B., Pitt, L., Love, M., Biohydrogen production: Prospects and limitations to practical application, *Int. J. Hydrogen Energy*, 2004, 29, 173-185.
22. FY 2003 Progress Report on Hydrogen, Fuel Cells and Infrastructure Technologies, [http://www.eere.energy.gov/hydrogenandfuelcells/pdfs/iic5\\_miller.pdf](http://www.eere.energy.gov/hydrogenandfuelcells/pdfs/iic5_miller.pdf).
23. Kalamaras, C. M., Efstathiou, A. M., Hindawi Publishing Corporation Conference Papers in Energy, Article ID 690627, <http://dx.doi.org/10.1155/2013/690627>.
24. Balat, H. and Kirtay, E., Hydrogen from biomass—present scenario and future prospects, *Int. J. Hydrogen Energy*, 2010, 35, 7416-7426.
25. Balat, M. and Balat, M., Political, economic and environmental impacts of biomass based hydrogen, *Int. J. Hydrogen Energy*, 2009, 34, 3589-3603.
26. Deluga, G. A., Salge, J. R., Schmidt, L. D., Verykios, X. E., Renewable hydrogen from ethanol by autothermal reforming, *Science*, 2004, 303, 993-997.
27. Licht, F. O., cited in Renewable Fuels Association, Ethanol Industry Outlook 2008-2013 reports Available at [www.ethanolrfa.org/pages/annual-industry-outlook](http://www.ethanolrfa.org/pages/annual-industry-outlook).
28. Fatsikostas A.N., Verykios X.E., Reaction network of steam reforming of ethanol over Ni-based catalysts, *Journal of Catalysis*, 2004, 225, 439.

29. Ni M., Leung D.Y.C., Leung M.K.H., A review on reforming bio-ethanol for hydrogen production, *Int. J. Hydrogen Energy*, 2007, 32, 3238-3247.
30. Freni, S., Maggio, G. and Cavallaro, S., Ethanol steam reforming in a molten carbonate fuel cell: a thermodynamic approach, *Journal of Power Sources*, 1996, 62, 67-73.
31. Benito, M., Padilla, R., Sanz., J. L. and Daza L., Thermodynamic analysis and performance of a 1kW bioethanol processor for a PEMFC operation, *Journal of Power Sources*, 2007, 169, 123–130.
32. Vaidya, P. D. and Rodrigues, A. E., Insight into steam reforming of ethanol to produce hydrogen for fuel cells, *Chemical Engineering Journal*, 2006, 117, 39-49.
33. Mas, V., Kipreos, R., Amadeo, N. and Laborde, M., Thermodynamic analysis of ethanol/water system with the stoichiometric method, *International Journal of Hydrogen Energy*, 2006, 31, 21-28.
34. Garcia, E. Y., Laborde, M. A., Hydrogen production by the steam reforming of ethanol: Thermodynamic analysis, *Int. J. Hydrogen Energy*, 1991, 16, 307-312.
35. Vasudeva, K., Mitra, N., Umasankar, P., Dhingra, S. C., Steam reforming of ethanol for hydrogen production: thermodynamic analysis, *Int. J. Hydrogen Energy*, 1996, 21, 13-18.
36. Fishtik, I., Alexander, A., Datta, R., Geana, D., A thermodynamic analysis of hydrogen production by steam reforming of ethanol via response reactions, *Int. J. Hydrogen Energy*, 2000, 25, 31-45.
37. Wang, W., Wang, Y. Q., Thermodynamic analysis of steam reforming of ethanol for hydrogen generation, *Int. J. Energy Res.*, 2008, 32, 1432-1443.

38. Ionnides, T., Thermodynamic analysis of ethanol processors for fuel cell applications, *Journal of Power Sources*, 2001, 92, 17-25.
39. Erdohelyi, A., Raskó, J., Kecskés, T., Tóth, M., Dömök, M. & Baán, K., Hydrogen formation in ethanol reforming on supported noble metal catalysts, *Catalysis Today*, 2006, 116, 367-376.
40. Hernández, L. and Kafarov, V., Thermodynamic evaluation of hydrogen production for fuel cells by using bio-ethanol steam reforming: Effect of carrier gas addition, *Journal of Power Sources*, 2009, 192, 195-199.
41. Silveira, J. L., Braga, L. B., de Souza, A. C. C. and Antunes J. S., The benefits of ethanol use for hydrogen production in urban transportation, *Renewable and Sustainable Energy Reviews*, 2009, 13, 2525-2534.
42. Comas, J., Dieuzeide, M. L., Baronetti, Laborde, M., Amadeo, N., Methane steam reforming and ethanol steam reforming using a Ni(II)-Al(III) catalyst prepared from lamellar double hydroxides, *Chem. Eng. Journal*, 2006, 118, 11-15.
43. Yang, Y., Ma, J., Wu, F., Production of hydrogen by steam reforming of ethanol over a Ni/ZnO catalyst, *Int. J. Hydrogen Energy*, 2006, 31, 877-882.
44. Barroso, M. N., Gomez, M. F., Arrua, L. A., Abello, M. C., Hydrogen production by ethanol reforming over NiZnAl catalysts, *Appl. Catal. A: General*, 2006, 304, 116-122.
45. Akande, J., Master of Science Thesis submitted to University of Saskatchewan, Canada, Feb. 2005.

46. Sun, J., Qiu, X., Wu, F., Zhu, W., Wang, W., Hao, S., Hydrogen from steam reforming of ethanol in low and middle temperature range for fuel cell application, *Int. J. Hydrogen Energy*, 2004, 29, 1075-1081.
47. Comas, J., Marino, F., Laborde, M., Amadeo, N., Bio-ethanol steam reforming on Ni/Al<sub>2</sub>O<sub>3</sub> catalyst, *Chem. Eng. Journal*, 2004, 98, 61-68.
48. Fatsikostas, A. N., Kondarides, D. I., Verykios, X. E., Production of hydrogen for fuel cells by reformation of biomass-derived ethanol, *Catal. Today*, 2002, 75, 145-155.
49. Batista, M. S., Santos, R K. S., Assaf, E. M., Assaf, J. M., Ticianelli, E. A., High efficiency steam reforming of ethanol by cobalt-based catalysts, *J. Power Sources*, 2004, 134, 27.
50. Batista, M. S., Santos, R K. S., Assaf, E. M., Assaf, J. M., Ticianelli, E. A., Characterization of the activity and stability of supported cobalt catalysts for the steam reforming of ethanol, *J. Power Sources*, 2003, 124, 99.
51. Llorca, J., de la Piscina, P, R., Dalmon, J. A., Sales, J., Homs, N., CO-free hydrogen from steam-reforming of bioethanol over ZnO-supported cobalt catalysts: Effect of the metallic precursor, *Appl. Catal. B: Environ.*, 2003, 43, 355-369.
52. Llorca, J., Dalmon, J. A., de la Piscina, P. R., Homs, N., In situ magnetic characterisation of supported cobalt catalysts under steam-reforming of ethanol, *Appl. Catal. A: General*, 2003, 243, 261-269.
53. Haga, F., Nakajima, T., Miya, H., Mishima, S., Catalytic properties of supported cobalt catalysts for steam reforming of ethanol *Catal. Lett.*, 1997, 48, 223-227.

54. Boudart, M., Perspectives in catalysis, J. M. Thomas, K. I. Zamaraev (Ed) Blackwell, Oxford, 1992, 183.
55. Augustine, R. L., Heterogeneous Catalysis for the Synthetic chemist, Supported Metals, Marcel Dekker, New York, 1996.
56. Oye, G., Sjöblom, J., Stöcker, M., Synthesis, characterization and potential applications of new materials in the mesoporous range, Advances in Colloid and Interface Science, 2001, 89-90, 439-466.
57. Corma, A., From microporous to mesoporous molecular sieve materials and their use in catalysis, Chem. Rev., 1997, 97, 2373-2419.
58. Vartuli, J. C., Roth, W. J., Degnan, T. F., Mesoporous materials (M41S): From discovery to application, Dekker Encyclopedia of Nanoscience and Nanotechnology, 2004.
59. Topsoe, H., Clausen, B.S., Massoth, F.E., Hydrotreating Catalysis, Springer: Berlin, 1996, 310.
60. Fang, X. S. Ye, C.H. Xu, X.X. Xie, T. Wu, Y.C.; Zhang, L.D., J. Phys.: Condens. Matter, 2004, 16, 4157–4163.
61. Boissiere, C., Nicole, L., Gervais, C., Babonneau, F., Antonietti, M., Amenitsch, H., Sanchez, C., Grosso, D., Nanocrystalline Mesoporous  $\gamma$ -Alumina Powders “UPMC1 Material” Gathers Thermal and Chemical Stability with High Surface Area, Chem. Mater. 2006, 18, 5238–5243.
62. Zhao, R. H., Li, C. P., Guo, F., Chen, J. F. Scale-up Preparation of Organized Mesoporous Alumina in a Rotating Packed Bed, Ind. Eng. Chem. Res. 2007, 46, 3317–3320.

63. Zima, T. M., Baklanova, N. I., Lyakhov, N. Z., Mesoporous structure of  $\text{Al}_2\text{O}_3$  prepared from poly(*N*-vinylpyrrolidone)-modified sols of hydrous metal oxides *Inorg. Mater.* 2008, 44, 146–153.
64. Vaudry, F., Khodabandeh, S., Davis, M. E., Synthesis of pure alumina mesoporous materials, *Chem. Mater.* 1996, 1451–1464.
65. Yang, P., Zhao, D., Margolese, D. I., Chmelka, B. F., Stucky, G. D., Generalized syntheses of large-pore mesoporous metal oxides with semicrystalline frameworks, *Nature* 1998, 396, 152–155.
66. Niesz, K.; Yang, P., Somorjai, G. A., Sol-gel synthesis of ordered mesoporous alumina, *Chem. Commun.* 2005, 15, 1986–1987.
67. Zhang, Z., Pinnavaia, T. J., Mesostructured forms of  $\gamma\text{-Al}_2\text{O}_3$ , *J. Am. Chem. Soc.* 2002, 124, 1592–1593.
68. Liu, Q., Wang, A., Wang, X., Zhang, T., Ordered crystalline alumina molecular sieves synthesized via a nanocasting route, *Chem. Mater.* 2006, 18, 5153–5155.
69. Yuan, Q., Yin, A. X., Luo, C., Sun, L. D., Zhang, Y. W., Duan, W. T., Liu, H. C., Yan, C. H., Facile Synthesis for Ordered Mesoporous  $\gamma$ -Aluminas with High Thermal Stability, *J. Am. Chem. Soc.* 2008, 130, 3465–3472.
70. Kuemmel, M., Grosso, D., Boissiere, C., Smarsly, B., Brezesinski, T., Albouy, P. A., Amenitsch, H., Sanchez, C., Thermally Stable Nanocrystalline  $\gamma$ -Alumina Layers with Highly Ordered 3D Mesoporosity, *Angew. Chem., Int. Ed.* 2005, 44, 4589–4592.

71. Gu, D., Schüth, Ferdi, Synthesis of non-siliceous mesoporous oxides, *Chem. Soc. Rev.*, 2014, 43, 313.
72. Hartmann, S., Sachse, A., Galarneau, A., Challenges and strategies in the synthesis of mesoporous alumina powders and hierarchical alumina monoliths, *Materials*, 2012, 5, 336-349.
73. Panpranot, J., Goodwin, J. G., Sayari, A., Synthesis and characteristics of MCM-41 supported CoRu catalysts, *Catalysis Today*, 2002, 77, 269-284.
74. Haga, F., Nakajima, T., Miya, H., Mishima, S., Catalytic properties of supported cobalt catalysts for steam reforming of ethanol, *Catalysis Letters*, 1997, 48, 223-227.
75. Llorca, J., Homs, N., Sales, J., Piscina, P., Efficient production of hydrogen over supported cobalt catalysts from ethanol steam reforming, *Journal of Catalysis*, 2002, 209, 306-317.
76. Lin, S., Kim, D. H., Ha, S. Y., Hydrogen production from ethanol steam reforming over supported cobalt catalysts, *Catal. Lett.*, 2008, 122, 295-301.
77. Haga, F., Nakajima, T., Yamashita, K., Mishima, S., Effect of crystallite size on the catalysis of alumina-supported cobalt catalyst for steam reforming of ethanol, *React. Kinet. Catal. Lett.*, 1998, 63, 253-259.
78. Song, H., Mirkelamoglu, B., Ozkan, U., Effect of cobalt precursor on the performance of ceria-supported cobalt catalysts for ethanol steam reforming, *Applied Catalysis A: General*, 2010, 1-7.
79. Ma, Y., Zeng, M., He, J., Duan L., Wang, J., Wang, J., Syntheses and characterizations of cobalt doped mesoporous alumina prepared using natural rubber latex as template and its catalytic oxidation of tetralin to tetralone, *Applied Catalysis A: General*, 2011, 396, 123-128.

80. Zhe, W., Zhu, B., Liao, T., Li, Z., Yang, H., Wang, X., Wang, J., Syntheses and Characterizations of Cobalt doped Mesoporous Alumina Templated by Rubber Latex and its Adsorption of Acetaldehyde, *Advanced Materials Research*, 2013, 742, 346, 350.
81. Wosciezjak, R., Monteverdi, S., Mercy, M., Nowak, I., Ziolk, M., Bettahar, M. M., Nickel containing MCM-41 and AlMCM-41 mesoporous molecular sieves characteristics and activity in the hydrogenation of benzene, *Applied Catalysis A: General*, 2004, 268, 241-253.
82. Encyclopedia Britannica 'Hertz: Radio-wave experiments'.
83. Spencer, P. L., U. S. Pateny, 1950, 2 495 429.
84. Durka, T., Microwave assisted low temperature steam reforming of methanol for hydrogen production, Master Thesis, May 2010.
85. Durka, T., van Gerven, T., Stankiewicz, A.I., "Microwaves in Heterogeneous Gas-Phase Catalysis: Experimental and Numerical Approaches", *Chem. Eng. Technol.* (2009), 9, 1301-1312.
86. *Microwaves in Nanoparticle Synthesis*, First Edition. Edited by Satoshi Horikoshi and Nick Serpone. © 2013 Wiley-VCH Verlag GmbH & Co. KGaA.
87. Horikoshi, S., Serpone, N., Role of microwaves in heterogeneous catalytic systems, *Catalysis Science & Technology*, DOI: 10.1039/c3cyoo753g.
88. Will, H., Scholz, P., Ondruschka, B., Microwave-assisted heterogeneous gas-phase catalysis, *Chem. Eng. Technol.*, 2004, 27, 113-122.
89. *Microwaves in organic synthesis*, ed. A. De la Hoz and A. Loupy, Wiley-VCH Verlag, Weinheim, Germany, 2012.



90. Reus, M., Microwave-assisted low temperature steam reforming of methanol for hydrogen production, MSc Thesis, TU Delft, 2010.
91. Hayes, B. L., Recent advances in microwave-assisted synthesis, *Aldrichimica ACTA*, 2004, 37, 66-76.
92. Jacob, J., Chia, L. H. L., Thermal and non-thermal interaction of microwave radiation with materials, *Journal of Material Science*, 1995, 30, 5321-5327.
93. Galema, S., Microwave chemistry, *Chemical Society Reviews*, 1997, 26, 233-238.
94. Meredith, R., *Engineers' handbook of industrial microwave heating*, Published by: The Institution of Electrical Engineers, 1998, London, United Kingdom.
95. Perry, W. L., Datye, A. K., Prinja, A. K., Brown, L. F., Katz, J. D., Microwave heating of endothermic catalytic reactions: Reforming of methanol, *AICHE J.*, 2002, 48, 820.
96. Conde, L. D., Marun C, Suib, S. L., Fathi, Z., Frequency Effects in the Catalytic Oligomerization of Methane via Microwave Heating, *J. Catal.*, 2001, 204, 324.
97. Zhang X. L., Hayward, D. O., Lee, C., Mingos, D. M. P, *Appl. Catal. B: Environ.*, 2001, 33, 137.
98. Zhang, X., Hayward, D.O., Michael, D., and Mingos, P., 2003, Effects of microwave dielectric heating on heterogeneous catalysis, *Cat. Lett.*, 2003, 88.
99. Perry, W.L., et al., Kinetics of the Microwave-Heated CO Oxidation Reaction over Alumina-Supported Pd and Pt Catalysts. *Journal of Catalysis*, 1997(171): p. 431–438.

- 100.**Will, H., et al., Multimode Microwave Reactor for Heterogeneous Gas-Phase Catalysis, *Chemical Engineering & Technology*, 2003, 26, 1146-1149.
- 101.**Beckers, J., et al., Clean Diesel Power via Microwave Susceptible Oxidation Catalysts. *ChemPhysChem*, 2006, 7, 747-755.
- 102.**Koch, T.A., et al., Improved safety through distributed manufacturing of hazardous chemicals. *Process Safety Progress*, 1997, 16, 23-24.
- 103.**Sinev, I., et al., Interaction of vanadium containing catalysts with microwaves and their activation in oxidative dehydrogenation of ethane. *Catalysis Today*, 2009, 141, 300-305.
- 104.**Cooney, D.O. and Z. Xi, Production of hydrogen from methane and methane/steam in a microwave irradiated char-loaded reactor. *Petroleum Science and Technology*, 1996, 14, 1111 - 1141.
- 105.**Bi, X.J., et al., Microwave effect on partial oxidation of methane to syngas. *Reaction Kinetics and Catalysis Letters*, 1999, 66, 381-386.
- 106.**Domínguez, A., et al., Microwave-assisted catalytic decomposition of methane over activated carbon for CO<sub>2</sub>-free hydrogen production. *International Journal of Hydrogen Energy*, 2007, 32, 4792-4799.
- 107.**Fidalgo, B., et al., Microwave-assisted dry reforming of methane. *International Journal of Hydrogen Energy*, 2008, 33, 4337-4344.
- 108.**Perry, W.L., et al., Microwave heating of endothermic catalytic reactions: Reforming of methanol. *AIChE Journal*, 2002, 48, 820-831.
- 109.**Chen, W.-H., et al., Hydrogen generation from a catalytic water gas shift reaction under microwave irradiation. *International Journal of Hydrogen Energy*, 2008, 33, 4789-4797.

- 110.**Zhang, X. R., et al., A unique microwave effect on the microstructural modification of Cu/ZnO/Al<sub>2</sub>O<sub>3</sub> catalysts for steam reforming of methanol, Chem. Comm. 2005, 4104 – 4106.
- 111.**Brundle, C. R.; Evans, C. A., Jr., & Wilson, S. (1992). Encyclopedia of Materials Characterization: Surfaces, Interfaces, Thin Films, Butterworth-Heinemann & Manning Publications Co., ISBN 978- 0-750-69168-0, Boston, MA, U.S.A.
- 112.**Yue, W., Zhou, W., Porous crystals of cubic metal oxides templated by cage-containing mesoporous silica, J Mater Chem, 2007, 4947-4952.
- 113.**Bayram B, et al., Ethanol steam reforming over Co-based catalysts: Investigation of cobalt coordination environment under reaction conditions, J of Catalysis, 2011, 77-89.
- 114.**Chen Z, et al., Hydrothermal synthesis and optical property of nano-sized CoAl<sub>2</sub>O<sub>4</sub> pigment, Materials Letters, 2002, 281-284.
- 115.**Jacobs G, et al., Fischer-Tropsch synthesis: study of the promotion of Pt on the reduction property of Co/Al<sub>2</sub>O<sub>3</sub> catalysts by in-situ EXAFS of Co K and Pt L<sub>III</sub> edges and XPS, J Synchrotron Rad., 2004, 414-422.
- 116.**Chu, W., et al., Cobalt species in promoted cobalt alumina-supported Fischer-Tropsch catalysts, Journal of Catalysis, 2007, 215-230.
- 117.**Takenaka, S., Shimizu, T., Otsuka, K., Complete removal of carbon monoxide in hydrogen-rich gas stream through methanation over supported metal catalysts, Int. J. Hydrogen Energy, 2004, 29, 1065-1073.

- 118.**Duprez, D., DeMicheli, M. C., Marecot, P., Barbier, J., Ferretti, O. A., Ponzi, E. N., Deactivation of steam-reforming model catalysts by coke formation: I. Kinetics of the formation of filamentous carbon in the hydrogenolysis of cyclopentane on Ni/Al<sub>2</sub>O<sub>3</sub> catalysts, *J. Catal.*, 1990, 124, 324.

## APPENDICES

### A. THERMODYNAMIC ANALYSIS

Thermodynamic equilibrium analysis was performed in order to analyze the effects of operating conditions on hydrogen percentage in the product stream and product distributions. A program called GASEQ which is based on the minimization of free energy method (NASA method) was used for equilibrium calculations. Calculations were performed considering the product stream includes  $H_2$ ,  $CO$ ,  $CH_4$ ,  $CO_2$ ,  $C_2H_4$  and  $CH_2O$ .

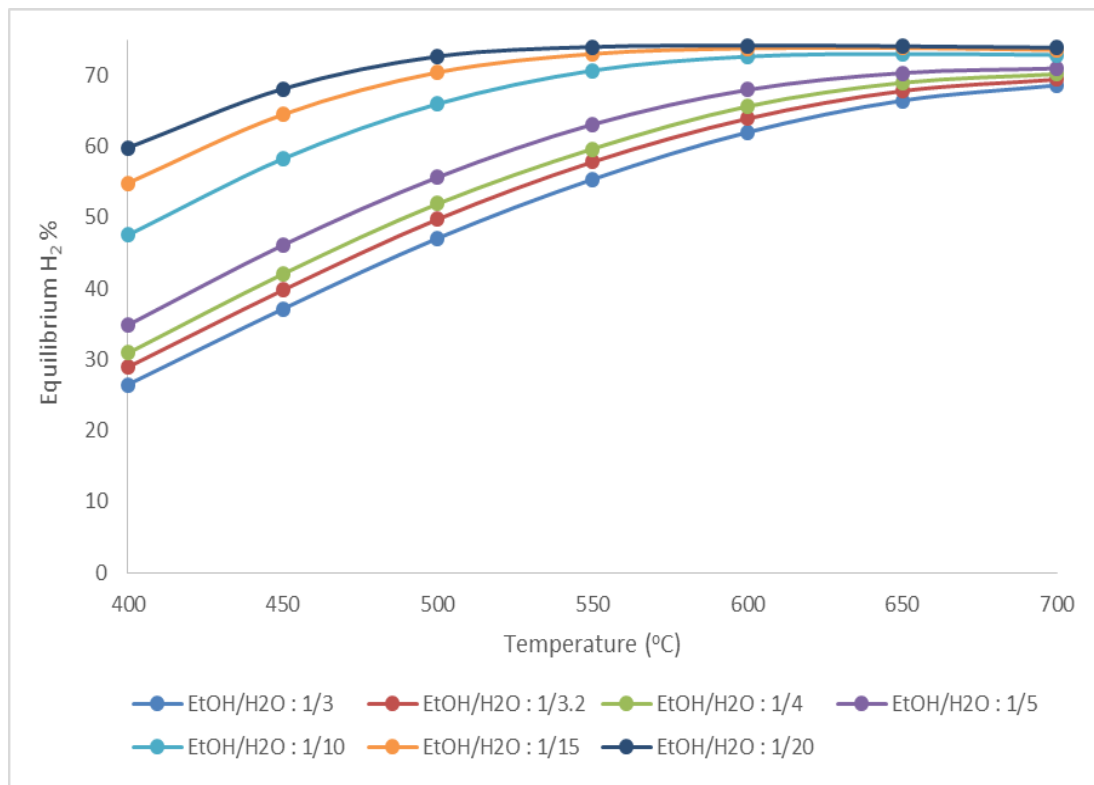


**Figure A. 1.** Equilibrium  $H_2\%$  in product stream between  $400^{\circ}C$  and  $700^{\circ}C$  with steam to ethanol ratio changing between 3 and 20

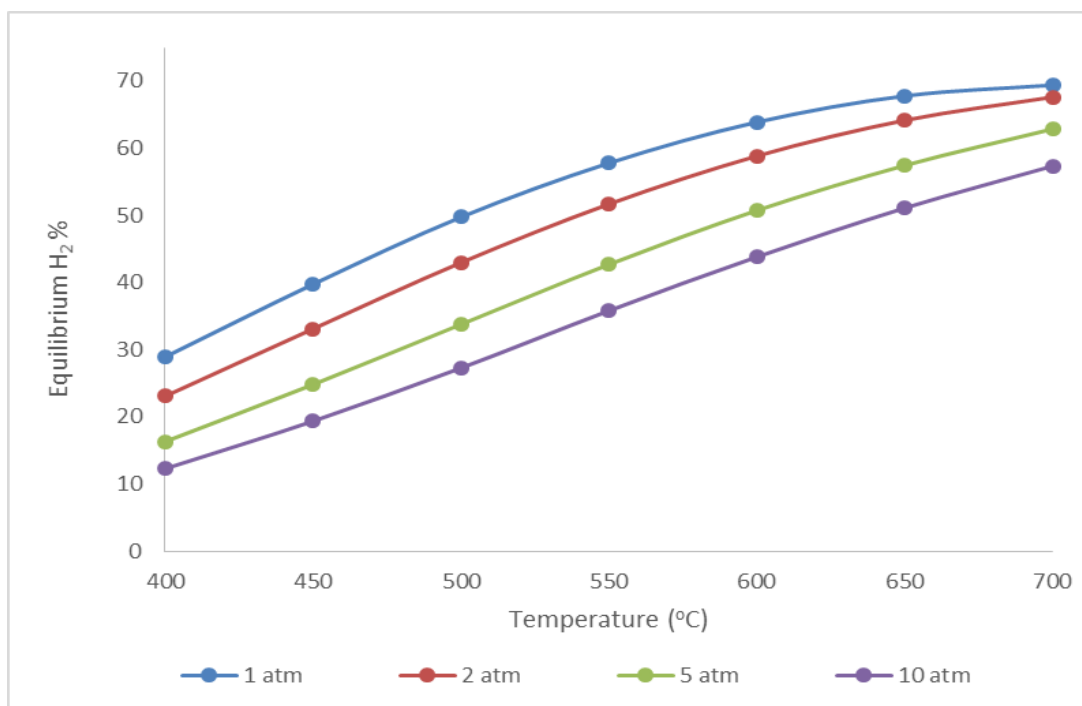


**Figure A. 2.** Equilibrium H<sub>2</sub>% in product stream between 400°C and 700 °C at pressure changing between 1 atm and 10 atm

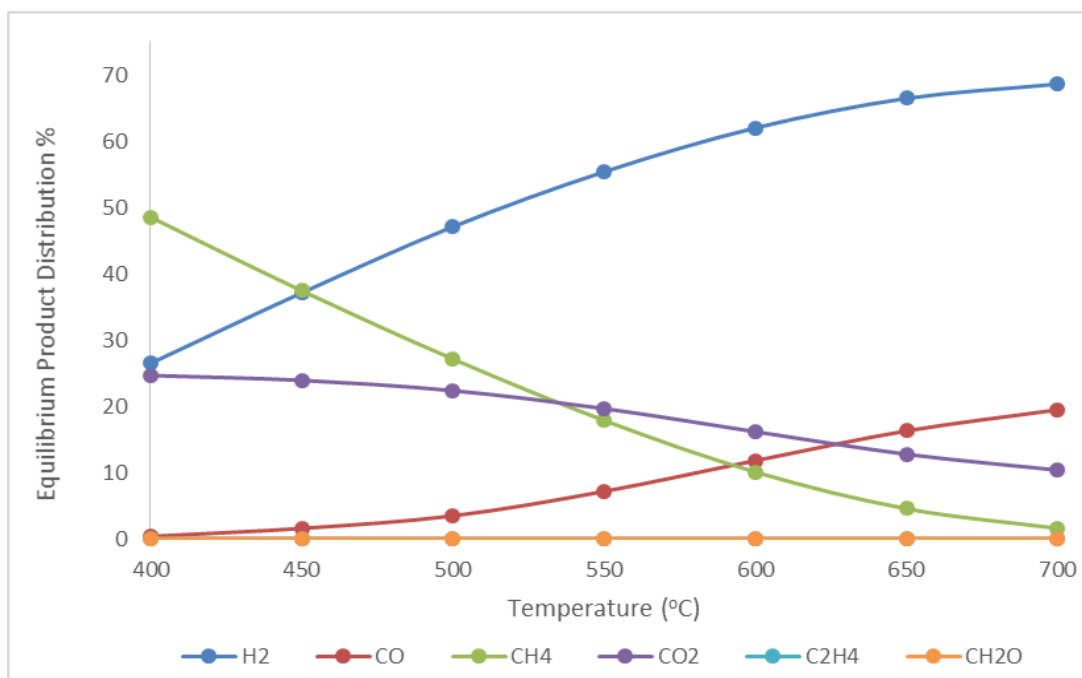


**Figure A. 3.** Equilibrium product distributions between 400°C and 700 °C with steam to ethanol ratio of 3

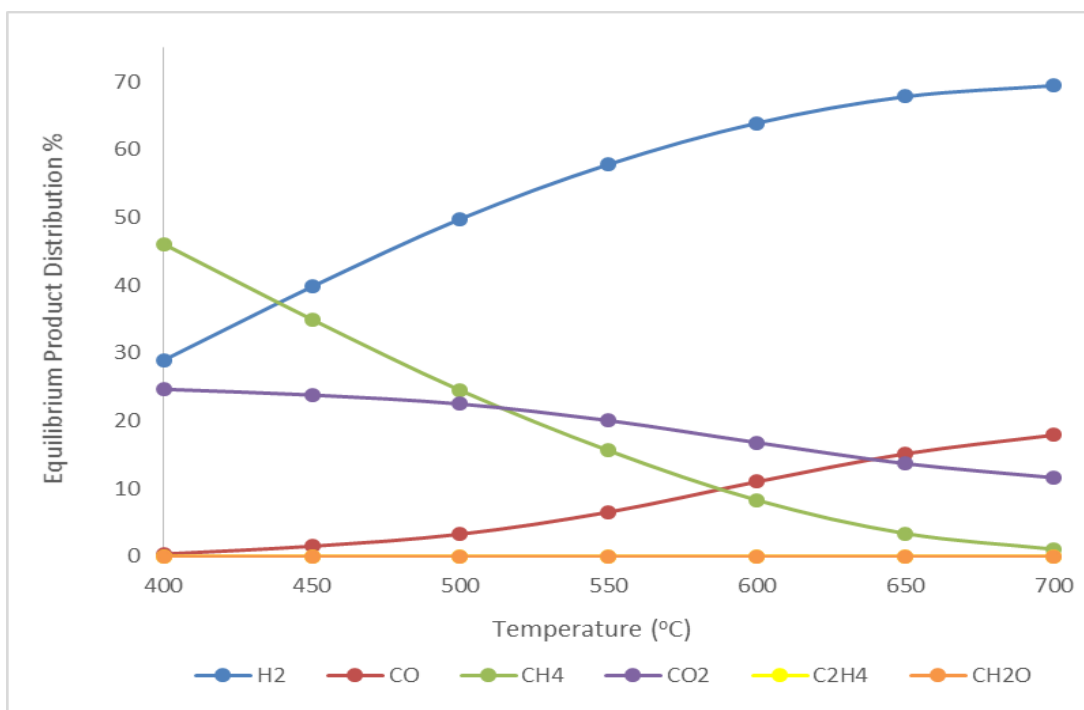


**Figure A. 4.** Equilibrium product distributions between 400°C and 700 °C with steam to ethanol ratio of 3.2

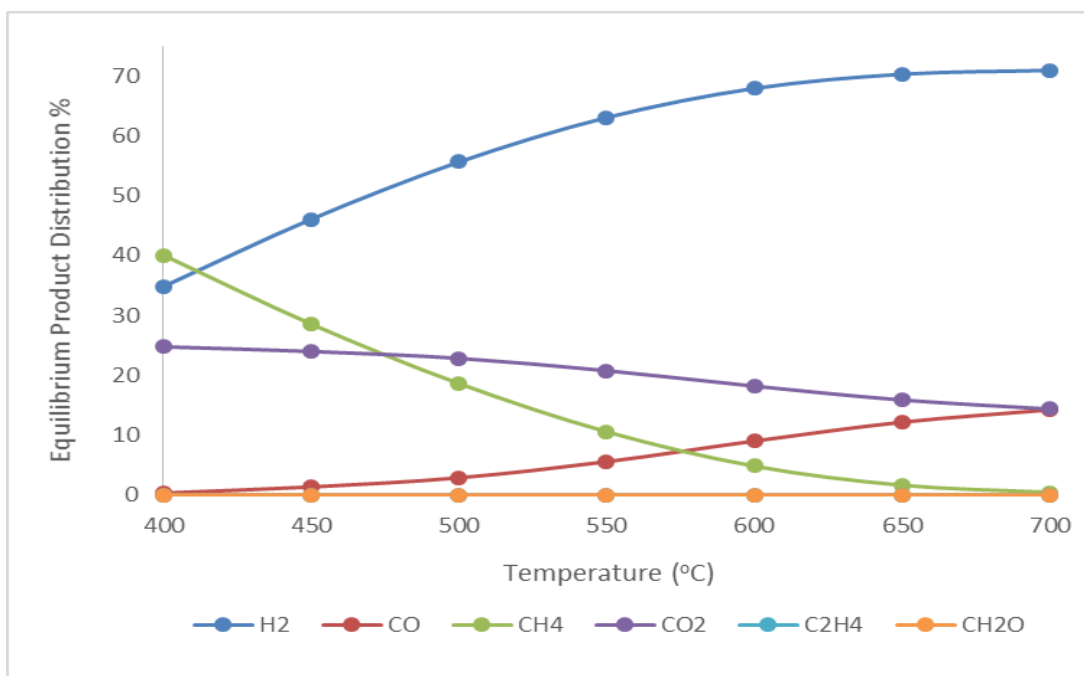


**Figure A. 5.** Equilibrium product distributions between 400°C and 700 °C with steam to ethanol ratio of 5

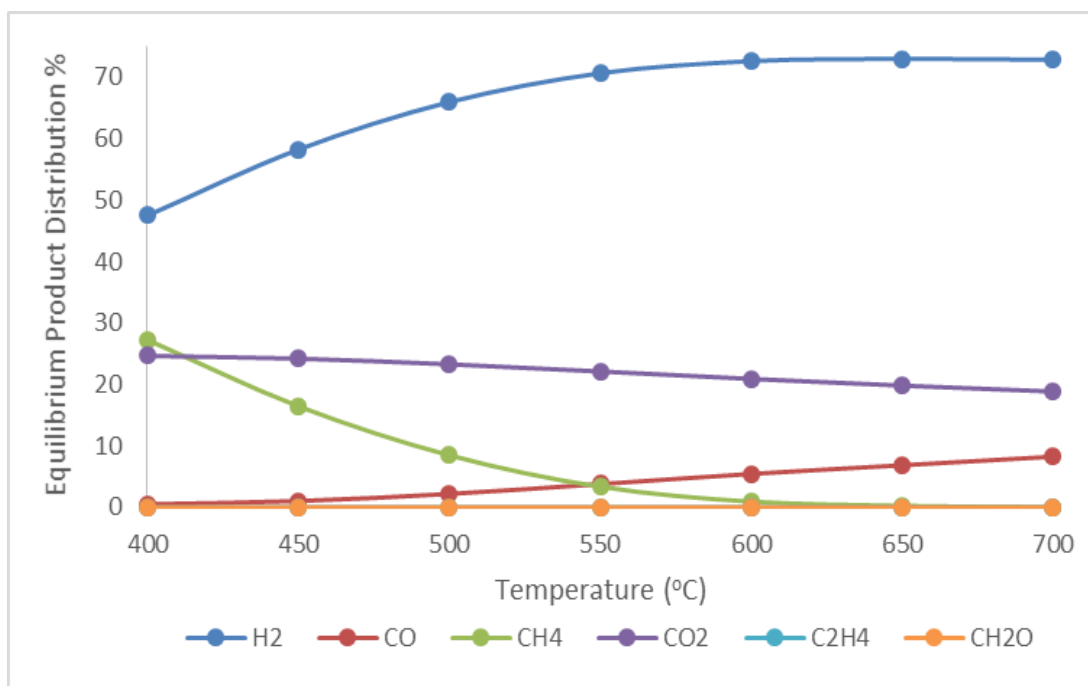


**Figure A. 6.** Equilibrium product distributions between 400°C and 700 °C with steam to ethanol ratio of 10

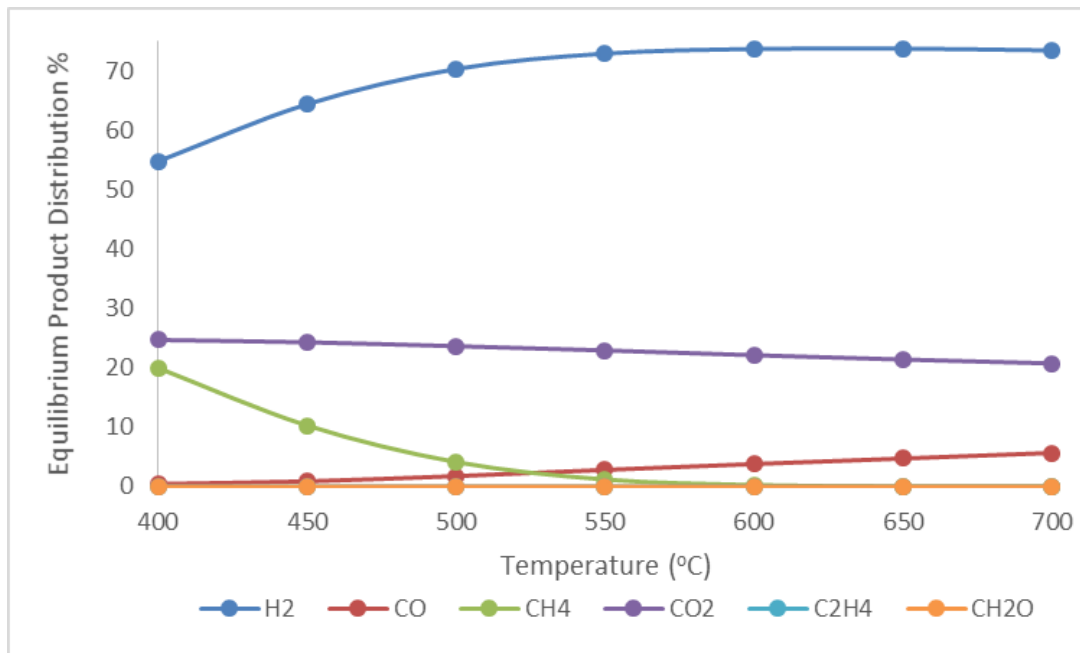


**Figure A. 7.** Equilibrium product distributions between 400°C and 700 °C with steam to ethanol ratio of 15



## **B. FOCUSED - MICROWAVE REACTOR COMPONENTS**

The components of the focused-microwave reactor available in our laboratory are analyzed in detail as follows;

### **B.1 Microwave Generator**

Microwave generator is composed of a power supply (Figure B.1) equipped with a front panel (Figure B.2) and compact size-microwave head (Figure B.3).



**Figure B.1.** Power supply of focused-microwave reactor

In our microwave reactor system, 2 kW power supply which is based upon the latest switch mode power technology with good power stability and significantly reduced electrical losses is used.

As shown in Figure B.2, the front panel of the power supply consists of a large white over blue graphical LCD screen 240x180 pixels, 3 push buttons and a knob for menu navigation and power control. All operating parameters, control status, any possible fault, forward power and reflected power are displayed on the screen.



**Figure B.2.** Front panel of the power supply

Compact size-microwave head is responsible for converting electricity to microwave energy. This microwave head includes a water cooled-magnetron and filament transformer. An isolator equipped with reflected power crystal detector is connected to the microwave head. A water flow meter is connected at the exit of the cooling circuit of the isolator. This flow meter acts as an interlock that will completely shut down the microwave generator if not enough water flow is sensed.



**Figure B.3.** Compact size-microwave head of focused-microwave reactor

## B.2 Adjustable Iris

The variable iris (Figure B.4) is designed for adaptation of a resonant monomode rectangular cavity. This part of the reactor allows to adjust the Q factor of the resonant monomode cavity and the position of the maximum electric field with the position of the sample to be heated.

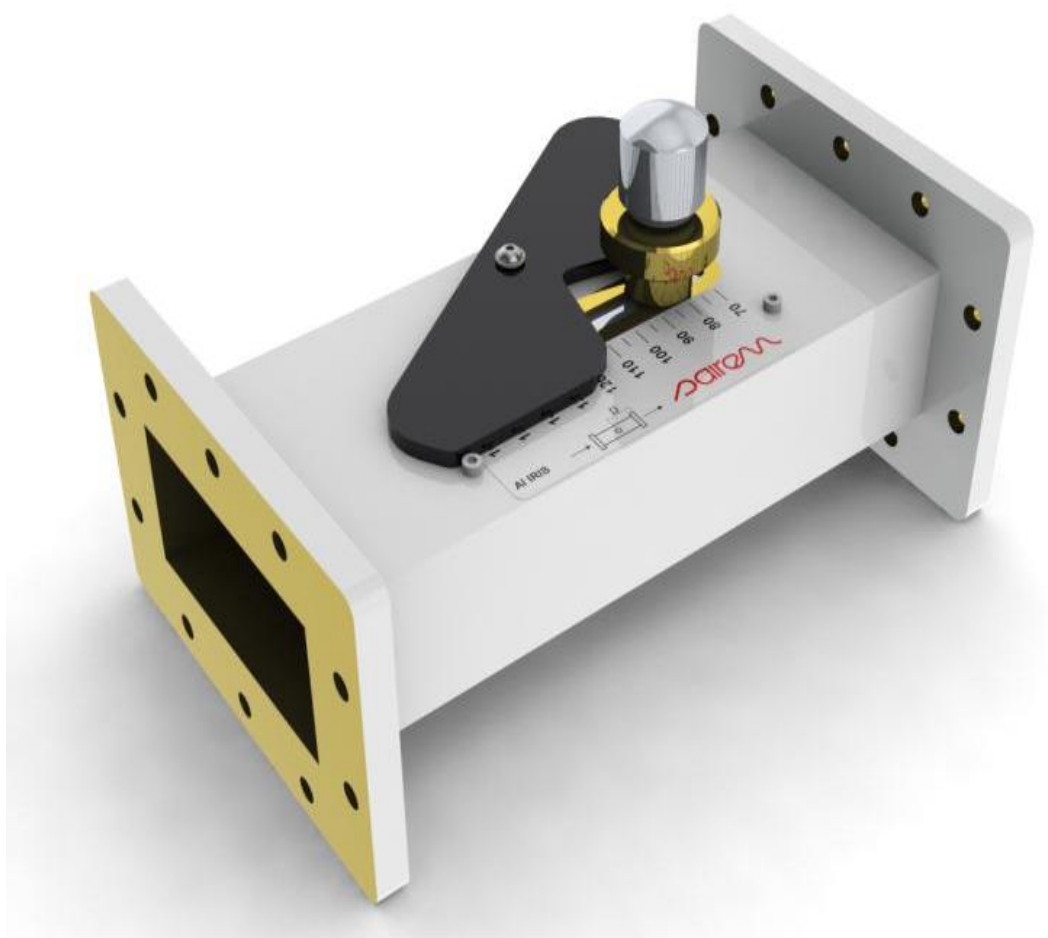


**Figure B.4.** Adjustable iris of focused-microwave reactor

### **B.3 H-Bend Waveguide**

H-bend waveguide (Figure B.5) allows linking together waveguide elements that are not in the same plane.

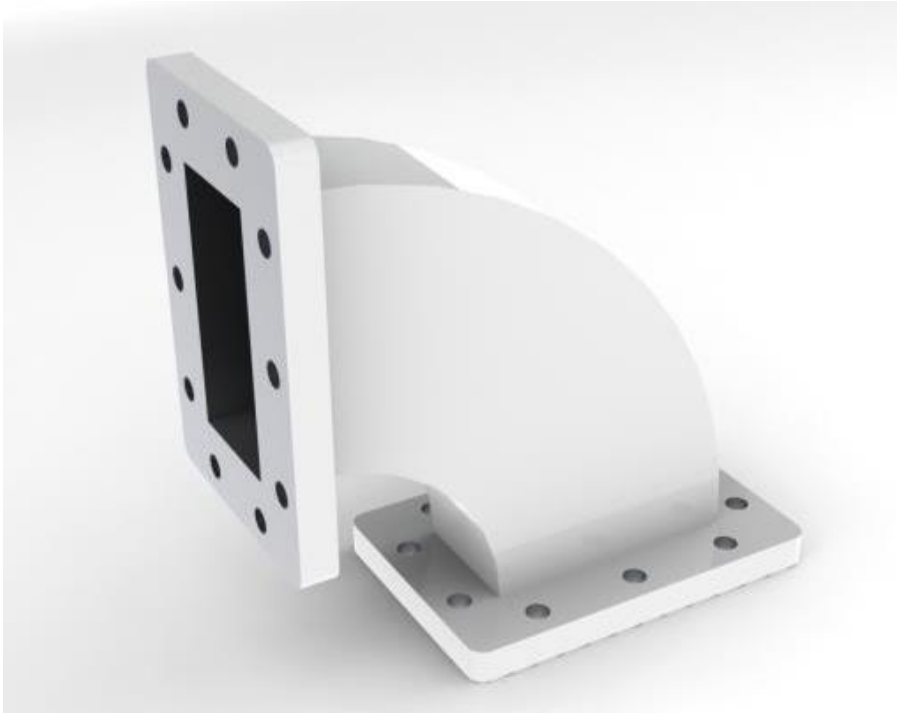


**Figure B.5.** H-bend waveguide element of microwave reactor

### **B.4 Downstream Plasma Source**

The plasma downstream source (Figure B.6) is designed to generate plasmas whose parameters depend on the gas type, pressure and the total microwave power absorbed by the plasma.

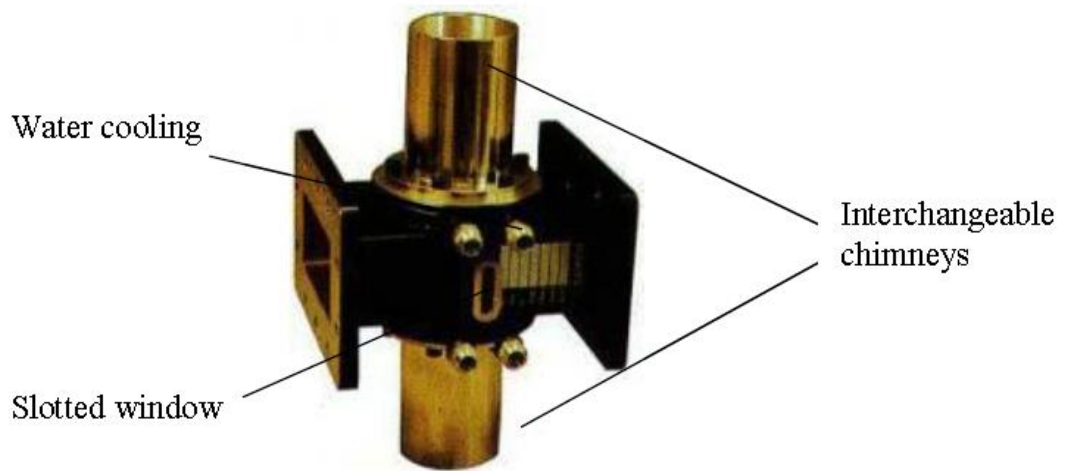


**Figure B.6.** Plasma downstream source of microwave reactor

### B.5 Sliding Short Circuit

Sliding short circuit (Figure B.7) is designed for tuning applications for the adjustment of resonance frequency of a monomode cavity. This tuner consists of a waveguide with standard flange at one end and a short circuit that can be moved inside the guide. There is a handle to help the movement of the sliding short circuit as well as a blocking screw to fix it in position once the tuning is achieved. The plunger allows quick adjustment while fine tuning can be achieved via a tuning screw.

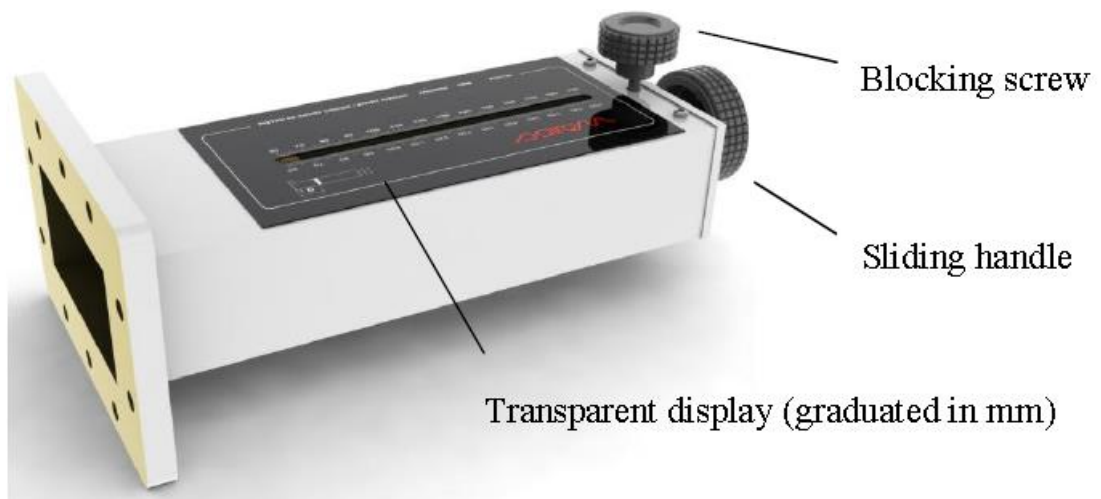


**Figure B.7.** Sliding short circuit of microwave reactor



### C. SAMPLE PARTICLE SIZE CALCULATION

Particle sizes of the crystals were calculated using Scherrer equation (Equation C.1). Sample calculation of crystal size determination was performed using raw XRD data of Co-Mg-MA catalyst (Table C.1).

$$t_{\text{particle}} = \frac{C \times \lambda}{B \times \cos\left(\frac{2\theta}{2}\right)} \quad (\text{C.1})$$

**C:** crystal shape factor (0.89)

**$\lambda$ :** Wavelength (0.154 nm)

**B:** Full width at half maximum

**$2\theta$ :** Peak angle

**Table C.1.** Raw XRD data of Co-Mg-MA

2-theta(deg)	d (Å)	Int. I(cps deg)	FWHM(deg)
19.01(3)	4.664(7)	299(13)	0.71(2)
31.34(2)	2.8516(18)	571(13)	0.73(2)
36.895(9)	2.4342(6)	2045(15)	0.743(9)
44.916(19)	2.0164(8)	1234(17)	0.76(2)
59.45(4)	1.5536(10)	906(21)	0.83(4)
65.376(18)	1.4263(4)	1446(16)	0.747(17)
77.53(11)	1.2303(15)	143(14)	0.75(12)

Cluster size of  $\text{Co}_3\text{O}_4$  was estimated from the characteristic peak at the  $2\theta$  value of 19.01.

$$B = \text{FWHM} \times \frac{3.14}{180} = 0.71 \times \frac{3.14}{180} = 0.01239 \text{ radians}$$

$$t_{\text{particle}} = \frac{0.89 \times 0.154}{0.01239 \times \cos\left(\frac{19.01}{2}\right)} = 11.2 \text{ nm}$$



## D. CALIBRATION OF GAS CHROMATOGRAPH

The outlet stream emerging from the reactor is analyzed by an online gas chromatography instrument. Gas chromatograph was calibrated with respect to ethanol which means that ethanol calibration factor was assumed as 1.00. For the species A, calibration factor is calculated by using the formula below:

$$\frac{X_A}{X_{C_2H_5OH}} = \frac{\text{Peak area of A} \times \beta_A}{\text{Peak area of } C_2H_5OH \times \beta_{C_2H_5OH}}$$

Retention times and calibration factors of the gas chromatography are given in Table D.1.

**Table D.1.** Calibration parameters of reaction gases

<b>Gas</b>	<b>Retention Time</b>	<b>Calibration Factor</b>
H <sub>2</sub>	0.98-1.00	0.35
CO	1.20-1.30	4.40
CH <sub>4</sub>	1.60-1.80	0.92
CO <sub>2</sub>	3.70-4.00	3.30
C <sub>2</sub> H <sub>2</sub>	5.10-5.30	1.23
CH <sub>2</sub> O	8.20-8.40	3.80
C <sub>2</sub> H <sub>4</sub> O	10.30-10.80	1.68
C <sub>2</sub> H <sub>5</sub> OH	12.20-12.80	1



### E. SAMPLE CALCULATION FOR CATALYST ACTIVITY TOWARDS SRE

The data for 60<sup>th</sup> minute of Co-Mg@MA catalyst at 550°C is used for the sample calculation. Raw data obtained at the 60<sup>th</sup> minute of the activity test is presented in Table E.1.

**Table E.1.** Raw data for 60<sup>th</sup> minute of activity test of Co-Mg@MA catalyst at 550°C

Component	Peak Area
H <sub>2</sub>	2322.6
CO	11.3
CH <sub>4</sub>	126.0
CO <sub>2</sub>	45.0
C <sub>2</sub> H <sub>4</sub>	5884.6
CH <sub>2</sub> O	61.3
C <sub>2</sub> H <sub>4</sub> O	0.00
C <sub>2</sub> H <sub>5</sub> OH	0.00

From the gas chromatography analysis, several peaks corresponding to different chemicals were collected and each peak area was multiplied with their calibration factors as listed in Table D.1. Calculated numbers represent the mole numbers with respect to ethanol.

Mole calculations of each species observed in product stream and total mole calculation with respect to ethanol are shown below.

$$n_{\text{H}_2} = \beta_{\text{H}_2} \times A_{\text{H}_2} = 0.35 \times 2322.6 = 812.91$$

$$n_{\text{CO}} = \beta_{\text{CO}} \times A_{\text{CO}} = 4.4 \times 11.3 = 49.72$$

$$n_{\text{CH}_4} = \beta_{\text{CH}_4} \times A_{\text{CH}_4} = 0.92 \times 126.0 = 115.92$$

$$n_{\text{CO}_2} = \beta_{\text{CO}_2} \times A_{\text{CO}_2} = 3.3 \times 45.0 = 148.50$$

$$n_{\text{C}_2\text{H}_4} = \beta_{\text{C}_2\text{H}_4} \times A_{\text{C}_2\text{H}_4} = 1.23 \times 5884.6 = 7238.06$$

$$n_{\text{CH}_2\text{O}} = \beta_{\text{CH}_2\text{O}} \times A_{\text{CH}_2\text{O}} = 3.80 \times 61.3 = 232.94$$

Total mole number of inlet stream is calculated by the carbon balance of outlet stream flow as shown below.

$$n_0 = n_{\text{C}_2\text{H}_5\text{OH}} + 0.5 n_{\text{CO}_2} + 0.5 n_{\text{CO}} + 0.5 n_{\text{CH}_4} + 0.5 n_{\text{CH}_2\text{O}} + n_{\text{C}_2\text{H}_4} + n_{\text{C}_2\text{H}_4\text{O}}$$

$$n_0 = 0 + 0.5 \times 148.50 + 0.5 \times 49.72 + 0.5 \times 115.92 + 0.5 \times 232.94 + 7238.06 + 0 = 7511.60$$

To find the ethanol conversion, converted amount of ethanol is divided into the total carbon inlet stream and hydrogen yield is calculated by dividing the mole numbers of hydrogen produced by mole numbers of inlet stream.

$$\text{EtOH Conversion} = \frac{n_{\text{converted}}}{n_0} \times 100 = \frac{n_0 - n_{\text{C}_2\text{H}_5\text{OH}}}{n_0} \times 100 = \frac{7511.6 - 0}{7511.60} = 100\%$$

$$\text{Hydrogen Yield} = \frac{n_{\text{H}_2}}{n_0} = \frac{812.91}{7511.60} = 0.11$$

The outlet product stream composition is calculated by dividing the mole number of any component to total number of all components.

$$\text{H}_2\% = \frac{n_{\text{H}_2}}{n_{\text{total}}}$$

where;

$$\begin{aligned}n_{\text{total}} &= n_{\text{H}_2} + n_{\text{C}_2\text{H}_5\text{OH}} + n_{\text{CO}_2} + n_{\text{CO}} + n_{\text{CH}_4} + n_{\text{C}_2\text{H}_4} + n_{\text{C}_2\text{H}_4\text{O}} + n_{\text{CH}_2\text{O}} \\n_{\text{total}} &= 812.91 + 0 + 148.50 + 49.72 + 115.92 + 7238.06 + 0 + 232.94 \\&= 8598.05\end{aligned}$$

$$\text{H}_2\% = \frac{n_{\text{H}_2}}{n_{\text{total}}} \times 100 = \frac{812.91}{8598.05} \times 100 = 9.5$$

$$\text{CO}\% = \frac{n_{\text{CO}}}{n_{\text{total}}} \times 100 = \frac{49.72}{8598.05} \times 100 = 0.58$$

$$\text{CH}_4\% = \frac{n_{\text{CH}_4}}{n_{\text{total}}} \times 100 = \frac{115.92}{8598.05} \times 100 = 1.35$$

$$\text{CO}_2\% = \frac{n_{\text{CO}_2}}{n_{\text{total}}} \times 100 = \frac{148.50}{8598.05} \times 100 = 1.73$$

$$\text{C}_2\text{H}_4\% = \frac{n_{\text{C}_2\text{H}_4}}{n_{\text{total}}} \times 100 = \frac{7238.06}{8598.05} \times 100 = 84.18$$

$$\text{CH}_2\text{O}\% = \frac{n_{\text{CH}_2\text{O}}}{n_{\text{total}}} \times 100 = \frac{232.94}{8598.05} \times 100 = 2.71$$



## CURRICULUM VITAE

Name :SEVAL GÜNDÜZ  
Title :Research Assistant  
Employer :Middle East Technical University (METU), Ankara, Turkey  
Telephone :(90) 312 2104363  
Fax :(90) 312 2102600  
Mobile :(90) 505 4555470  
E-mail :gseval@metu.edu.tr  
Date of birth :08.04.1985

### EDUCATION

- |          |                                     |      |
|----------|-------------------------------------|------|
| 1. Ph.D. | METU, Chem. Eng. Department, Ankara | 2014 |
| 2. M.S.  | METU, Chem. Eng. Department, Ankara | 2011 |
| 3. B.S.  | METU, Chem. Eng. Department, Ankara | 2008 |

### ACADEMIC POSITIONS / TITLES

- |                       |                                     |       |
|-----------------------|-------------------------------------|-------|
| 1. Research Assistant | METU, Chem. Eng. Department, Ankara | 2012- |
|-----------------------|-------------------------------------|-------|

### AWARDS-SCHOLARSHIPS

- |  |           |
|--|-----------|
| 1. METU Graduate Courses Academic Performance Award  | 2009      |
| 2. Best Poster Award (3 <sup>rd</sup> National Catalysis Congress)                         | 2010      |
| 3. TUBITAK Research Scholarship  | 2010-2011 |
| 4. TUBITAK Research Scholarship  | 2011-2013 |
| 5. Prof. Dr. Hasan Orbey Memorial Award for Research Excellence in Graduate Studies (Ph.D) | 2013      |
| 6. Best Poster Award (5 <sup>th</sup> National Catalysis Congress)                         | 2014      |
| 7. Best Oral Presentation (20 <sup>th</sup> World Hydrogen Energy Conference)              | 2014      |

## **RESEARCH INTERESTS:**

Synthesis and characterization of nanostructured mesoporous catalysts; chemical reaction engineering; heterogeneous catalysis; steam reforming of ethanol; hydrogen production; microwave assisted heterogeneous reactions.

## **PROJECTS:**

1. TUBITAK Project (108M571): Dizel Alternatifi Dimetileter Sentezi: Katalitik Çalışmalar, 'Diesel Alternate DME Synthesis: Catalytic Studies', 15/10/2010-15/10/2011, project scholar.
2. TUBITAK Project (111M338): Etanol Reformlama ile Yüksek Hidrojen Verimi için Adsorpsiyon-Reaksiyon Kombinasyonu ve Uygun Mezogözenekli Katalizörlerin Geliştirilmesi, 'Adsorption-Reaction Combination for High Hydrogen Production through Ethanol Reforming and Synthesis of Suitable Mesoporous Catalysts', 01/10/2011-01/10/2013, project scholar.
3. METU BAP Project (BAP-03-04-2010-011): Mikrodalga Enerjisi Altında Yeni Mezogözenekli Katalizörler Yardımıyla Buhar Reform Reaksiyonu Kullanarak Etanolden Sentez Gazı Üretimi, 'Synthesis Gas Production over Novel Mesoporous Catalysts with Microwave Assisted Steam Reforming of Ethanol', 01/01/2010-31/12/2010.
4. METU BAP Project (BAP-03-04-2011-007): Adsorpsiyon Destekli Etanol Reformlama Reaksiyonu ile Hidrojen Üretimi, 'Hydrogen Production with Sorption Enhanced Reforming of Ethanol', 01/01/2011-31/12/2013.

## **COMPUTER SKILLS:**

Programming: FORTRAN, POLYMATH, MATHCAD

## **TEACHING EXPERIENCE:**

Served as a Teaching Assistant for the following courses at METU:

ChE 203 - Chemical Process Calculations

ChE 222 - Fluid Mechanics



ChE 311 – Chemical Reaction Engineering  
ChE 327 - Heat and Mass Transfer Operations  
ChE 410 - Chemical Engineering Laboratory II  
ChE 420 - Chemical Engineering Laboratory III  
ChE 426 - Reactor Design  
ChE 501 - Advanced Thermodynamics

### **EQUIPMENT SKILLS:**

Gas Chromatograph (Agilent 6850)  
TGA (Perkin Elmer TGA7)  
Diffuse Reflectance FT-IR (Perkin Elmer Instrument One)  
Focused-Microwave Ssystem (SAIREM)

### **PUBLICATIONS:**

#### **THESIS**

**Ph.D Thesis:** Gunduz, S., ‘Hydrogen Production From Ethanol over Mesoporous Alumina based Catalysts and Microwave Reactor Applications’, ODTÜ, Ankara, 2014.

**M.Sc Thesis:** Gunduz, S., ‘Sorption Enhanced Ethanol Reforming over Cobalt, Nickel Incorporated MCM-41 for Hydrogen Production’, ODTÜ, Ankara, 2011.

#### **ARTICLES**

1. Gunduz, S., Dogu, T., ‘Sorption Enhanced Reforming of Ethanol over Ni- and Co-Incorporated MCM-41 Type Catalysts’, Ind. Eng. Chem. Res. 2012, 51, 8796-8805.
2. Arslan, A., Gunduz, S., Dogu, T., ‘Steam Reforming of Ethanol with Zirconia Incorporated Mesoporous Silicate Supported Catalysts’, International Journal of Hydrogen Energy 2014, DOI: 10. 1016/j.ijhydene.2014.09.030.

3. Gunduz, S., Dogu, T., ‘Hydrogen by Steam Reforming of Ethanol over Co-Mg Incorporated Novel Mesoporous Alumina Catalysts in Tubular and Microwave Reactors’ (in progress).

### **SYMPOSIUM PRESENTATIONS/PUBLICATIONS**

1. Gunduz, S., Dogu, T., ‘Ethanol Steam Reforming over Ni Impregnated MCM-41 Type Mesoporous Materials’, 3<sup>rd</sup> National Catalysis Congress, 28 April-1 May 2010, Zonguldak/Turkey. (Poster)
2. Gunduz, S., Dogu, T., ‘Hydrogen Production by Steam Reforming of Ethanol over Co/MCM-41’, 6<sup>th</sup> EFCATS Summer School Catalysis and Surface Sciences for Renewables and Energy, 13-19 September 2010, İzmir/Turkey. (Poster)
3. Gunduz, S., Dogu, T., ‘Ni, Rh, Cu and Co Impregnated MCM-41-Like Mesoporous Catalysts for Ethanol Reforming’, 6<sup>th</sup> Chemical Engineering Conference for Collaborative Research in Eastern Mediterranean Countries, 7-12 March 2010, Antalya/Turkey. (Poster)
4. Gunduz, S., Dogu, T., ‘Sorption Enhanced Reforming of Ethanol Over Ni and Co Incorporated MCM-41 Type Catalysts’, Catalysis in Multiphase Reactors CAMURE-8 and International Symposium on Multifunctional Reactors ISMR-7, 22-25 May 2011, Naantali/Finland. (Poster)
5. Gunduz, S., Dogu, T., ‘Hydrogen by Sorption Enhanced Ethanol Reforming over Cobalt Incorporated Mesoporous Catalysts’, 12<sup>th</sup> Mediterranean Congress of Chemical Engineering, 15-18 November 2011, Barcelona/Spain. (Poster)
6. Gunduz, S., Dogu, T., ‘Co-Mg Incorporated Mesoporous Alumina with Ordered Pore Structure for Steam Reforming of Ethanol to Produce Hydrogen Rich Gas’, MRS Materials Research Society Spring Meeting, 9-13 April 2012, San Francisco/ABD. (Poster)
7. Gunduz, S., Dogu, T., ‘Sorption Enhanced Ethanol Reforming over Co and Mg Incorporated Mesoporous Alumina and Silica, 4<sup>th</sup> National Catalysis Conference, 21-24 March 2012, Kocaeli/Turkey. (Oral)
8. Gunduz, S., Dogu, T., ‘Sorption Enhanced Ethanol Reforming over Nickel and Magnesium Incorporated Mesoporous Alumina and Silica’, ISCRE 22

International Symposium on Chemical Engineering, 2-5 September 2012, Maastricht/Netherlands. (Poster)

9. Gunduz, S., Dogu, T., ‘Performance Comparison of Co-Mg Incorporated Mesoporous Alumina Prepared by the One-Pot and Impregnation Routes on Product Distribution and Hydrogen Yield in Reforming of Ethanol, HYPOTHESIS 2013 Conference, 11-12 June 2013, Edinburgh/Scotland. (Oral)
10. Gunduz, S., Dogu, T., ‘Ni-Mg Eklenmiş Mezogözenekli Alumina Tipi Katalizör ile Buharlı Etanol Reformlama Sonucu Hidrojen Üretimi’, 1. Ulusal Kataliz Yaz Okulu, 24-28 August 2013, Malatya/Turkey. (Poster)
11. Gunduz, S., Dogu, T., ‘Effect of Co-Mg Incorporation Method on Hydrogen Production Performance of Mesoporous Alumina based Catalysts’, International Porous Powder Materials Symposium and Exhibition PPM 2013, 3-6 September 2013, İzmir/Turkey. (Poster)
12. Gunduz, S., Dogu, T., ‘Activity Comparison of Ni and Mg Incorporated Mesoporous Alumina and Silica Catalysts in Reforming of Bio-Ethanol in Tubular and Microwave Reactors’, National Catalysis Congress NCC 5, 23-26 April 2014, Adana/Turkey. (Poster)
13. Gunduz, S., Dogu, T., ‘Hydrogen by Steam Reforming of Ethanol over Co-Mg Incorporated Novel Mesoporous Alumina Catalysts in Tubular and Microwave Reactors’, 20<sup>th</sup> World Hydrogen Energy Conference 2014, 15-20 June 2014, Gwangju/Korea. (Oral)
14. Arslan, A., Gunduz, S., Dogu, T., ‘Steam Reforming of Ethanol with Zirconia Incorporated Mesoporous Silicate Supported Catalysts’, 20<sup>th</sup> World Hydrogen Energy Conference 2014, 15-20 June 2014, Gwangju/Korea. (Oral)